Basma Tamasas

Program Authorized to Offer Degree:

Oral Biology

# Salivary Gland and Tooth Abnormalities Massively Increase Caries Susceptibility in A Mouse Model of Cleft Lip/Palate

Basma Tamasas

A dissertation submitted in partial fulfillment of the

requirements for the degree of

Doctor of Philosophy

University of Washington

2016

Reading Committee:

Timothy Cox, Chair

Susan Herring

Jeffrey S. McLean

Hitesh Kapadia

University of Washington

*Abstract*

**Salivary Gland and Tooth Abnormalities Massively Increase Caries Susceptibility in A Mouse Model of Cleft Lip/Palate**

Basma Ibrahim Tamasas

Chair of the Supervisory Committee:

Timothy Cox

Oral Health Sciences

**Objectives:** Cleft lip and palate (CLP) is one of the most common birth defects and has been found to be associated with multiple dentofacial anomalies, including hypoplastic teeth, and defects of the orbicularis oris muscle. In view of this associated spectrum of anomalies, numerous studies have investigated the risk of caries development in the CLP population, with the vast majority reporting an increase in caries incidence and severity. However, the cause of the observed increase in caries is largely unknown, making it difficult to manage and significantly prevent. Conditionally targeted mice for the cleft gene, Irf6 (*Irf6 Null-E*) have been established by deleting the gene only in the oral epithelium after the development of the lip has been completed, thus permitting investigation of the gene's other roles in the oral phenotypes. Therefore, these mice provide an ideal system with which to investigate the susceptibility and risk factors for caries progression. The overall goal of this research is to assess the function of Irf6 in oral epithelia during morphogenesis of teeth and salivary glands, and in particular how it

later impacts tooth structure, salivary function and caries susceptibility. I hypothesize that mice lacking the expression of Irf6 in oral epithelia will have a higher caries incidence compared to matched controls because of abnormal crown morphology and decreased enamel mineralization, as well as altered salivary gland function.

**Methods:** A dental epithelium-specific Irf6 knockout (*Irf6 Null-E*) mouse was generated using a Pitx2-Cre driver line. Dental development was analyzed by microcomputed tomography, and immuno-histochemistry. Salivary glands were assessed functionally using pilocarpine and histologically postmortem. We then employed an established caries induction protocol that involved infection of the oral cavity with *S. mutans*, a cariogenic bacterium, followed by feeding with a high-sucrose diet for eight weeks. Bacteria were then recovered from the animals by sonication of the lower jaw in normal saline, bacterial numbers counted to investigate the extent of oral cavity colonization, and the incidence and severity of caries scored under a dissecting microscope and following microCT imaging.

**Results:** I here found, as other previously did (Chu, 2015), that *Irf6 Null-E* mice recapitulate the dental phenotype observed in patient with cleft lip and palate, such as hypodontia, supernumerary teeth, and misshapen teeth (i.e., flat crown and root taurodontism), as well as enamel mineralization defects that were associated with delayed polarization of ameloblasts.

This thesis demonstrated that Irf6 ablation drastically alters the structure of major salivary glands. Histologically, salivary glands from *Irf6 null* mice exhibited persistent dysplastic

changes, disorganized structure that were associated with reduced and disorganized expression of adhesion proteins, altered salivary cell polarization, increased salivary cell proliferation, and reduced acinar cell differentiation. As a consequence, salivary gland hypofunction including low flow rate and reduced buffering capacity, as well as changes in mucin distribution, were observed in the null mice.

A striking increase in caries was observed in *Irf6 Null* mice compared to controls ($P<0.0001$), and this was associated with a significant increase in both total cultivable flora and the *S. mutans* population ($P <0.001$).

**Conclusions:** In addition to altered tooth morphology and decreased enamel mineralization, abnormal salivary gland function may be significantly increasing bacterial colonization and caries susceptibility and severity in the CLP population. For children with IRF6 mutations, implementation of early oral health strategies may be warranted.

**ABBREVIATIONS**

AMBN: ameloblastin

AMEL: amelogenin

AP-2: adaptor protein complex 2

AQP5: Aquaporin 5

ARHGAP: Rho GTPase activating protein

BMP: bone morphogenic protein

BSA: Bovine serum albumin

BPS: Bartsocas-Papas syndrome

CDH-1: Cadherin 1, Type 1

CLP: clefts with or without palatal involvement

CO2: Carbon Dioxide

Cre: Cre recombinase

DEJ: Dentino-enamel junction

DEFB1: Defensin beta 1

Dlx: The Distal-less family of genes

DVL: Dishevelled

EIIA: adenovirus EIIa promoter

EDA: Ectodysplasin A

EDAR: Ectodysplasin A receptor

EDTA: ethylene diamine tetraccetic acid

EEC: Ectrodactyly-ectodermal dysplasia-clefting syndrome

EGF: Epidermal growth factor

EMT: epithelial to mesenchymal transition

ENAM: Enamelin

FGF: fibroblast growth factor

FGFR: fibroblast growth factor receptor

GLI: Glioma-associated oncogene homolog

GTPase: guanosinetriphosphatase

HCL: Hydrochloric acid

HEK293T: human embryonic kidney 293 cells

HED: Hypohidrotic ectodermal dysplasia

HERS: Hertwig's epithelial root sheath

IEE: Inner enamel epithelium

IHC: Immunohistochemsitry

IRF5: Interferon Regulatory Factor 5

IRF6: Interferon Regulatory Factor 6

K14: Keratin 14

$KHCO_3$: Potassium Carbonate

KLK4: Kallikrein 4

LNP: Lateral nasal processes

MAPK: Mitogen-activated protein kinase

MEE: medial edge epithelium

MES: midline epithelial seam

MMP20: Matrix metalloproteinase 20

MNP: median nasal processes

MSA: Mitis Salivarius Agar

MXP: maxillary processes

NaCl: Sodium Chloride

NCCs: Neural crest cells

NME1: Nucleoside Diphosphate Kinase 1

NME2: Nucleoside Diphosphate Kinase 2

OEE: Outer enamel epithelium

P63: tumor protein 63

PAS: Periodic acid–Schiff

PCNA: Proliferating cell nuclear antigen

PCR: Polymerase chain reaction

PFA: paraformaldehyde

PITX2: Paired-Like Homeodomain 2

PPS: popliteal pterygium syndrome

PBS: phosphate buffered saline

Rac1: Ras-related C3 botulinum toxin substrate 1

RGS19: regulator of G protein signaling 19

Rho: Ras homolog gene family

RhoA: Ras homolog gene family, member A

RIPK4: receptor interacting serine-threonine kinase 4

ROCK: Rho-associated coiled-coil containing protein kinase

SHH: Sonic hedgehog

SI: Stratum Intermidium

SMG: Submandibular salivary gland

SLG: Sublingual salivary gland

SR: Stellate reticulum

Tabby: Spontaneous Eda-null mouse strain

TFAP2A: Transcription Factor AP-2 Alpha

TGFβ: transforming growth factor beta

TNF: Tumer necrosis factor

VWS: Van der Woude Syndrome

Wnt: wingless type

WT: Wild Typ

# TABLE OF CONTENTS

## LIST OF FIGURES

LIST OF TABLES

## ACKNOWLEDGEMENTS

I express my deepest gratitude to my supervisor, Prof. Timothy Cox for giving me the opportunity to carry out independent research. He was always open to new ideas, and we shared great scientific discussions. I have been privileged to benefit from his expertise and interest in this work. I am also extremely grateful for giving me the opportunities to work at a valuable institute such as Seattle Children Research Institute.

I would like to dedicate very special thanks to Prof. Susan Herring, a member of my advisory committee; she has truly inspired my passion for research, helped me continue believing in myself and strengthened my motivation to continue moving forward along this journey.

I am also profoundly grateful to my thesis committee members Dr. Hitesh Kapadia, Jeffrey S. McLean and Rebeca Slayton for their guidance, their insightful comments and encouragement and endless help. I also offer special thanks to the Oral Health Science Department especially Dr. Richard Presland, and Kathy Hobson, for their support and guidance throughout my PhD career.

During my PhD, I had the privilege to mentor Lucy Li, an undergraduate student from the University of Washington, Biology Department. She provided assistance during the carious induction, and the bacterial counting parts of the project and I am thankful for all the hard work she has done.

Special thanks also to all my fellow lab-mates for their valuable discussion, advice and help throughout the study. Thank you for supportively sharing the moments of desperation and frustration, as well as the moments of happiness, all of which have been so vital to get me through this journey. I also extend my sincere thanks to all members of Seattle Childrens Research Institute for a friendly company and unforgettable events throughout my PhD years.

I am thankful to have been blessed with a wonderful family, loving husband and children, as well as great friends. Your inspiration, prayers, and belief in me have sustained me through some of the hardest times, helped me to pursue my dream, and making it a reality.

Last but not the least, I wish to express my deep appreciation, and sincerest gratitude to my country Libya, I acknowledge that this research would not have been possible without their financial assistance.

# 1 Chapter 1: Introduction

## 1.1 Development of the lips, primary and secondary palate, salivary glands and teeth: related developmental processes

### *1.1.1 Morphogenesis of the Lips and palate*

Craniofacial development is the result of highly coordinated processes of outgrowth, apoptosis, and fusion of facial prominences. It starts with the ventrolateral migration of cranial neural crest cells (CNCCs) to form the ectomesenchymal core of the facial primordia (i.e., frontonasal, maxillary and mandibular prominences) (Chai et al., 2006), surrounded by an epithelium of ectodermal origin. Interaction between NCCs and the adjacent surface ectoderm, both during migration and at their final destination, is key for proper development of the craniofacial region (Cox, 2004; Dupin et al., 2006; Sandell et al., 2006). In humans, the face begins to take shape during the 4$^{th}$ week after conception, starting with the formation of the nasal placode, which will further subdivide to the lateral and medial nasal processes (figure 1.A). While the lower lip begins to form from the continuation of the paired mandibular prominences, the upper lip forms from the paired maxillary processes, the lateral nasal process and the intermaxillary segment. The two medial nasal projections of the intermaxillary segment adhere with each maxillary process and lateral nasal process to form the lip and more ventrally the primary palate during the 7th week (figure 1.B). As a consequence of this initial adhesion, a bilayered epithelial seam is formed, which must then be removed by a combination of apoptosis and radial cell migration to permit the formation of a mesenchymal bridge and consolidation of the lip (Jiang et al., 2006;

Jugessur et al., 2009; Stanier et al., 2004).

Development of the upper lip and the secondary palate is largely driven by rapid proliferation of CNCC-derived mesenchymal cells. The secondary palate originates from the palatal shelves that grow medially from the maxillary prominence. The palatal shelves first grow vertically and parallel to the side of the tongue (figure 1.C). Then, due to the downward and forward growth of the lower jaw and the tongue, the shelves then re-orient and continue to grow horizontally, merging in the midline above the tongue (figure 1.D) and contacting, on its dorsal surface, the ventrally projecting nasal septum. As with the forming lip, the resultant midline epithelial seam (MES) must be removed to ensure a proper functional palate is formed (Cox, 2004; Krapels et al., 2006; Mossey et al., 2009) (figure 1.E,F). In humans, secondary palatal fusion is completed during the $10^{th}$ week of development.

Bone centers will develop within maxillary and medial nasal processes and this process begins after the initial contact and fusion of the tissue primordia. These centers ultimately grow out to form the maxilla, and premaxilla in mice, including the alveolar process. Insufficient outgrowth of bone centers of the palate causes submucous clefts of the secondary palate (Meng et al., 2009). In contrast, altered adhesiveness or competency of the early oral epithelium, or subtle disruptions in the rate or the timing of mesenchymal cell migration that drives outgrowth of the facial prominences, can lead to a variety of abnormalities ranging from small notch of the lip, cleft lip with or without cleft palate (CL/P), or isolated cleft palate (CP). Moreover, CP can also occur secondary to various craniofacial developmental abnormalities such as enlarged or poorly

positioned tongue or a failure to elevate the palatal shelves above the tongue. Therefore the underlying pathogenic processes are quite variable and distinct (Johnston et al., 1995; Jugessur et al., 2009).

### *1.1.2 Morphogenesis of teeth*

Oral ectoderm gives rise to the teeth and salivary glands with the first morphological sign of their development being placode formation (i.e., local epithelial thickening). In each case, early development is characterized by ingrowth of these epithelial placodes into the underlying mesenchyme to form a bud (bud stage). After this early invagination, the unique differences in epithelial morphogenesis of both organs becomes notable (Catón et al., 2009; Tucker, 2007) (figure 1.2).

Tooth inductive signals arise initially in the dental epithelium up to the early bud stage. As development proceeds, the dental epithelium loses inductive potential, while simultaneously the underlying dental mesenchyme develops the capability to instruct tooth morphogenesis (Mina et al., 1987). During the bud stage, cells at the tip of the molar tooth buds stop dividing and form the primary enamel knot which acts as a signaling center to regulate dental epithelial growth and folding. It also stimulates the adjacent epithelial cells to proliferate to form the cervical loop and secretes growth factors that regulate the proliferation of the condensed underlying mesenchyme. As the cellular proliferation of the tooth bud continues to fold and invaginate further, the dental epithelium of the bud encloses the condensing mesenchyme (dental papilla) and forms the cap

stage (Thesleff et al., 1981).

The histodifferentiation process of the cap stage results in the organization of the dental organ into three structures: the enamel organ, the dental papilla, and the dental follicle. The enamel organ forms from the differentiation of the epithelial tissue. The mesenchymal cells, on the other hand, proliferate to form the dental papilla beneath the inner enamel epithelium, and the dental follicle (or dental sac) surrounding the tooth germ (Yildirim, 2013). This is followed by the bell stage, during which specific cusp patterns emerge, and the dental epithelium segregates into four distinct cell layers, including a single layer of epithelial cells adjacent to underlying mesenchyme, inner enamel epithelium (IEE), two layers of stratum intermedium cells (SI), several layers of stellate reticulum (SR) cells and a layer of outer enamel epithelium (OEE). The OEE cells help to maintain the shape of the enamel organ and regulate substance exchange between the enamel organ and the surrounding dental follicle. The cells of the stellate reticulum play a protective and a nutritive role during enamel development, while the stratum intermedium cells, with high alkaline phosphatase activity, produce cytokines and function in protein synthesis and transport to and from ameloblasts. Together, the SI, SR, and OEE cells have a shared role of reabsorbing water to expand the ameloblast cells and provide more space for subsequent enamel deposition. As development proceeds, IEE cells differentiate into the enamel-producing ameloblasts, and the mesenchymal cells underneath differentiate into the dentin-producing odontoblasts. The matrices for both enamel and dentin are then first formed followed by their subsequent mineralization (Catón et al., 2009; Thesleff et al., 1981).

Enamel formation, or amelogenesis, is preceded by initiation of dentin formation through the

process of dentinogenesis. Amelogenesis is recognized into four phases, defined mainly by the morphology and function of ameloblasts (the enamel forming cells). These are presecretory, secretory, transition, and maturation phases. In the presecretory stage of enamel development, the inner enamel epithelium cells gradually elongate in morphology and reverse the cell polarity to form pre-ameloblasts. The pre ameloblasts have the ability to secrete several enamel matrix proteins. They also signal to the adjacent cells of the dental papilla to undergo cytodifferentiation into pre-odontoblasts, which further polarize and differentiate into dentin-producing odontoblasts (Catón et al., 2009; Hu et al., 2007; Thesleff et al., 1981).

During the secretory stage, the preameloblasts differentiate into tall columnar ameloblasts, further polarize, form Tomes' processes (the projections of ameloblasts into the enamel matrix), and secrete large amounts of enamel matrix proteins (amelogenin, ameloblastin, and enamelin). When the first layer of enamel is formed, matrix degradation, particularly of amelogenin, via matrix metalloproteinase 20 (MMP20) occurs. Consequently, the ameloblasts, which are attached to one another by junctional complexes laterally and to cells in the stratum intermedium by desmosomes, start to move vertically and away from the dentin to provide space for the full enamel thickness. Once the enamel gets its full thickness, the Tomes' processes are lost and the secretory stage ameloblasts shorten into transition stage ameloblasts, under which a basement membrane reforms, and the stratum intermedium reduces to a single cell layer. Then, the transition stage ameloblasts transform into short cuboidal maturation stage ameloblasts (Bei, 2009; Simmer et al., 2010).

During the maturation stage, the ameloblasts change their function from matrix production to the

degradation and transportation of enamel matrix proteins out of the enamel via the smooth-ended ameloblasts, and to mineral ion deposition (i.e. calcium and phosphorus) into the enamel via the ruffle-ended ameloblasts. This results in the loss of organic material and water from enamel and an increase in inorganic components leading to enamel maturation and completion of the mineralization process. Once enamel formation is completed, ameloblasts undergo apoptosis, which is in contrast to odontoblasts which persist throughout the lifespan of the tooth (Bartlett et al., 2013; Simmer et al., 1995, 2010; Smith, 1998).

An epithelial-mesenchymal interaction also regulates tooth root development. Hertwig's epithelial root sheath (HERS) and the root sheath diaphragm (the apical-most portion of the HERS) are the main structures that guide and regulate root development. They consist of a double layer of inner and outer enamel epithelium cells extending apically from the cervical area of the enamel organ. At the beginning of root formation, the epithelial diaphragm bends at the future cemento- enamel junction into a horizontal direction, turns inward toward the radicular pulp cavity, and extends around the primary and secondary apical foramina. This narrows the wide cervical opening, and determines the number of roots as well as the level of the floor of the pulp chamber (Kumakami-Sakano et al., 2014).

The diaphragm maintains a constant size while the root sheath grows in length. The apical growth of the HERS induces the dental papilla cells to become root dentin forming odontoblasts. After this time, the epithelial root sheath begins to be perforated. This allows communication between the dental follicle cells and newly formed root dentin. As a consequence, cells of the

inner layer of the dental follicle differentiate into cementoblasts to form cementum. Cells of the outer layer differentiate into fibroblasts and osteoblasts to form periodontal ligament and alveolar bone. As the tooth root develops, the tooth starts to move occlusally to erupt into the oral cavity (Huang et al., 2009; Kumakami-Sakano et al., 2014; Luan et al., 2006).

### *1.1.3 Morphogenesis of salivary gland*

In human and mouse, the three pairs of major salivary glands - the parotid (P), sublingual (SLG) and submandibular (SMG) glands - develop in a similar manner. However, the development of the submandibular gland is best described in the literature. For this reason this gland is going to be the main focus of this research.

In contrast to the process of tooth formation from the dental epithelium, the glandular bud epithelium further proliferates to invade the underlying ectomesenchyme and reorganizes into a cord-like structure(Janebodin et al., 2013; Patel et al., 2011). As growth proceeds, the terminal part of the epithelial cord elongates and undergoes branching morphogenesis, enabling the primary bud to be divided into multiple buds. At this stage, the continuation with the oral ectoderm is still maintained through the epithelial cord. The lumen of the epithelial cord starts to form and progress toward the terminal buds. The lumenization process is not completely understood. It has been proposed that lumenization occurs as a result of differential rates of cell proliferation, and increased hydrostatic pressure due to fluid secretion by marginal (presumptive ductal) cells. It includes a number of cellular processes; active proliferation of the epithelial cells surrounding the lumen and apoptosis of the cells occupying the center of the presumptive lumen. These processes are accompanied by modulation of epithelial cell-cell adhesion, and changes in

polarity of the epithelial cells lining the lumen (Jaskoll et al., 1999; Melnick et al., 2000).

Lumen formation gives rise to terminal tubules lined by progenitor cells which eventually differentiate into intercalated duct cells and other specialized cells including acinar cells, striated duct cells, and myoepithelial cells. The proximal lumenized branched epithelial cord give rise to excretory and main ducts, while the distal lumenized branched epithelial cords gives rise to striated ducts. Simultaneously, the inner layer of the lumenized terminal buds remains a round-shaped, less organized population of round cells, which will develop mainly into the intercalated ducts, whereas the outer layer is organized into columnar epithelium, which will later form the main secretory units of the salivary gland (i.e., acini). During acini differentiation, a layer of myoepithelium develops and surrounds the acini, providing mechanical contraction to support saliva secretion.

Cell differentiation takes over as branching morphogenesis attenuates during development. Ductal development is largely completed during the prenatal period while acinar differentiation will continue to form the complex tubular glandular structure, surrounded by a mesenchymal capsule, with final differentiation at puberty in mice, at ~ 6 weeks of age, and at ~2 years of age in humans (Tucker, 2007).

## 1.2 Epithelial polarity and adhesion as crucial processes in lip, palate, teeth, and salivary gland morphogenesis

Epithelia are composed of sheets of cells that form a physical barrier between the body interior

and the external environment, but also play many essential roles during tissue development. External organs contain multiple layers of epithelial cells (i.e. skin, oral epithelium) in order to protect vital internal organs. On the other hand, the ducts of internal organs contain a monolayer of epithelial cells (i.e. mammary and salivary gland, and lung) which typically forms of two structures: epithelial cysts and tubules. In both structures, epithelial cells undergo a process of polarization to form distinct apical versus basolateral surfaces, with their apical cell surface facing the hollow lumenal center and their basal surface contacting the basement membrane.

Epithelial cells establish polarity as a result of cell-to-cell contact points known as epithelial junctions. Junctional complexes are composed of tight junctions and adherens junctions. Tight junctions form both paracellular and intramembrane diffusion barriers and regulate the permeability of the epithelial layer, i.e. the diffusion of lipids and proteins between the apical and basolateral membranes. The main proteins involved in tight junction formation are the transmembrane proteins claudin and occludin. These proteins localize within the tight junction and facilitate the bond between basolateral membranes of the adjacent cells (Itoh et al., 2003; Shin et al., 2006) .

On the other hand, mature adherens junctions form through calcium-dependent interactions between cadherin molecules on adjacent epithelial cells. E-cadherin, the main cell adhesion protein in epithelial adherens junctions, forms membrane anchor sites for the actin cytoskeleton through interactions with P120 catenin, α-catenin and β-catenin. This cadherin/catenin complex provides strong adhesion between adjacent cells and mediates adherens junctions' regulation under different physiological conditions (Harris et al., 2010). Other regulatory proteins, such as

kinases, members of the small guanosine triphosphatase (GTPase) families, including Rho and Rac, and transcription factors, are also fundamental for the modulation of the assembly, stability and function of both tight and adherens junctions (Kuroda et al., 1997; Takaishi et al., 1995).

Alterations of adhesion complexes can disrupt fusion of facial primordia. During palate development, formation of the midline epithelial seam (MES) itself requires modulation in polarity and adhesion of the contacting epithelia. Then, following initial contact, the MES has to disintegrate for the underlying mesenchyme of palatine shelves to consolidate. This is believed to occur through a combination of apoptosis and collective / radial cell migration (Jiang et al., 2006), processes that require both reorganization and alteration of cell-cell adhesion complexes and cytoskeletal components. E-cadherin is down-regulated during the breakdown of the epithelial seam formed during both lip and secondary palate development (Cox, 2004; Zhou et al., 2010), and persistence of E-cadherin has been found to impair fusion and mesenchymal convergence of the developing palate. Mutations in E-cadherin have also been detected in families with CLP (Frebourg et al., 2006).

Cadherins and P120 catenin, as integral components of the adherens junctions, have been shown to be expressed during both tooth and salivary gland development (Alves Pereira et al., 2010; Menko et al., 2002). E-cadherin expression is prominent in inner enamel epithelium cells, whereas N-cadherin, a related cadherin, is upregulated in differentiating ameloblasts. This specific cadherin expression pattern is thought to be key for ameloblast transformation and polarization, and thus for enamel matrix secretion (Heymann et al., 2002). E-cadherin is also an

essential regulator of branching morphogenesis and growth during salivary gland development. E-cadherin stabilizes the apical-basal polarity in acinar and ductal progenitors and protects the differentiating duct cells surrounding the lumen from apoptotic death (Walker et al., 2008).

Alterations in other components of the E-cadherin/catenin complex also disrupt tooth and salivary gland development. When p120 catenin was ablated in teeth, mice developed rough, hypomineralized teeth with defective secretory ameloblast morphology and organization. Adhesion proteins such as E- and N- cadherins were also reduced in mutants (Bartlett et al., 2010). Furthermore, these mice exhibited severe salivary gland defects. Acinar cell development was completely blocked in mutant animals, and the glandular ducts were severely misshapen and occluded by epithelial masses of precancerous-like intraepithelial neoplasia (Davis et al., 2006). Additionally, blocking or silencing of E-cadherin during early salivary gland morphogenesis resulted in severe structural defects including dilated lumen and massive apoptosis of the ductal cells (Walker et al., 2008).

In a similar way, Rac1 regulates both tooth and salivary glands morphogenesis through modulation of E-cadherin–mediated cell–cell adhesion. Rac1 conditional knockout mice exhibited rough, hypomineralized enamel and disorganized ameloblasts that were detached from the enamel matrix (Huang et al., 2011), similar to that seen in P120 knockout mice. Furthermore, the inhibition of Rac1 function in developing Drosophila salivary glands leads to failure of cell migration, leading to defective salivary duct invagination and reduced lumen length. In contrast,

constitutive activation of Rac 1 leads to marked increases in cell death and loss of gland integrity (Pirraglia et al., 2006).

## 1.3 Molecular mechanisms underlying lip, palate, teeth, and salivary gland formation

Much of craniofacial development is based on the reciprocal interaction between the developing oral ectoderm and neural crest-derived mesenchyme. Despite the diversity in the appearance and function of different craniofacial structures, the same gene pathways are often involved in regulating the early developmental steps of many of these structures, as evidenced by the fact that mutations in a gene encoding a signaling molecule or transcription factor can often affect more than one ectodermal derivative. A signaling center often forms within the developing organ and guides morphogenesis. These signals instruct the surrounding cells to proliferate and determine their positioning within the developing structure by differential regulation of the dynamic processes of adhesion and selective apoptosis, and then ultimately inducing the cells to differentiate into organ-specific cell types.

Examples of the main signaling pathways involved in the early stages of lip and palate development that are also crucial for tooth and salivary gland development, include the Fibroblast Growth Factor (FGF), Hedgehog (HH), Wingless (WNT), and Transforming Growth Factor beta (TGF- β) pathways (Kouskoura et al., 2011). Mutations in different components of these pathways as well as genes encoding downstream transcription factors, IRF6, P63, and

TFAP2A have been linked to both syndromic and non syndromic forms of CLP, as well as tooth and salivary gland anomalies (Salahshourifar et al., 2012; Stanier et al., 2004).

Nonsense and missense mutations in the transcription factor IRF6 have been identified in the allelic conditions of van der Woude syndrome (VWS) and popliteal pterygium syndrome (PPS), which account for ~2% of all syndromic forms of clefting. These syndromes are characterized by a varied phenotype that ranges from lip pits alone to bilateral cleft lip and palate in VWS, to the involvement of webbing of skin behind the knees, genital anomalies, syndactyly, and oral adhesions in PPS (Kondo et al., 2002; Little et al., 2009; Wang et al., 2003). Both conditions also exhibit notable dental anomalies like hypoplastic, malformed, supernumerary, and taurodont teeth. Mutations in the transcription factor TFAP2A cause branchio-oculofacial syndrome, featuring anomalies of the skin, eyes and ears, in addition to clefting and tooth abnormalities (Milunsky et al., 2008). Mutations in P63 caused the ectrodactyly-ectodermal dysplasia-clefting syndrome (EEC), featuring orofacial clefting, dental and salivary gland defects (van Straten et al., 2013; Yildirim et al., 2012). These latter two genes also have a connection with IRF6 through its upstream enhancer element MCS-9.7. Therefore genes involved in IRF6 regulation also seem to present with craniofacial defects. So what we learn about the shared morphogenetic and molecular mechanisms in normal and abnormal craniofacial development will contribute significantly to better diagnosis, new methods of treatment, and possibly prevention of diverse craniofacial defects and disorders.

## 1.4 Orofacial cleft, associated oral anomalies, and caries risk

### *1.4.1 Orofacial clefting and the associated anomalies*

CL/P and CP is the most prevalent birth defect in humans with a global incidence of ~1 in 700 live births (Mossey, 2003). Serious complications may be associated with cleft lip and cleft palate including feeding difficulties, ear infections, and dental and speech problems. Current treatments are costly and require a multidisciplinary approach involving both medical and dental professionals (Stanier et al., 2004). Oral clefts can present as an isolated anomaly or with an array of other defects often as part of a recognizable syndrome (Cobourne, 2004). Oral clefts have been associated with ~300 Mendelian syndromes, however, the majority of oral clefts are non-syndromic (~70%) (Jiang et al., 2006). The etiology of oral clefts is very complex including both genetic and environmental factors (Murray, 2002). The contribution of many genes is supported by experiments in animal models such as the mouse and chick, genome-wide association studies in patient cohorts and investigations of familial inheritance (Jugessur et al., 2009; Olasoji et al., 2005; Stanier et al., 2004). Environmental factors such as toxins, drugs, maternal smoking and alcohol use, as well as severe nutrient and vitamin deficiencies are all believed to contribute to the high incidence of clefting (Jugessur et al., 2009; Stanier et al., 2004).

A range of dental abnormalities is frequently observed in cleft affected individuals. Hypodontia, where one or more teeth are missing, is a common dental anomaly in CLP individuals with the incidence directly associated with severity of cleft presentation (Karsten et al., 2005). However, supernumerary teeth, particularly around the cleft area, are also commonly seen in cleft cases. Delayed tooth development/eruption ranging from 2, 6.5, and 7 months for CL, unilateral CL/P,

and bilateral CL/P respectively is another common dental presentation (Harris et al., 1990; Pöyry et al., 1989). Abnormal tooth morphology including peg lateral incisors, with frequencies ranging from 61.3%, 58%, 48.2%, 45%, and 10% for unilateral CL, bilateral CL/P, unilateral CL/P, unilateral, and CP respectively, is also common (Wu et al., 2011). Tooth size reduction and enamel hypoplasia, mainly of the incisor teeth adjacent to the cleft area, have also been described (Ruiz et al., 2013; Shashni et al., 2015). Taurodontism, an apical shift of the root furcation, is another common abnormality observed in cleft individuals (Al Jamal et al., 2010). In both permanent and the primary dentition, maxillary teeth have a higher frequency of dental anomalies than mandibular teeth (Rawashdeh et al., 2009). Interestingly, studies showed that both clefting subjects and their non-presenting siblings have a higher frequency of tooth abnormalities than the general population (Eerens et al., 2001; Küchler et al., 2011), supporting a shared genetic mechanism for both craniofacial developmental defects. Despite the shared molecular mechanisms, shared early morphological similarities, and the close anatomical location of teeth and salivary glands, very little is known about salivary gland anomalies in clefting populations. Major salivary gland hypoplasia and aplasia has been demonstrated in a few reports of patients with non-syndromic CLP but is not generally examined in this population. A change in saliva composition, including higer antioxidant levels which are known to increase in response to an infection (Aizenbud et al., 2008), and an increase in salivary clearance time (Ahluwalia et al., 2004) , have also been reported in cleft children. Despite the frequent presence of dental anomalies, and the suggestive salivary gland abnormalities, the association between these two factors and the incidence of dental caries in this population is not well understood. Because of the unique availability of a mouse model deficient in *Irf6* in the latter dental and salivary gland epithelium, this project will focus on investigating these dental

conditions.

### *1.4.2 Dental caries in cleft population*

Dental caries, characterized by soluble demineralization of the enamel structure by acid producing bacteria, is the most prevalent and costly infectious disease worldwide. Among children age 5 to 17 years, 43.6%, and 23% of low and high socioeconomic status children respectively had one or more untreated decayed primary and/or permanent teeth (Rockville, 2000). Several studies have been conducted to assess the prevalence of dental caries in cleft lip and/or palate patients, with somewhat contradictory results. As an example, Kirchberg et al, and Bokhout et al., found the incidence of caries to be 2, and 3.5 times higher in cleft affected subjects compared to the control group respectively (Bokhout et al., 1997; Kirchberg et al., 2004). Turner et al. found that 82% of the 100-clefting individuals included in the study had a moderate to high caries rate, of whom 66% had poor oral hygiene (Turner et al., 1998). The most recent meta-analysis of data on the risk of caries in individuals born with clefts also concluded that individuals born with these defects have a higher risk of developing dental caries (Wells, 2014). On the other hand, a few other studies reported no difference in caries experience in the clefting and non-clefting group ( Lauterstein et al.,1964; Lages et al., 2004; Lucas et al., 2000). Non-significant difference in caries experience have been attributed to poorly matched control demographics, differential fluoride exposure and /or the multifactorial nature of dental caries ( Lauterstein et al.,1964; Lages et al., 2004; Lucas et al., 2000; Hasslöf et al., 2007). Nevertheless, the majority of studies do support the notion of high caries activity in clefting individuals.

Children with clefting are often reported to have poor oral hygiene habits due to the fear of tooth brushing around the cleft area, difficulty in cleaning the displaced teeth, and decreased access to dental brushing due to scars from surgical procedures that can often limit mobility of the upper lip (Lam L et al. 2007; Hunt et al. 2005). The use of a pre-and post-surgical infant orthopedic appliance (e.g. an acrylic obturator) has also been associated with increased risk of *Streptococcus mutans* (caries causing bacteria) colonization (Bokhout et al., 1996). Orthodontic treatment may also increase caries risk in this population due to the difficulty to clean their teeth with appliances attached (Gaudilliere et al., 2014). Oral bacterial loads have also been found to be different in children with orofacial clefts due to open communication with the nasal cavity with any remaining defects in the palate acting as a reservoir for bacteria (Weiss et al., 2005). Intriguingly, an elevated frequency of high sugar diets, and prolonged feeding times, have also been reported in the clefting population. This would result in a prolonged period of acid production influenced by the retention of high starch containing food (Gaudilliere et al., 2014). Saliva has both cleansing action and an antimicrobial component (e.g. immunoglobulin and lysozyme), which can directly attack cariogenic bacteria and help maintain oral health. Ahluwalia et al. reported that children with clefting have significantly prolonged salivary clearance times compared to control children (Ahluwalia et al., 2004), a factor that has been significantly associated with high caries experience in both the elderly and 'dry mouth' patients. Therefore, in this proposal, I will further investigate the contribution of different host factors to the caries process using the unique dental epithelium-specific *Irf6* animal model, as discussed in the next section.

## 1.5 Role of IRF6 in craniofacial development

### *1.5.1 Irf6 structure and regulation*

IRF6 is a 467 amino acid protein that is encoded by seven of the gene's nine exons. It is part of a larger family of transcription factors and possesses the conserved functional domains of the IRF family, namely the DNA binding domain (DBD), and a less conserved protein-binding domain (PBD). The DBD consists of a helix-turn-helix motif that recognizes a DNA: 5'-AANNGAAA-3' termed the Interferon Stimulated Response Element (ISRE) (Mamane et al., 1999; Taniguchi et al., 2001). IRF6 is most similar to IRF5 (~89% sequence similarity). IRF5 plays a role in interferon activation after viral infection and in cell cycle regulation and apoptosis promotion (Barnes et al., 2003). All IRF members have been implicated in innate immune response, cell cycle regulation, and tumor suppression (Taniguchi et al., 2001). However, IRF6 is unique among this family in that it is the only member with restricted epithelial expression and in having a major role outside the immune system. IRF6 is an essential regulator of epithelial cell proliferation and differentiation and is important for formation of the barrier function of skin (Richardson et al., 2009). Recently, IRF6 was also shown to act as a regulator of the inflammatory response of oral epithelial cells by regulating the MyD88-dependent toll like receptor activation (Kwa et al., 2014).

IRF6 is regulated by an enhancer element MCS9.7, located 9.7 kilobases upstream of the IRF6 (Fakhouri et al., 2012). This enhancer element is sufficient to recapitulate the endogenous expression of IRF6 in most tissues during murine craniofacial development except for the medial

edge epithelium and the oral periderm (Fakhouri et al. 2012). This enhancer region contains a conserved binding site for the transcription factor p63 (Rahimov et al., 2008). p63 binds directly to this upstream enhancer element in the IRF6 locus to activate its transcription. This, in turns, results in p63 degradation (Gritli-Linde, 2010; Moretti et al., 2010). Recent work expanded the IRF6 gene-regulatory network to include an upstream, Pbx-dependent regulation. Pbx proteins control the expression of *Wnt9b* and*Wnt3*, regulating p63, which then binds the MCS9.7 to regulate *Irf6* expression (Ferretti et al., 2011). Therefore, IRF6 may also be a feature of other signaling pathways (e.g. Wnt pathway) that contribute to the regulation of epidermal/epithelium development.

Phosphorylation is a key factor in the activation and regulation of all IRF family members including IRF6 (Bailey et al., 2008). During cellular proliferation, IRF6 is phosphorylated by kinase activity, which thus directs its proteasomal degradation (Bailey et al., 2008). In mammary cells, and keratinocytes both phosphorylated and nonphosphorylated forms of IRF6 exist, with the last form being localized primarily in the cytoplasm, suggesting either the cytoplasmic sequestration of the IRF6 until needed or that it has other roles besides acting as a transcription factor. IRF6 has been shown to maintain the epithelial apical junction complex, and to regulate epithelial cell adhesion (Richardson et al., 2009). Receptor interacting protein kinase 4 (RIPK4), a critical regulator of keratinocyte differentiation and cytoskeleton organization, has been shown recently to directly activate IRF6 and prompt its nuclear translocation. In the same study, RIPK 4, similar to IRF6, null mice showed a defective skin barrier, fusion of the opposed epithelia, and cleft palate. Interestingly, these mice showed an abnormal apical localization of E-cadherin (cell

adhesion protein) in the defective fused periderm (De Groote et al., 2015). Recent data from our lab showed that IRF6 bind to Nucleoside Diphosphate Kinase (NME1/2) complex in a phosphorylation-enhanced manner (Parada Sanchez, 2012). The NME complex plays a significant role in regulating epithelial cell adhesion. All together, these data provide further evidence for a crucial role for IRF6 to maintain the oral epithelium integrity, and to regulate cell-cell adhesion, which will be further investigated in this proposal.

### *1.5.2 Irf6 in craniofacial development*

During mouse palate development, IRF6 expression is evident in the ectoderm covering the developing facial primordia, as well as the medial edge epithelium (MEE) of the palatal shelves, especially right before the fusion of the shelves (Knight et al., 2006). Mice deficient for both *Irf6* alleles develop craniofacial abnormalities, including cleft of the secondary palate, a thick skin which lacks the superficial cornified layer, especially in the oral cavity, exposing the underlying hyperproliferative spinous layer, leading to adhesion between adjoining tissues, failure of the elevation of the palatal shelves, and the prenatal lethality of these mice (Ingraham et al., 2006; Knight et al., 2006). Irf6 has been postulated to be involved in the disintegration of the MEE although the exact mechanism is unknown (Cuervo et al., 2002; Martínez-Alvarez et al., 2000). A recent study showed that loss of irf6 in the epithelium results in absence of apoptosis and maintenance of proliferation in MEE cells during palatal fusion (Iwata et al., 2013). Our own studies in the Cox lab have found that knockdown of Irf6 in the prefusion oral epithelia leads to a redistribution of adherens junctions proteins and increased proliferation of the basal layer. Irf6 is also expressed in the epithelia of the developing incisor and molar tooth germ. However, during

the embryonic stage of tooth development, only the incisors have been reported to be affected by *Irf6* mutation. Specifically, the incisor epithelium was reported as failing to invaginate properly into the underlying mesenchyme, with enamel knot marker gene expression being displaced to the outermost tip of the epithelia compared to the central expression in wild type embryos (Blackburn et al., 2012). IRF6 is also expressed in embryonic submandibular salivary gland epithelium, suggesting an important role for *Irf6* in salivary gland development (Fakhouri et al., 2012; Laugel-Haushalter et al., 2012). However, the effect of *Irf6* ablation on either postnatal tooth and salivary gland development is currently unknown. The Cox lab has already established a homozygous mouse line with *Irf6* conditionally ablated in oral epithelia. Homozygotes, and to a much lesser degree heterozygotes, show an array of tooth anomalies (resembling those described in patients with CLP), increased enamel wear, as well as abnormal salivary gland morphology, and thus they provide an ideal system with which the role of *Irf6* in tooth and salivary gland development can be investigated.

## 1.6 Hypothesis and Specific Aims

The overall goal of this research is to assess the function of Irf6 in oral epithelia during morphogenesis of teeth and salivary glands, and in particular how it later impacts tooth structure, salivary function and caries susceptibility. I hypothesize that mice lacking the expression of Irf6 in oral epithelia will have a higher caries incidence compared to matched controls because of abnormal crown morphology and decreased enamel mineralization, as well as altered salivary gland function. The results emerging from this research will contribute toward the understanding of the role of *Irf6* in CLP in epithelial-derived tissues in generals, and the functional

consequences. It is anticipated that findings from this study will open up new research opportunities investigating possible preventative approaches and treatment strategies for tooth-related problems in patients with CLP. Moreover, understanding the role of *Irf6* in salivary gland development can enhance the ongoing efforts to develop better regenerative therapies for damaged salivary glands. The following aims were pursued:

***Aim 1: Assess the role of Irf6 in postnatal tooth development.***

Using epithelial conditional knockout mice and matched controls, the effect of Irf6 ablation on tooth morphology, and mineralization were evaluated. 3D morphometric analysis using micro-computed tomography was utilized to quantify mineral density and volume of different tooth structures (enamel and dentin).

***Aim 2: Investigate the impact of Irf6 loss on salivary gland morphology and function.***

Saliva was collected from live animals of each genotype to test the functionality of the salivary glands. Salivary flow rate, protein constituents, buffer capacity and pH were measured. Salivary gland tissues were harvested from *Irf6* conditional knockout mice, and controls and a histological time course were conducted. Protein expressions of critical regulators of salivary gland development were evaluated using immunohistochemistry.

***Aim 3: Investigate the influence of Irf6 ablation on dental caries development and bacterial viability.***

*Irf6* conditional knockout mice along with matched controls were infected with *S. mutans* by oral

swabbing on 3 consecutive days, and fed Diet 2000 (56% sucrose) and 5% sucrose water ad libitum. All animals were followed for 8 weeks from the initial inoculation. At the terminal procedure, mice were euthanized with an overdose of CO2 and subjected to imaging by dissecting microscopy and microCT for caries scoring. After scanning, the lower jaws were dissected and sonicated with saline solution. The suspensions from this mix were streaked on mitis salivarius agar plus erythromycin and blood agar to estimate the *S. mutans* population, and to determine the total cultivable oral flora respectively.

## 1.7 Figures and tables

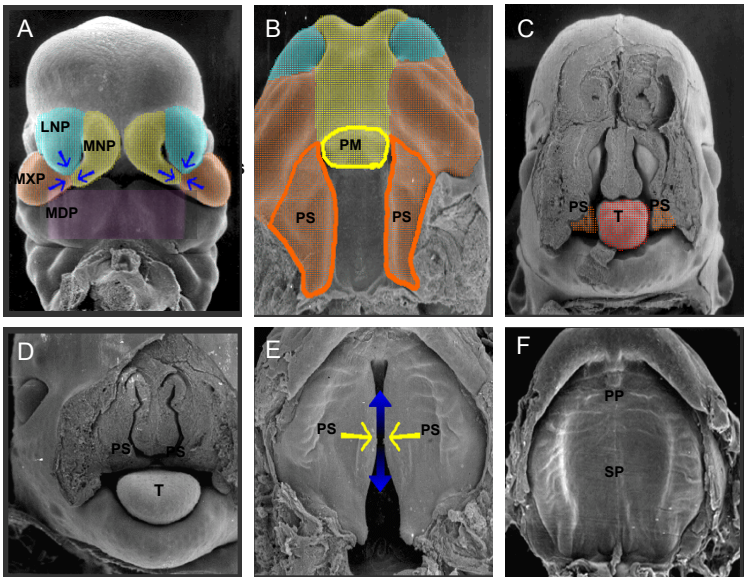


**Figure 1.1: Lip and Palate development.** Scanning electron micrographs of human embryos, except C, and D are mouse embryo. A) The medial nasal, lateral nasal, and the maxillary processes fuse to form the upper lip, and continuation of the mandibular processes establishes the lower lip. B) The medial nasal processes have fused to form the premaxilla, while the palatal shelves will later elevate and fuse to form the secondary palate. C) The margins of palatal shelves are extending to the level of the lateral borders of the tongue. D) The palatal shelves are positioned above the tongue to facilitate their fusion E), the palatal shelves approximate each other, and fuse anteriorly and posteriorly (arrow direction). F) Complete fusion of the palatal shelves. MXP: Maxillary process, MDP: Mandibular process, MNP: Medial nasal process, LNP: Lateral nasal process, PM: Premaxilla, PS: Palatal shelves. PP: Primary palate, SP: Secondary palate, T: Tongue. Images from: https://syllabus.med.unc.edu

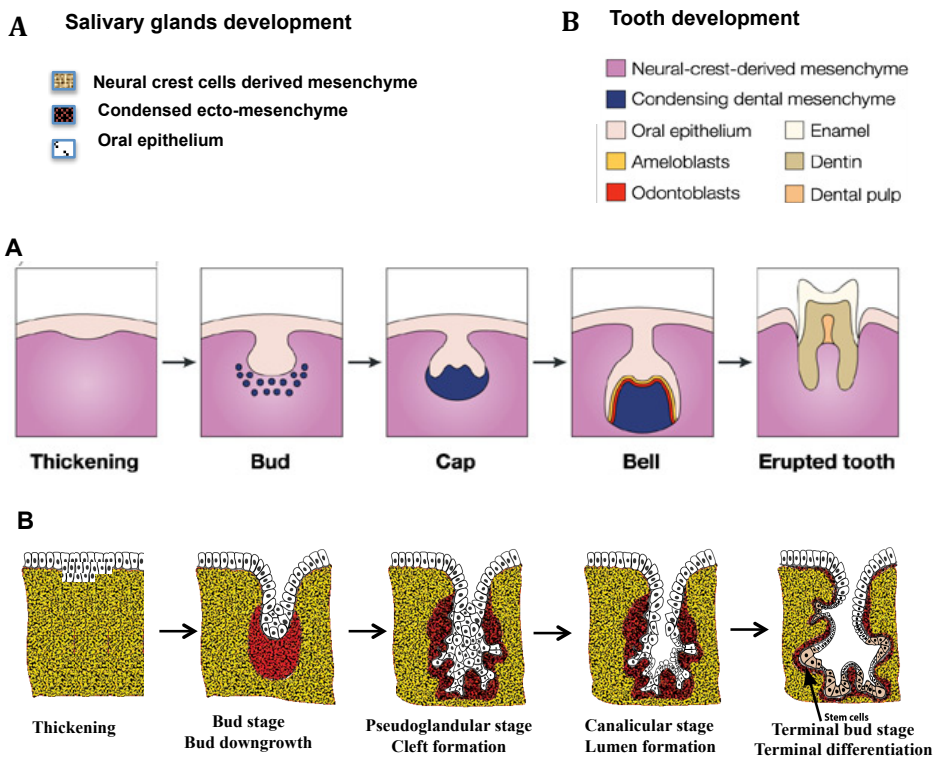


**Figure 1.2: A schematic diagram of tooth and salivary gland development in the mouse embryo** Both tooth germ and salivary gland are formed from the oral epithelium and neural-crest-derived mesenchyme, started as a thickening of the oral epithelia followed by bud formation and mesenchymal condensation. Tooth development images by Tucker A, Sharpe P. The cutting-edge of mammalian development; how the embryo makes teeth. Nat Rev Genet. 2004 Jul;5(7):499-508. Salivary gland development images by Dr. Susanne Jeffrey. Adapted with modification

# 2 Chapter 2: Materials and methods

## 2.1 Generating the *Irf6* knockout

The Cox lab has established a breeding line in which both copies of *Irf6* are conditionally ablated in oral epithelia. This line was generated by crossing floxed *Irf6* mice, harboring loxP sites flanking exons 3 and 4, which encode the DNA binding domain, with a transgenic Cre line in which Cre is driven by the paired-like homeodomain2 (*Pitx2*) promoter. In this *Pitx2*-Cre conditional disruption of *Irf6*, deletion occurs specifically in the oral epithelium, dental lamina, and ameloblasts, and consequently produces viable offspring (Li et al., 2014; Liu et al., 2003). However, homozygotes for the epithelial-specific knockout, and to a much lesser degree heterozygotes, show an array of tooth anomalies (resembling those described in patients with CLP), and increased enamel wear and thus they provide an ideal translational system with which to investigate caries susceptibility in this condition.

To investigate whether a sub-threshold genetic susceptibility (mimicking carriers in human populations) also leads to increased caries susceptibility, the lab also produced ubiquitously heterozygous *Irf6* mice using the adenovirus *EIIa* promoter *(EIIa)-Cre* driver line, in which the adenovirus EIIa promoter directs expression of Cre recombinase in preimplantation mouse embryos, and thus expresses the Cre recombinase in all tissues. Hereafter, mice of the *Irf6* $^{fl/fl}$

genotype are denoted as wild type mice (*Irf6* WT). *Irf6*$^{fl/fl}$; Pitx2-Cre mice are denoted as epithelial-specific homozygous *Irf6* knockouts (Null, *Irf6 Null-E*). *Irf6*$^{fl/+}$; *Pitx2*-Cre mice are denoted as epithelial-specific heterozygous *Irf6* knockouts (*Irf6 Het-E*). Mice of the *Irf6*$^{fl/+}$*; EIIa*-Cre genotype are denoted as "ubiquitous" heterozygous *Irf6* knockouts mice (*Irf6 Het-U*). These genotypes were each confirmed by a PCR-based genotyping assay: 0.5 cm tail snips were collected and digested using 50mM NaOH, at 95 °C for 30 min. PCR reactions were performed for 35 cycles of 95°C for 30 seconds, 60°C for 1 minute, and 72°C for 1 minute using the KAPA2G Fast Genotyping Mix and the relevant primer sets (table1). All products were resolved on 1% agarose/TAE gels, at 200V for 10 mins. All mice were housed at Seattle Children's Research Institute and all experimentation approved by the Institutional Animal Care and Use Committee.

## 2.2 3D Morphometric Analysis of the teeth "Micro-CT"

A 3D technique, based on micro-computed tomography, was designed to detect and quantify differences in mineral density, tooth morphology and tooth volume between animals carrying different numbers of *Irf6* knockout alleles (0, 1 or 2), and Pitx2 Cre control mice, in order to get a better understanding of dental phenotype genotype associations. The heads of mice collected at P28 were scanned at 55 kV, 180 μA, at an isotropic resolution of 9 μm using a Skyscan 1076 micro CT scanner (Bruker, Kontich, Belgium). A camera exposure time of 1480 ms, a rotation step of 0.5°, frame averaging of 3 and medium filtering (1mm aluminum) were applied during data acquisition. Images were then reconstructed using NRecon 1.11.4.2 (Bruker). Reorientation of the head sagittal images was done in DataViewer (Bruker). Segmentation of incisor, first and

second molar teeth was undertaken using the built in region of interest CTAnalyser function (Bruker). Binarisation and morphometric analysis of the segmented teeth images were performed using CTAnalyser functions following thresholding (15 to 225) to permit identification of the whole tooth volume with low noise. Intensity ranges of 40 to 99 (for dentin) and 100 to 225 (for enamel) were used for binarization. Filtering operations were performed on each tooth to reduce the noise. Unattached objects (structures that were difficult to remove during segmentation) were removed using a "Despeckle" operation (sweep). A "Remove pores" operation was also performed to remove the root canals and exclude them from the dentin volume (Figure 2.1). The following morphometric parameters were calculated in CTAnalyser: Total tooth volume (TV, mm3), enamel volume (EV, mm3), dentin volume (DV, mm3), enamel volume fraction (EV/TV, %), and dentin volume fraction (DV/TV, %). The density of different tooth tissues was measured by grayscale analysis and expressed as enamel mineral density (index), and dentin mineral density (index). 3D renderings of reconstructed data were generated using Drishti v2.4 (Limaye, 2012) or CTVox (Bruker).

## 2.3 Histology

Heads and salivary glands from mice euthanized at postnatal (P) days 3, 60, and 70 were fixed in 4% paraformaldehyde, demineralized in 14% EDTA solution (pH 7.5), dehydrated with a sequential concentration of alcohol and xylene, and finally embedded in paraffin. Sections were cut to 7μm thickness. Multiple sections from each sample were stained with standard hematoxylin and eosin staining (tooth, and salivary gland), and alcian blue/PAS double staining (salivary gland). For alcian blue/PAS double staining, sections were first stained with alcian blue for 30 minutes, and then with periodic acid 5 minutes and Schiff's reagent for 10 minutes. All

images were captured using a light microscope (DM 4000B, Leica).

## 2.4 Immunohistochemistry

Sections to be used for immunohistochemistry were deparaffinized, rehydrated and treated with 10 mM citrate buffer (pH 6.0) for antigen retrieval. Sections were then treated with 3% hydrogen peroxide to block the endogenous peroxidase activity. Subsequently, sections were incubated with either 3% goat serum or 3% rabbit serum (Vector Laboratories) for I hour at room temperature, followed by overnight incubation at 4°C with a primary antibody (diluted 1:200) against one of the following proteins: Irf6 (LS-B3231, Lifespan Biosciences), PCNA (sc-9857, Santa Cruz Biotechnology), P63 (sc-8431, Santa Cruz Biotechnology), E cadherin (610181, BD Biosciences), or AQP5 (sc-9890, Santa Cruz Biotechnology). After washes, the slides were incubated with either peroxidase conjugate anti-rabbit secondary antibody (A0545, Sigma) or biotinylated anti-goat secondary (PK-6105, Vector Laboratories) at a concentration of 1:300. Immunodetection was performed by Vectastain Elite ABC Kit, and substrate development by DAB substrate (SK-4100, Vector Laboratories).

## 2.5 Caries Induction Protocol

The main steps of the caries induction experiment are summarized in Figure 2.2

### *2.5.1 Bacterial strain and culture condition*

A 16% glycerol stock of *Streptococcus mutans* UA159 was kept at -80°C throughout the experiment. Strains were maintained at 37˚C in 5% $CO_2$ on blood agar plates (221239, Becton

Dickinson) for 24 – 48 hours. For subculture, individual colonies were inoculated into 5 mL brain-heart infusion broth media (237500, BD Bacto) supplemented with 0.5% glucose and pre-reduced overnight in anaerobic conditions (37˚C in 5% $CO_2$). After 18 hours growth, the concentration (Colony Forming Unit per milliliter (CFU/ml)) was estimated by measuring the optical density at a wavelength of 600 nm (OD600) using a Nano Drop spectrophotometer (ND-1000 UV-Vis Spectrophotometer, NanoDrop Technologies), assuming an OD600 of 1 approximately equals $8x10^8$ cells per ml. For mouse inoculation, the volume was adjusted based on the concentration so that the absolute number of *S. mutans* was the same, at $10^8$ CFU/ml, for all infections. The bacteria were then recollected by centrifugation and resuspended in 10 µl of medium density carboxymethylcellulose (C4888, Sigma-Aldrich).

### *2.5.2 Mouse infections*

This experiment was performed using the oropharyngeal swabbing method (Culp et al., 2011; Paper et al., 2005). Briefly, all mice were infected with the same volume of *S. mutans* by oral swabbing on three consecutive days starting at 17 days of age for the pilot study, and 15 days of age for the caries experiment. Prior to swabbing with the inoculum (2 days before), all animals were swabbed to test for indigenous *S. mutans* in their oral flora. Only mice that tested negative were included in the study. Mice were screened for infection 5 days and 8 weeks after the initial inoculation by streaking oral swabs on mitis salivarius agar (MSA) (BD 229810, Fisher Scientific) containing 1% Potassium tellurite (Aldrich P0677, Sigma-Aldrich), and 1% streptomycin (S6501, Sigma-Aldrich).

### *2.5.3 Cariogenic diet*

Mice were fed 56% sucrose powdered diet (LabDiet® 5BCB Cariogenic Purified Rodent Diet) and 5% sucrose water *ad libitum* starting from the first day of inoculation. All animals were followed for eight weeks from the initial inoculation, weighed weekly and physically observed. At the terminal procedure, saliva was collected. Mice were then immediately euthanized with an overdose of $CO_2$ and subjected to imaging by dissecting microscope and micro-CT for caries scoring.

### *2.5.4 Blood glucose levels*

To determine whether the mice that were fed high-sucrose diet developed diabetes, blood from two animals of each genotype chosen randomly was collected during the last week of the experiment, from the tail vein using a capillary tube collecting method, and blood glucose level was measured using a digital glucometer (ACCU-CHEK Aviva meter).

## 2.6 Caries scoring

Each molar tooth was evaluated utilizing two different scoring systems, after which total caries scoring for each tooth and mean caries scoring for each animal were calculated.

### *2.6.1 Caries severity scoring*

The heads of mice collected at P70 were scanned using a Skyscan 1076 micro CT scanner (Skyscan, Kontich, Belgium) under scanning settings similar to those mentioned above, except

that no filtering was applied during data acquisition. Images were then reconstructed using NRecon 1.11.4.2 (Bruker). The severity of the carious lesions was evaluated using DataViewer, according to Keyes' scoring system with modification as shown in figure 2.3.A (Keyes, 1958). A score of 1 was given for a radiolucent area within the enamel up to the dentino-enamel junction (DEJ) (Enamel only, E), 2 for a radiolucent area through the dentin to just below the DEJ (slight dentin, Ds), 3 for a radiolucent area through at least 1/3 the dentin thickness (moderate dentin, Dm), and 4 for a radiolucent area involving all the dentin and reaching to the pulp (extensive dentin, Dx).

### *2.6.2 Caries incidence per tooth surface scoring*

After scanning, the lower jaw was aseptically dissected from the skulls and sonicated in 5 ml of 0.9% sterile NaCI solution using ultrasonic dispersion for three pulses of 10 seconds with 30 second intervals, for biofilm detachment. After this the lower jaw and the rest of the skulls were manually defleshed over 24 h. All dental deposits were carefully removed from the teeth using a small soft toothbrush under a 10×stereo dissecting microscope (Leica; Carl Zeiss Microimaging, Inc, Thornwood, NY). A determination of the number of surfaces involved in carious teeth was evaluated under the dissecting microscope (Figure 2.3.B), and scored as follows; 0 for intact surface, 1 for decay affecting only the occlusal surface of the tooth, 2 for decay affecting only one smooth surface (mesiodistal, buccal or lingual surface), 3 for decay affecting both the occlusal surface and one of the smooth surfaces, 4 for decay affecting occlusal and two smooth surfaces, and 5 for decay affecting occlusal and more than two smooth surfaces.

## 2.7 Colony counting

To quantify bacteria, the lower jaw sonicated suspension from each animal was diluted one to 1000, and 100 µl was streaked on mitis salivarius agar containing 0.01 M Streptomycin (MSA-S) and blood agar plates to estimate the *S. mutans* population, and to determine the total cultivable oral flora respectively. The MSA-S plates were incubated for 48h at 37$^{o}$C, under anaerobic conditions using an anaerobic jar supplied with anaerobe sachets (GasPak™ EZ Anaerobe Container System Sachets, BD 260678, Becton Dickinson), and anaerobic indicator (GasPak Dry Disposable Anaerobic Indicator, BD 271041, Becton Dickinson). The blood agar plates were incubated for 24 h at 37 $^{o}$C under aerobic conditions. All colonies on MSA-S and blood agar plates were recorded for enumeration of oral *S.mutans* and total aerobic oral flora respectively, using the formula:

$$\frac{\text{Number of CFU}}{\text{Volume plated (ml) x total dilution used}} \rightarrow \text{Number of CFU/ml}$$

Only colonies with granular "frosted-glass" morphology, characteristic for *S.mutans* on MSA-S plates (Emilson 1983; Gold et al. 1973) were counted. A smear from the S. mutans isolates was Gramstained. A positive staining reaction and appearance of streptococci was considered indicative of *S. mutans*. The minimum significant level was set at 1000 CFU/ml.

## 2.8 Stimulated saliva collection method

Mice were anesthetized with an intraperitoneal (IP) injection of ketamine (110 mg/kg) and xylazine (10 mg/kg). Salivary secretion was stimulated using pilocarpine (10 mg/kg, IP). Each

mouse was positioned at 45 degrees on its side; saliva was collected for 5 min using a capillary tube that was placed through the side of the cheek and ended in a pre-weighed 1.5 ml centrifuge tube from the other side (Figure 4.) All samples were maintained at 4$^{o}$C for no longer than several hours, before freezing them at -80 $^{o}$ C.

## 2.9 Salivary gland function Tests

Before freezing the samples, salivary flow was measured as mg/min. Given that we combine both males and females of the same genotype together, the weighted salivary flow rate was calculated using the following formulla

$$\frac{\text{Saliva weight (mg)}}{\text{Total time (5 min) x body weight (g)}} \rightarrow \text{Flow rate (mg/min/g of body weight)}$$

Salivary pH was measured with a digital pH meter (pHBOY-P2, SU-19A, Shindengen Electric). The digital meter was initially calibrated using buffered solutions with pH 4.0 and pH 7.0. After that 10 µl of saliva was added to the surface of the meter where it remained for 1 minute, thus yielding automatic pH reading.

Buffering capacity was measured using Ericson's method (Ericson et al., 1989) with

modification. Briefly, 15 µl of hydrochloric acid (HCL) 0.005 M/L was mixed with 5 µl of the collected stimulated saliva. After 20 minutes the pH of the solution was measured using the calibrated digital meter. A buffering capacity of > 6.5 was considered high, > 5.75- 6 was

considered normal, < 5.74 was considered low, and < 4.5 was considered very low.

## 2.10 Statistical Analysis

All statistical analyses, including initial descriptive statistics, were processed using IBM SPSS Statistics for Windows (Version 21.0. Armonk, NY: IBM Corp) statistical software. The tooth 3D morphometric analyses were analyzed using one-way ANOVA with Tukey's post hoc test (after Bonferroni corrections). Differences among the four experimental groups in relation to salivary gland weight, salivary functions, caries score, and bacterial count were statistically analyzed using Kruskal-Wallis with Dunn's nonparametric multiple comparison tests (after Bonferroni corrections). The critical level of significance was set at 0.05 for ANOVA and Kruskal-Wallis, and at 0.01 for Tukey's and Dunn's multiple comparison tests. Box plots display median, $25^{th}$ and $75^{th}$ percentiles and whiskers show the minimum and maximum values. All quantified results are presented as the mean ± standard deviation unless stated otherwise. Graphs were created using SPSS ver. 21.0

## 2.11 Figures and tables

**Table 1: Sequence of primers used for genotyping in this study**

| Primer | Allele Targeted | Sequence (5' to 3') |
|---|---|---|
| MHOX | Pitx2-Cre | GCCACTCCCACTGTCCTTTC |
| PITX2-FLEXB | Pitx2-Cre | TTCTGGAGGGTTTTCTTGTTCTAGG |
| 3318 | Irf6-floxed | TGGCAAAATCTATTTCGAGTGG |
| 3319 | Irf6-floxed | CACACTGACCTCAATGCCTCCAA |
| 4380 | Irf6-floxed | GCAGAGTGGAGCACACTTCA |
| WNT1-RVS | EIIa-Cre | ATTCTCCCACCGTCAGTACG |
| WNT1-FWD | EIIa-Cre | CGTTTTCTGAGCATACCTGGA |

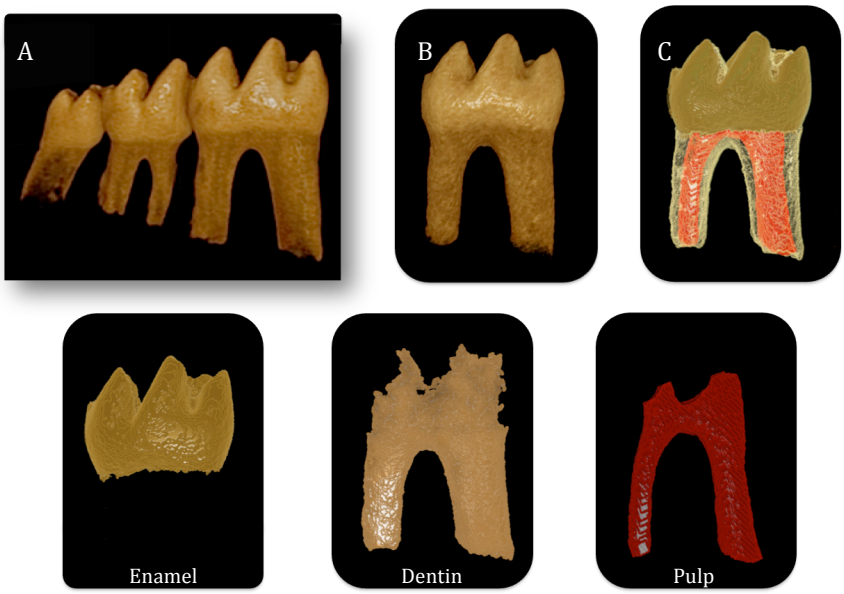


**Figure 2.1: Illustration of 1st molar segmentation.** 3D rendering of microCT images, segmentation and color maps of first mandibular molars in WT mice at 28 days of age.

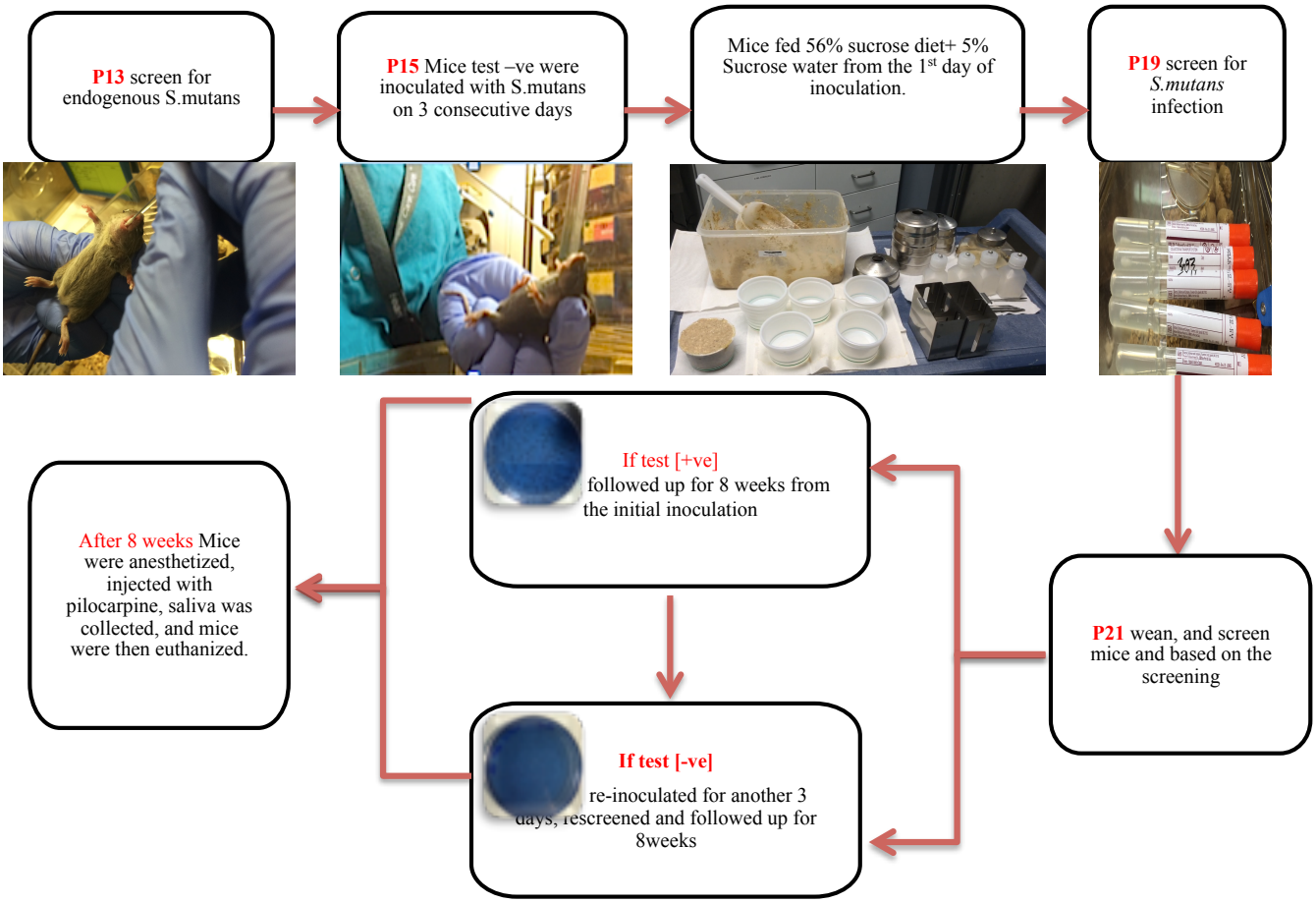


**Figure 2.2: Illustration of the caries induction protocol.**

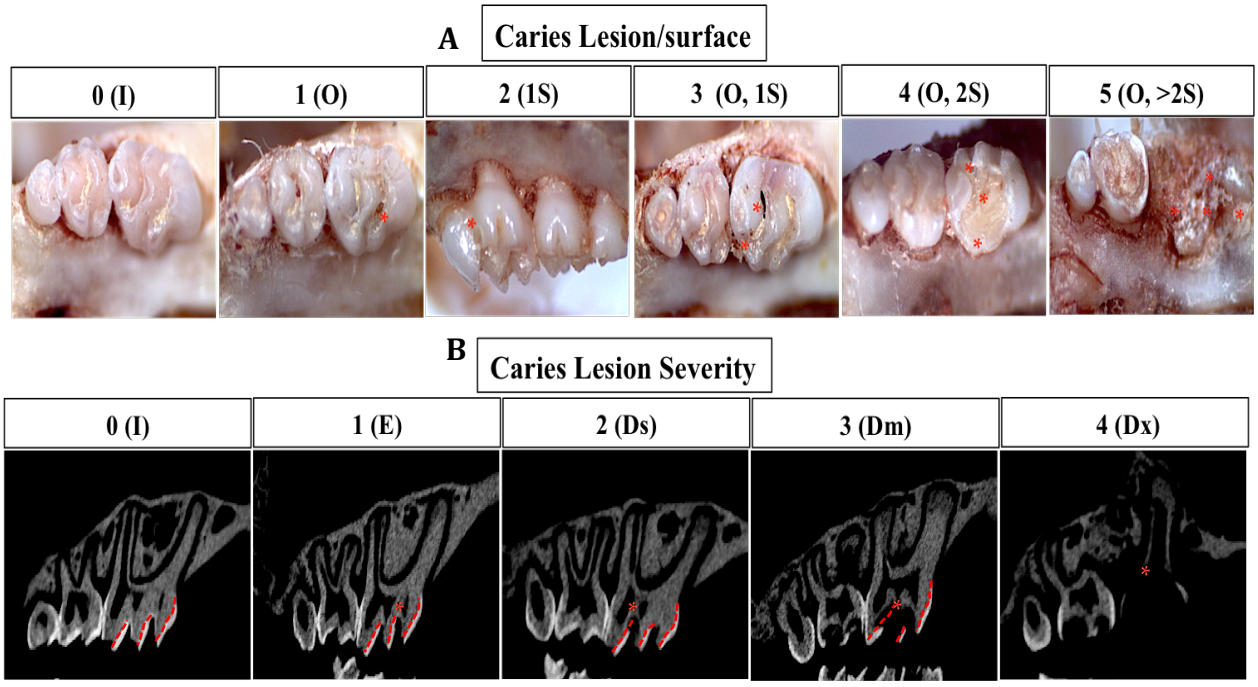


**Figure 2.3: Caries lesion scoring.** A) Determination of the number of surfaces involved in carious teeth were evaluated under dissecting microscope and scored as 0 (Intact surface, I), 1 (occlusal surface only, **O**), 2 (one smooth surface only, **1S**), 3 (occlusal and one smooth surfaces, **O+1S**), 4 (occlusal and more than one smooth surface, **2S**) 5 (occlusal and more than two smooth surfaces, **O+ >2S**). B) Severity of carious lesions were evaluated following microCT imaging whereas score of 1 was given for enamel involvement only (**E**), 2 was for slight dentin involvement (**Ds**), 3 was for moderate dentin involvement **(Dm)**, and 4 was for extensive dentin involvement **(Dx)**. Asterisks indicate caries, and red dotted line indicate dentino-enamel junction.

# 3 Chapter3: Irf6 ablation results in enamel mineralization and crown morphology defects.

## 3.1 Introduction

Individuals with isolated or non-syndromic cleft lip with or without cleft palate (CLP) exhibit various dental defects, including high rates of tooth agenesis (missing teeth), supernumerary teeth, small or fused teeth, enamel hypoplasia, and taurodontism. They have been also found in some studies to exhibit a higher frequency of caries (Al Jamal et al., 2010; Hasslöf et al., 2007; Pegelow et al., 2012). The frequent coexistence of these craniofacial abnormalities is suggestive of a common underlying genetic etiology. Likewise, many CLP syndromes, for example autosomal dominant VWS which has been linked to pathogenic mutations in the *IRF6* gene, also present with an array of tooth abnormalities such as hypodontia and taurodontism in addition to the oral clefting. Moreover, specific common *IRF6* haplotypes have been found to be associated with isolated CLP where an association with dental abnormalities is also evident (Nawa et al., 2008; Pardo V et al., 2006; Salahshourifar et al., 2012).

In support of a possible common underlying etiology, expression of Irf6 has been reported in dental and oral epithelium during embryonic stages of both incisor and molar development. At the late bell stage, Irf6 is highly expressed in the proliferative cell population at the cervical loop and in the ameloblasts of the developing tooth (Blackburn et al., 2012; Laugel-Haushalter et al.,

2012). However, *Irf6* null mutant strains die before completion of tooth development due to ectopic intraoral adhesion and failure to form the appropriate skin barrier (Ingraham et al., 2006). Therefore, to facilitate our understanding of the molecular and genetic mechanisms underlying these defects, the Cox lab has developed a novel conditional knockout model of *Irf6* deficiency: Mice heterozygous for the *Pitx2-Cre* allele and homozygous for the floxed *Irf6* allele (conditional null; *Irf6 Null-E*). PITX2, a transcription factor belonging to the bicoid-related homeobox family, is a key regulator of tooth development. The *Pitx2-Cre* line used to generate these *Irf6* null mice is tissue specific; it expresses Cre in the developing oral and tooth epithelia, therefore the null mice lacks the expression of *Irf6* in these tissues only. The *Pitx2-Cre* mice used in our study are a knock-in Cre allele, wherein the homeodomain is replaced with Cre-neomycin cassette. Consequently, these Cre mice are also heterozygous for a *Pitx2* null allele (Liu et al., 2003). In humans, heterozygous mutations in *PITX2* have been linked to Rieger syndrome, which features a wide spectrum of developmental defects including craniofacial abnormalities and various dental defects (Idrees et al., 2006; Li et al., 2014). Although Pitx2-Cre heterozygous mice have not been reported as showing obvious craniofacial defects or dysmorphology, in all experiments, I also include the *Pitx2 Cre* mice as a separate control group. These mice also provide an opportunity to investigate the contribution of this gene to the dental phenotypes observed in the *Irf6* mutant mice.

The *EIIa Cre* transgene is expressed ubiquitously as early as the zygotic stage and therefore can be used to delete the *Irf6* floxed allele in all tissue (i.e., ubiquitous or general conditional knockout). As homozygous null *Irf6* mice are known to die prenatally, I use mice doubly

heterozygous for *EIIa-Cre* transgene and the floxed *Irf6* allele (*Irf6 Het-U*). In some ways these may more likely recapitulate the situation in patients (i.e., reduced but not completely absent IRF6 expression).

## 3.2 Results

### *3.2.1 Expression of Irf6 during normal tooth development*

To delineate the role of *Irf6* in postnatal tooth development, the expression pattern of Irf6 in the molar tooth of wild-type (WT) mice was examined (figure 3.1). As *Irf6* has previously been implicated in regulating cell proliferation and differentiation, the relationship between cell proliferation and Irf6 expression during postnatal stages of tooth development was investigated. The Irf6 protein and proliferating cell nuclear antigen (PCNA), a protein associated with DNA replication, were immunostained using 5-μm consecutive paraffin embedded sagittal sections of the molar teeth from 3-day-old mice. The Irf6 protein was detected mainly in the dental epithelium during the amelogenesis stage, specifically, in cells of the epithelial enamel organ including the stratum intermedium and cervical loop as well as the inner and outer dental epithelium. Strong expression of the Irf6 protein in the highly proliferating cells of the cervical loop area and the presecretory ameloblasts primarily colocalized in the nucleus with proliferating cell nuclear antigen (PCNA), consistent with the previously described role for the *Irf6* in

regulating cell proliferation in keratinocytes and mammary epithelia (Ingraham et al., 2006; Richardson et al., 2006). However, at the cusp tip, the expression of Irf6, but not PCNA, was primarily localized in the cytosol and only weakly in the nuclei of the differentiating ameloblast

and stratum intermedium cells. This suggests that the localization of Irf6 may be actively regulated depending on the proliferative state of the cell or the local signals it receives.

### *3.2.2 Loss of Irf6 causes cusp, root patterning, and mineralization defects*

*Irf6* was conditionally knocked out in the oral ectoderm using the *Pitx2-Cre* driver line crossed to the *Irf6* floxed mouse, generating the *Irf6 Het-E* and *Irf6 Null-E* mice. A ubiquitously expressed Cre driver line, the *EIIa-Cre* mouse, was also used to generate *Irf6 Het-U* animals, which have a 50% reduction in *Irf6* expression in all tissues of the body. All generated mice were viable and the body weights of *Irf6* null mutants were not different from those of wild type or heterozygous animals at all ages.

To determine whether *Irf6* null mice and their heterozygous littermates develop an abnormal dental phenotype, gross tooth morphology and microCT scans of heads from the *Irf6* null mice and age-matched control mice (WT, *Irf6-Het-U* and *Irf6-Het-E*) at 2 and 4 weeks of age were examined. At P14 in wild type mice, incisors are fully erupted, upper and lower first molars are partially erupted, while the rest of the molar teeth are not yet erupted but visible on microCT imaging in the alveolar bone. At P28 in wild type animals, all incisor and molar teeth were

erupted. Although eruption timing was essentially the same in null animals, as early as 2 weeks postnatal, the tooth shape, size, and color were distinguishable from wild type mice, with the incisors of *Irf6* conditional null mice showing an abnormally roughened/pitted, hypoplastic labial

surface compared to those of controls (figure 3.2). At 4 weeks, the occlusal two-thirds of the maxillary incisors from *Irf6* null, and to lesser degree the *Irf6 Het-E* and *Pitx2 Cre*

mice, appeared greyish-white in color compared to the normal brownish-yellow color observed in WT mice. In contrast, the teeth of *Irf6 Het-U* mice were similar in appearance to those of WT mice. The findings on the epithelial-specific alleles suggest a different degree of mineralization defect based on gene dosage of both *Pitx2* and *Irf6.* (i.e. the reduction (or heterozygosity) of *Pitx2* likely sensitizes the teeth to the effects of loss of *Irf6* since the ubiquitous heterozygotes did not show obvious mineralization issues). However, the sometimes mosaic activity of Cre in the latter (which I have noted by PCR-based genotyping of the Cre-mediated excision event) may also contribute to the lack of overt phenotype in these animals.

Three-dimensional rendered images from micro CT scans showed that all three molars of *Irf6 Null-E* mice exhibited reduced size and altered crown morphology with rounded cusp tips. The most distal cusp was absent from first and second lower molars of *Irf6 Null-E* mice. In addition, the buccal and lingual cusps were fused partially or completely together leaving a deep grove, and sometimes a fossa, in the center of the crown (figure 3.3) in the null animals. Besides altered crown morphology, the *Irf6 Null-E* molars, and to lesser degree the *Irf6 Het-E* and *Pitx2-Cre* mice showed taurodontic root morphologies, characterized by an enlarged pulp chamber with apical displacement or absent furcation, leading to short root formation. This was observed in the first and/or second molars, both in the upper and/or lower jaw (figure 3.3, and 3.4). However, the first and second molar root anomalies were more severe in the null mice suggesting that loss of *Irf6* exacerbates the root phenotype, or that heterozygosity of *Pitx2* sensitizes the animals as also suggested by the incisor enamel presentation noted earlier. Interestingly, of the ten Irf6 null mice examined in our study, two mice exhibited an extra tooth – one involving the incisor and

the other a molar (Figure 3.5 A and B), and two other mice exhibited a missing 3rd molar tooth (Figure 3.5 C).

### *3.2.3 Loss of Irf6 causes reduced tooth volume and a delay in mineralization*

In order to better understand dental phenotype-genotype associations, a 3D technique, based on micro-computed tomography, was employed to segment different tooth structures digitally (i.e., enamel, dentin, and pulp) using a thresholding-based methodology. Such segmentation enables the independent measurement of differences in volume and mineral density of different tooth structures between animals carrying different numbers of *Irf6* knockout alleles. The heads of mice collected at P28 were imaged using a Skyscan 1076 microCT scanner and the data reconstructed and segmented for 3D analysis of incisors and molar teeth as described in the methods (section 2.2). Differences were considered statistically significant for comparisons of datasets yielding $P<0.05$. Follow-up pairwise comparisons of the groups using Tukey Bonferroni correction of significance levels were additionally carried out (Table 3.1).

Differences in the percentages of enamel volume and dentin volume between each genotype were not statistically different. However, *Irf6 null* teeth showed a significant reduction in total tooth volume compared to all other genotypes – notably of the upper and lower first molars and the upper incisors. This finding is consistent with the gross observations.

Interestingly, the *Irf6* null animals, the *Irf6 Het-E* heterozygous mice, and the *Pitx2-Cre* mice all

showed a significant reduction in enamel but not dentin density when compared to WT animals. However there was no significant difference between each of these genotypes after Bonferroni correction, suggesting that the reduction in mineral density is a trait associated with heterozygosity for *Pitx2*. Taken together, these data suggest that complete loss of *Irf6* in oral epithelia is specifically associated with reduced tooth volume, blunted cusp morphology, and a delay in mineralization, including abnormal mineral composition. Moreover, given that the severity of taurodontism is commonly increased by the apical displacement of bifurcation or trifurcation of the root. The taurodontism phenotype was more severe in the *Irf6 Null-E* mice with a complete loss of the bifurcation/trifurcation (peg root) from first and/or second molars. Thus *Irf6* loss also has potentially increased severity of taurodontism.

## 3.3 Discussion

The finding that the teeth of *Irf6* null mice display anomalies in tooth size, number, cusp, root patterning and morphology, and enamel matrix mineralization, similar to tooth abnormalities observed in the cleft lip and palate population, supports the notion of a common etiology. Furthermore, it reveals a more significant role for *Irf6* in regulating tooth morphogenesis than previously appreciated. The specific expression of Irf6 in the enamel knot area during embryonic stages of murine tooth development (Blackburn et al., 2012) and in ameloblasts during postnatal stages (see figure 3.1) could explain the aberrant cusp and mineralization defects, respectively, that were observed when *Irf6* was ablated. At postnatal stages of tooth development, strong expression of Irf6 was also observed in stratum intermedium (SI) cells. SI is a cell layer between the inner dental epithelium and the stellate reticulum, which exhibits high Ca-ATPase and

alkaline phosphatase activities, suggestive of a role in enamel mineralization and calcium transportation (Sasagawa et al., 2005; Sasaki et al., 1986). Strong expression in the cells of the cervical loop area, where it co-localizes with PCNA in the nucleus, strongly suggests that *Irf6* is involved in the regulation of tooth root formation.

The enamel knot is a non-proliferating transient epithelial structure of the enamel organ that functions as a signaling center responsible for cusp formation and patterning during early stages of tooth development (Rothová et al., 2012). Due to the low proliferation within the knot and high proliferation outside, the epithelium of the tooth germ folds forming a cap-shaped structure, which ultimately determines the pattern of the cusp. As the primary enamel knot is removed by apoptosis, teeth with more than one cusp will start to develop a secondary enamel knot, which will dictate the future cusp pattern and determine the correct cusp position and size (Rothová et al., 2012; Thesleff, 2006). The enamel knot expresses several components of different signal pathways of transforming growth factor β (TGFβ), fibroblast growth factor (FGF), sonic hedgehog (SHH), and Wingless (WNT) signaling pathways (Liu et al., 2008; Luukko et al., 2014; Thesleff, 2006; Thesleff et al., 1996; Tucker et al., 1999). Knocking out many of these genes at the time of transition from bud to cap stage leads to an arrest of tooth development at bud stage in genetically modified mice, and their mutations cause tooth agenesis in humans (Bei, 2009; Dassule et al., 2000; Fleischmannova et al., 2008). In contrast, interference with any of these genes at the bell stage leads to defects in cusp patterning and morphology similar to the phenotype observed in the *Irf6* conditional null mice. Interestingly, *Irf6* homozygote null mutant mice exhibited defective invagination of incisor epithelium as well as a reduction and

displacement of enamel knot marker genes (*Shh, and Wnt*) from the normal location within the center of the invaginated incisor epithelium to the most outer part of the abnormally evaginated incisor epithelium (Blackburn et al., 2012), suggesting a prominent role for *Irf6* in regulating the invagination of the incisor epithelial preceding cusp formation.

Members of the Wnt signaling family play numerous roles throughout tissue morphogenesis including in the developing lip and palate. Individual Wnt ligands have been reported to induce various cellular responses from cell proliferation, and polarity to terminal differentiation depending on the cellular context. Parallel to the previous report of downregulation of Wnt expression upon ablation of *Irf6* (Blackburn et al., 2012), data from Cox lab showed transiently decreased Wnt10b mRNA expression in *Irf6 Null-E* P4 molars. A regulatory feedback loop between *Wnt, P63*, and *Irf6* has been reported in facial epithelia, supported by the reduction of *Irf6* and *P63* expression in *Wnt9b* null mice. Mutations in *P63* or *Irf6* disrupt this regulatory loop, leading to an altered balance between cell proliferation and differentiation that may ultimately lead to the morphogenetic defects.

Interestingly, both mouse and human mutations in the *Wnt10a* and *Wnt* signaling pathway, for example *Eda* and its components (i.e., *Eda, Edar or Edaradd*), lead to small teeth with reduced cusp number, hypodontia and taurodont teeth (Ahn et al., 2010; Blackburn et al., 2015; Laurikkala et al., 2001; Pispa et al., 1999; van den Boogaard et al., 2012; Yang et al., 2014), similar to the tooth phenotypes of *Irf6 Null-E* mice. On the other hand, overexpression of Eda in

oral epithelia, increasing Fgf signaling (via knockout of the Fgf pathway inhibitors, Spry2 and Spry4), or knockout of *Sostdc1*, a negative regulator for Bmp and Wnt signaling, produced an extra molar (Kangas et al., 2004; Kassai et al., 2005; Klein et al., 2006). The fact that the *Irf6 Null-E* mice exhibited both hypodontia and supernumerary teeth suggests possible positive and negative, or stage-specific, roles for Irf6 although this requires further investigation. Notably, a similar extra premolar-like tooth was also seen in animals doubly heterozygous for *Pitx2* and *Tbx1* (Cao et al, 2010), supporting the notion of a genetic interaction between *Irf6* and *Pitx2* or *Pitx2* as a sensitizer to these phenotypes.

Enamel development can be divided into four stages based on the morphology and function of ameloblasts: presecretory, secretory, transition, and maturation stages. During the secretory stage, the enamel crystallites form and the tall columnar ameloblasts secrete large volumes of enamel matrix proteins (amelogenin (AMELX), ameloblastin (AMEL), and enamelin (ENAM)). Simultaneously, ameloblasts start to retreat from the dentino-enamel junction (DEJ) to allow elongation of crystal ribbons to establish the thickness of the enamel. Once the enamel reaches its full thickness, the secretory-stage ameloblasts retract their cytoplasmic processes and shorten into transition-stage ameloblasts, and then into short cuboidal maturation-stage ameloblasts. During the maturation stage, the enamel matrix proteins are further degraded by enamel proteases, mainly by kallikrein-related peptidase 4 (KLK4) and matrix metalloproteinase 20 (MMP20), and are removed to provide space for ion deposition onto the sides of enamel crystallites to give the enamel its hardness (Bartlett et al., 2013; Catón et al., 2009; Simmer et al., 1995, 2010).

Defects in enamel formation are collectively referred to as Amelogenesis Imperfecta *(AI)*. The presentation encompassed by AI can range from hypoplastic to hypocalcified forms based on the thickness, hardness, and smoothness of the affected enamel (Hu et al., 2007). The *Irf6 Null E* mice, and to a lesser degree *Irf6 Het-E* and *Pitx2 Cre* mice, exhibited both hypoplastic incisors characterized by localized pitted enamel and hypo mineralized enamel characterized by significant reduction in enamel density. Previous data from the Cox lab showed that *Irf6-cKO* P14 and P28 samples presented with notably higher levels of AMEL in secretory and mature ameloblasts compared to *Irf6 Het-E* and WT controls; this was accompanied by a decrease in KLK4 expression in P14 samples (Chu, 2015). Mutations in the *AMEL* gene lead to hypoplastic teeth, while mutations in *KLK4* gene cause hypo-maturation forms characterized by normal enamel thickness but low mineral content (Hu et al., 2007). For proper mineral deposition, enamel matrix proteins including AMEL have to be removed for the enamel crystallites to grow in width and thickness. Failure to do so will result in smaller enamel crystallites and increased spacing between crystallites (Bartlett, 2013). Therefore, the increased AMEL could be the cause of the hypomineralized phenotype in the *Irf6-Null-E* mice.

Parallel to the abnormal tooth size and cusp patterning, the molars of *Irf6* null mice, and to lesser degree the mice doubly heterozygous for both the floxed allele and *Pitx2* allele, and the *Pitx2-Cre* mice, exhibit taurodontic root morphologies, which have been previously reported in VWS (*IRF6* mutation) and ARS (*PITX2* mutation) patients (Dressler et al., 2010; Küchler et al., 2011;

Nawa et al., 2008). During tooth root development, epithelial cells of the inner and outer enamel epithelium proliferate from the cervical loop to form two layers of epithelium called Hertwigs root sheath (HERS). Initially, the first formed part of the root sheath folds horizontally to form a disc like structure called the epithelial diaphragm, which encloses the primary apical foramen. As the root sheath grows in length, the cells of the lengthening root sheath induce the adjacent dental papilla cells to differentiate into odontoblasts, which then form the root dentine (Kumakami-Sakano et al., 2014). As the root lengthens the tooth continues to erupt. The epithelial diaphragm develops tongue-like extensions that grow until they contact each other to form the furcation area to separate the root into two or three roots (Bower 1983). Taurodont teeth develop as a consequence of failure or delay in the horizontal inward invagination of HERS leading to a low furcation point and an elongated root trunk (Kumakami-Sakano et al., 2014). *Irf6* has previously been demonstrated to play a critical role in regulating epithelial invagination (Blackburn et al., 2012). Here it is shown that Irf6 is highly expressed in the cells of the cervical loop area suggesting a potential role for *Irf6* in root development. Similar to *Irf6* null mice, several mouse models of important regulators of root development display taurodontism including conditional ablation of *Bmp2* (Rakian et al., 2013) and *Dlx3* in mouse dental mesenchyme (Duverger et al., 2012), *Wnt10a* null mice (Yang et al., 2014), and Tabby mice (*Edaa* mutation) (Pispa et al., 1999).

Interestingly, in our study the mice doubly heterozygous for the *Pitx2-Cre* and the *Irf6* floxed allele, as well as and the *Pitx2-Cre* mice, exhibited altered enamel mineralization as well as taurodontic roots. It has been shown that various dental defects, including microdontia,

hypodontia, enamel hypoplasia, and taurodontism are common findings in patients with Axenfeld-Rieger syndrome. The Pitx2 transcription factor has been shown to be important for amelogenesis by regulating Amelogenin production through binding to the 2.2 kb distal *Amel* promoter (Li et al., 2014). Loss of *Pitx2* function directly and indirectly perturbs activation of Amelogenin expression, leading to lower enamel deposition and ultimately hypoplastic enamel (Li et al., 2014). Pitx2 has also been reported as an activator of the *Dlx2* gene (Cox et al., 2002). The Distalless homeobox family (Dlx) plays a central role during tooth development. Various members of this family are expressed in ameloblasts during different stages of amelogenesis suggesting a main role in enamel formation (Lézot et al., 2008). A network of regulatory interactions among Dlx family members has been implied by the temporal pattern of *Dlx* gene expression (Beanan et al., 2000; Qiu et al., 1997). Mice carrying mutations in both *Dlx1* and *Dlx2* exhibit arrested maxillary molar development at the epithelial thickening stage (Thomas et al., 1997). *Dlx3* has also been shown to be important to proper ectodermal organ development and regulated by P63, which is part of the Irf6 regulatory pathway (Radoja et al., 2007). Mutations in human *DLX3* cause Tricho-Dento-Osseous (TDO) syndrome featuring both amelogenesis imperfecta and taurodontism. Furthermore, knockdown of *Dlx3* in a mouse ameloblast cell lineage resulted in down-regulation of several enamel matrix proteins including Amelx, Enam, and Klk4 (Zhang et al., 2015), whereas ablation of *Dlx3* in mouse dental mesenchyme *in vivo* resulted in taurodontic molars (Choi et al., 2010). Whether or not Pitx2 regulates Dlx family members other than *Dlx2*, these observations together with our findings in the heterozygous *Pitx2-Cre* mice are consistent with the notion that heterozygosity for the *Pitx2* allele increases the susceptibility to the enamel mineralization and root abnormalities observed in

the *Irf6* null mice.

Another mechanism by which *Pitx2* heterozygosity could sensitize our mice to loss of *Irf6* is through the Wnt pathway. In the canonical Wnt pathway, activation of Wnt signaling leads to association of the cytoplasmic scaffold protein Dishevelled (Dvl) and β-catenin, stabilizing the latter and allowing it to accumulate and translocate to the nucleus where it controls key developmental gene expression including *Pitx2* and *Lef1* (Amendt et al., 1999; Logan et al., 2004). Prior studies suggest a positive feedback loop between Pitx2 and the Wnt pathway. Pitx2 is potentially a direct Wnt/β-catenin target. Overexpression of Pitx2 inhibits phosphorylation of β-catenin, the central Wnt pathway molecule, ultimately leading to the activation of Wnt target genes to regulate proliferation (Kioussi et al., 2002; Li et al., 2014). A feedback loop between Irf6 and Wnt signaling has been also proposed to regulate morphological changes in the oral epithelium required during palatal fusion (Ferretti et al., 2011). Therefore, the disruption in the Wnt pathway could be intensified by heterozygosity of *Pitx2*. This could also explain why the *Irf6 Null-E*, *Irf6 Het-E*, and *Pitx2 Cre* mice exhibited significant reduction in enamel mineral density, and root taurodontism while ubiquitous heterozygotes did not show any issues.

## 3.4 Figures and tables

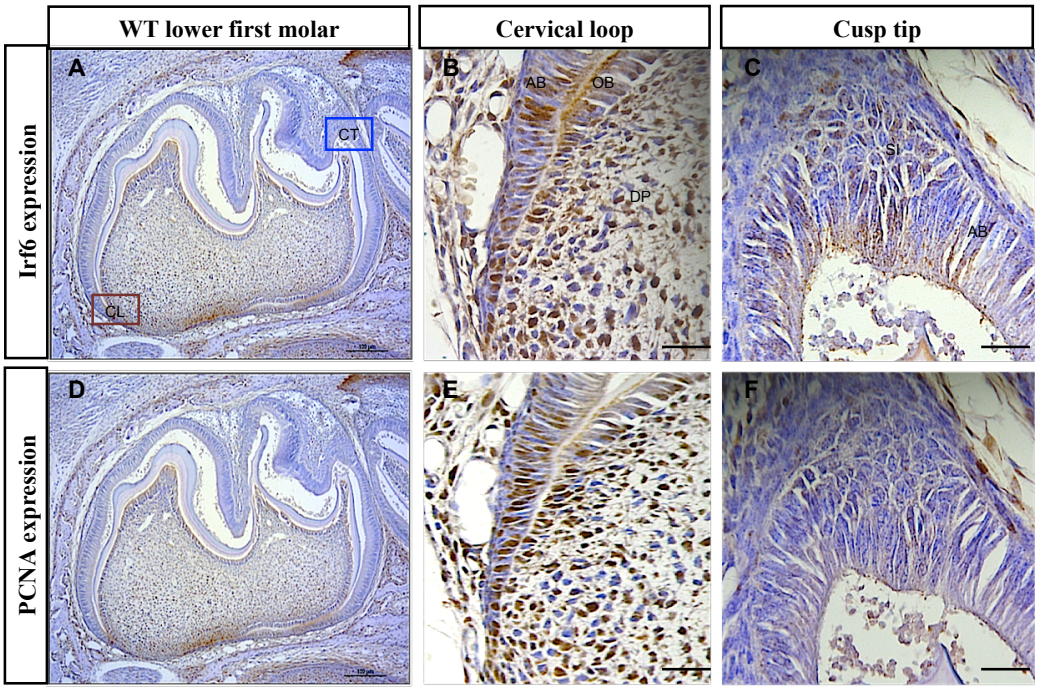


**Figure 3.1: Irf6 co-localization with PCNA in ameloblast at the cusp tip versus cervical loop area.** Immunohistochemical detection of Irf6 (A-C) and proliferating cell nuclear antigen (PCNA) (D- F) in the lower first molar of a wild type mouse at postnatal day 3 (P03). Strong nuclear Irf6 staining is seen in the highly proliferating area of the cervical loop and the pre-secretory ameloblasts (B), where it colocalized with PCNA (E), consistent with the previously described role for Irf6 in regulating cell proliferation. At the cusp tip (C, F), staining for Irf6 (C), but not PCNA (F), was evident. Of note, Irf6 staining was primarily cytosolic with only relatively light staining in nuclei of the differentiating ameloblasts and cells of the stratum intermedium. CT: Cusp tip, CL: Cervical loop, AB: ameloblast, OB: Odontoblast, DP: Dental papilla, SI: Stratum intermedium. Scale bars: 50 µm (B, C,E, and F); and 500 µm (A and D).

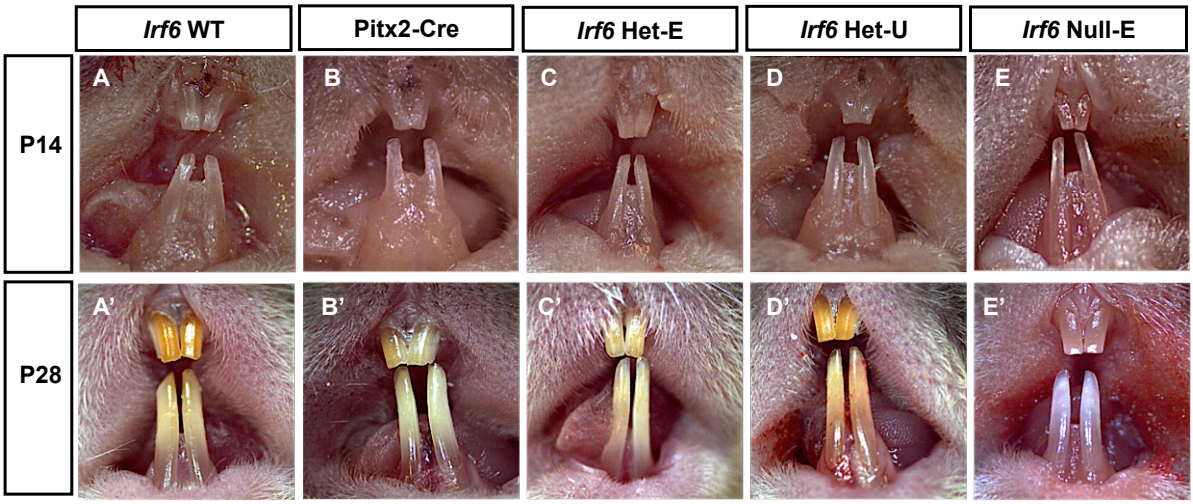


**Figure 3.2: Comparison of P14, and P28 *Irf6 null* incisors with matched controls.** Dissecting microscope images of *Irf6* null mice, those heterozygous for *Irf6* and either the ubiquitously expressed *EIIa-Cre* (*Irf6* Het-U) or oral epithelium-specific *Pitx2-Cre* (*Irf6* Het-E), *Pitx2-Cre* mice and background matched WT controls. (A-E) At 2 weeks of age (P14), the incisors of *Irf6* null mice showed abnormally roughened/pitted, hypoplastic labial surfaces, when compared to the normal surface of incisors of each of the other genotypes (*Pitx2-Cre*, WT and all heterozygotes). (A'-E') At 4 weeks the incisors of WT and *Irf6* Het-U animals showed the normal brownish-yellow color, a reflection of mineral deposition in rodent teeth. The yellowish brown color appeared less pronounced in both *Irf6* Het-E, and *Pitx2-Cre* incisors, while *Irf6* null incisors had greyish white color, indicating a mineralization defect in these animals.

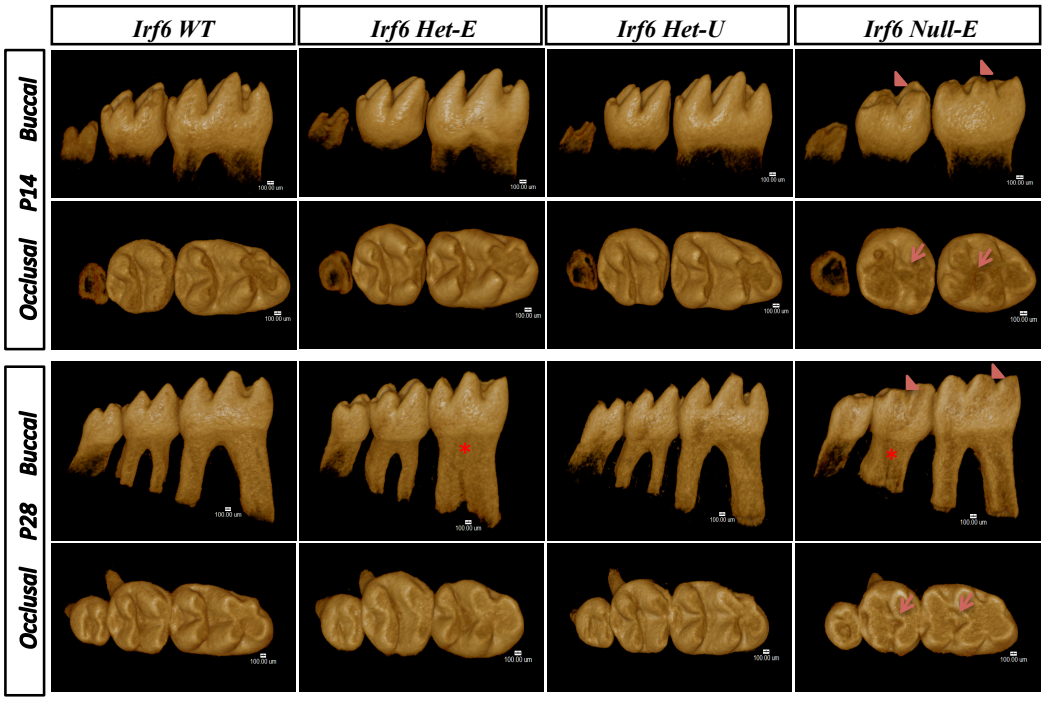


**Figure 3.3: Comparison of P14, and P28 *Irf6 null* Molars with matched controls.** 3D rendered micro-CT images of 2 and 4-week-old *Irf6* null and matched controls lower molars. At 2 weeks, molars of *Irf6* Null-E and to a lesser degree *Irf6* Het-E showed altered crown morphology with rounded cusp tips, and altered root morphology (taurodontism). Images of the occlusal surfaces of the mandibular molars indicated that the null first and second molars are smaller, their crowns lacking the distal cusp. The buccal and lingual are cusps connected, and form a deep fossa in the center (red arrow). At 4 weeks, the molars from *Irf6* null animals showed signs of wear (arrow heads) probably as a consequence of the mineralization defect. Scale bar = 100 µm.

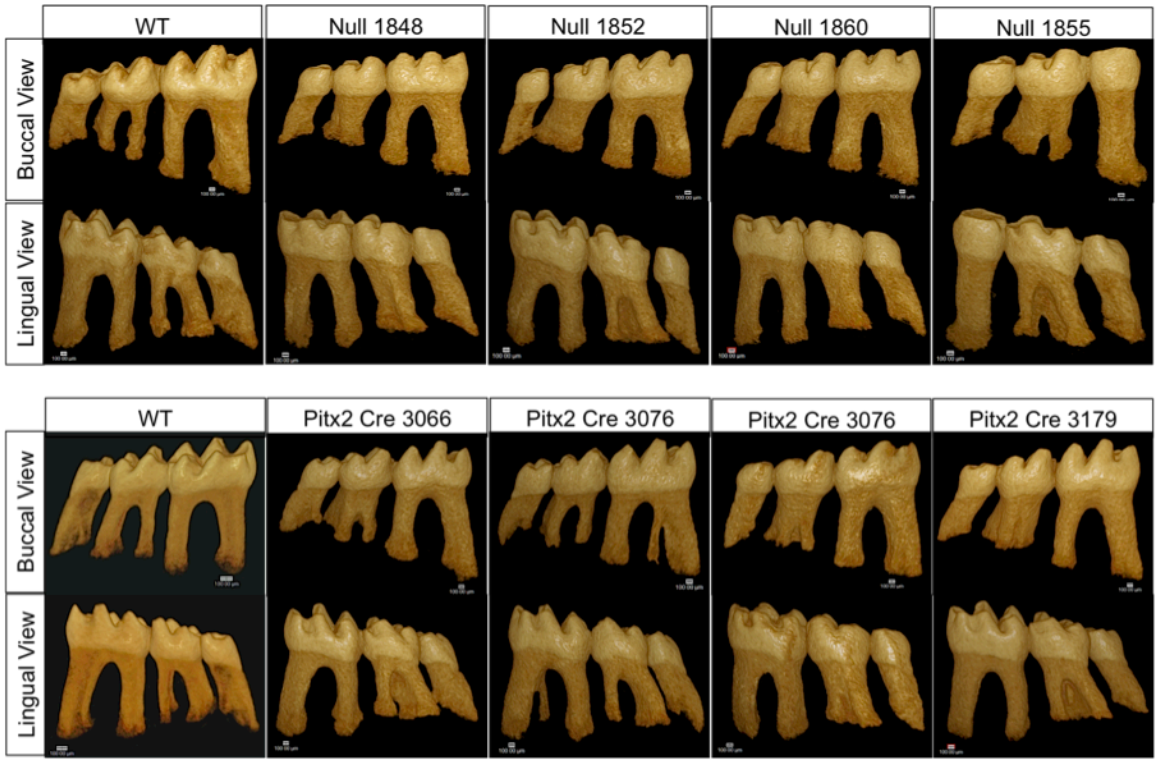


**Figure 3.4 Root phenotype in *Irf6 Null-E* and *Pitx2 Cre* mice.** rendered micro-CT images of lower molars from 12-week-old *Irf6* null and matched controls. Molars from *Irf6* null animals and at a slightly lower penetrance in *Pitx2-Cre* mice show altered root morphology (taurodontism). Scale bar = 100 μm.

**Table 2: Micro-CT parameters measured in different genotypes at 4 weeks**

| *Outcome unit (Mean ±SD)* | *Tooth* | *Genotype* | | | | | *ANOVA P-value* | *Pairwise Comparison* |
|---|---|---|---|---|---|---|---|---|
| | | **WT (a)** | ***Irf6 Null-E (b)*** | ***Irf6 Het-E (c)*** | ***Irf6 Het-U (d)*** | **Pitx2 Cre *(e)*** | | |
| **Tooth Volume, $mm^3$** | U I | 1.72±1.7 | 1.57±0.1 | 1.70±0.0 | 1.70±0.0 | 1.71±0.0 | *<0.001 | **b<a,c,d,e |
| | U 1M | 1.00±0.1 | 0.69±0.0 | 0.94±0.0 | 094±0.0 | 0.98±0.0 | *0.001 | **b<a,c,d,e |
| | U 2M | 0.48±0.0 | 0.41±0.0 | 0.47±0.0 | 0.47±0.0 | 0.48±0.0 | *0.028 | **b<a |
| | L I | 2.21±0.6 | 2.07±0.1 | 2.19±0.3 | 2.23±0.1 | 2.43±0.0 | 0.577 | N.S |
| | L 1M | 0.91±0.0 | 0.67±0.1 | 0.89±0.0 | 0.89±0.0 | 0.90±0.0 | *0.019 | **b<a,c,d,e |
| | L 2M | 0.56±0.1 | 0.52±0.1 | 0.55±0.0 | 0.55±0.0 | 0.54±0.0 | *0.001 | **b<a |
| **Enamel Volume, %** | U I | 14.6±3.3 | 13.1±1.8 | 13.8±1.9 | 13.7±2.3 | 14.1±1.8 | 0.141 | N.S |
| | U 1M | 24.4±2.1 | 22.9±1.8 | 23.5±2.0 | 24.3±1.8 | 23.0±1.8 | 0.061 | N.S |
| | U 2M | 30.1±0.8 | 29.4±1.7 | 30.2±2.8 | 31.3±1.9 | 30.6±2.1 | 0.163 | N.S |
| | L I | 20.6±1.3 | 19.4±1.2 | 19.9±0.5 | 19.9±1.2 | 19.6±0.2 | 0.127 | N.S |
| | L 1M | 22.7±0.9 | 20.6±1.9 | 22.8±1.9 | 22.1±2.0 | 22.3±0.8 | 0.062 | N.S |
| | L 2M | 27.8±1.6 | 26.9±2.1 | 26.9±2.0 | 28.5±1.2 | 27.2±0.6 | 0.113 | N.S |
| **Dentin Volume, %** | U I | 81.8±2.5 | 81.7±1.5 | 84.9±3.5 | 81.9±2.9 | 80.7±1.5 | 0.051 | N.S |
| | U 1M | 64.4±2.7 | 64.7±1.3 | 64.5±2.1 | 63.7±1.3 | 63.7±1.3 | 0.521 | N.S |
| | U 2M | 54.9±2.4 | 52.2±1.6 | 52.6±3.5 | 50.3±1.0 | 51.9±2.2 | 0.111 | N.S |
| | L I | 72.7±2.2 | 72.2±1.4 | 73.5±2.8 | 70.9±4.8 | 70.9±2.8 | 0.396 | N.S |
| | L 1M | 61.9±3.0 | 63.9±3.2 | 62.8±3.3 | 61.4±3.2 | 61.3±2.2 | 0.103 | N.S |
| | L 2M | 54.7±2.04 | 58.27±2.8 | 57.4±2.4 | 54.1±2.8 | 53.1±2.0 | 0.148 | N.S |
| **Enamel Density, index** | U I | 107.4±0.7 | 103.2±0.7 | 103.6±0.3 | 106.7±0.8 | 103.6±0.6 | *<0.001 | **a>b,c,e. d>b,c,e |
| | U 1M | 111.9±0.5 | 107.9±0.7 | 108.8±0.7 | 111.4±0.7 | 108±0.1 | *<0.001 | **a>b,c,e. d>b,c,e |
| | U 2M | 112.2±1.2 | 108.6±0.6 | 109.4±0.3 | 111.9±0.9 | 108.3±0.1 | *<0.001 | **a>b,c,e. d>b,c,e |
| | L I | 112.2±0.6 | 108.3±0.3 | 109.4±0.4 | 111.3±0.7 | 108±0.7 | *<0.001 | **a>b,c,e. d>b,c,e |
| | L 1M | 111.9±0.7 | 108.8±0.8 | 109.5±1.2 | 111.5±0.7 | 108.9±0.7 | *<0.001 | **a>b,c,e. d>b,c,e |
| | L 2M | 112.6±0.5 | 110.2±0.5 | 111.2±0.6 | 112.5±0.6 | 110±0.7 | *<0.001 | **a>b,c,e. d>b,c,e |
| **Dentin Density, index** | U I | 57.6±1.0 | 56.6±1.6 | 55.6±2.4 | 56.5±2.0 | 56.4±1.0 | 0.087 | N.S |
| | U 1M | 59.2±1.1 | 58.5±1.1 | 58.2±0.9 | 59.0±0.4 | 57.9±0.9 | 0.762 | N.S |
| | U 2M | 56.9±0.8 | 56.7±1.5 | 56.5±2.1 | 56.1±0.5 | 55.1±0.5 | 0.796 | N.S |
| | L I | 61.2±2.0 | 60.8±1.2 | 60.7±2.2 | 60.7±1.6 | 59.7±0.4 | 0.974 | N.S |
| | L 1M | 58.2±1.5 | 58.2±1.1 | 57.8±1.3 | 58.4±0.5 | 58.0±0.6 | 0.984 | N.S |
| | L 2M | 57.2±0.9 | 57.8±0.9 | 56.3±1.3 | 56.7±0.5 | 57.7±0.7 | 0.058 | N.S |

N.S. indicates non-significant difference at P>0.05. *Significant at P<0.05, **significant at P<0.005. Lower case letters indicate the pairwise comparison between groups among the values at the same horizontal line, based on a Bonferroni correction for multiple comparisons test. n= 6 mice/genotype.

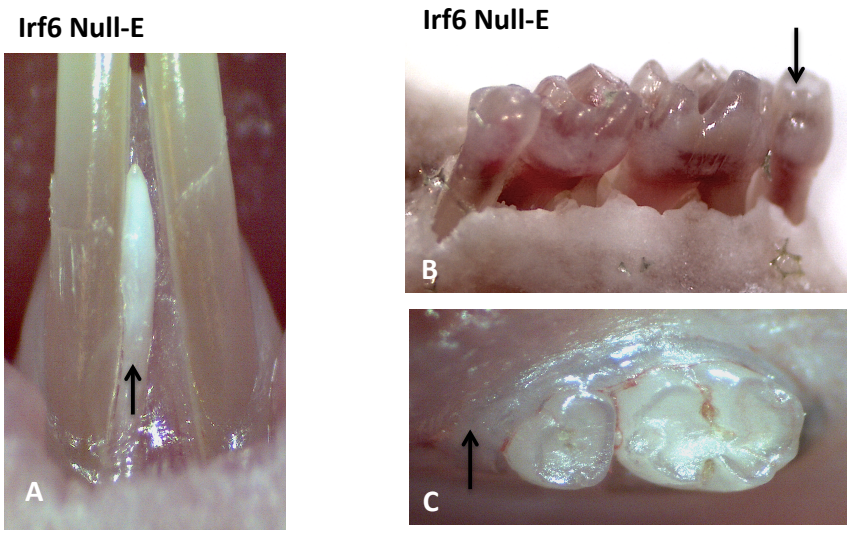


**Figure 3.5: Variations in tooth number observed in the *Irf6 Null-E* mice.** Similar to the findings in patients with CLP and in patients with VWS syndrome, two *Irf6* null animals exhibited supernumerary teeth. One had an extra incisor and the other an extra molar (arrows in A and B, respectively), and two animals were found with hypodontia (missing 3$^{rd}$ molar; arrow) (c).

# 4 Chapter 4: The impact of Irf6 loss on salivary gland morphology and function.

## 4.1 Introduction

Development of the salivary glands occurs through a process known as branching morphogenesis. It starts with the protrusion of an epithelial stalk and end bud into the surrounding mesenchyme, followed by subsequent epithelial cleft formation, progression, and differentiation of specialized cell types. This complex branched architecture provides maximum epithelial surface area for efficient fluid production and secretion (Tucker, 2007). Salivary glands are exocrine glands composed of three major epithelial cell types; 1) acinar cells, which form the secretory units, 2) ductal cells that form ducts for fluid transport, and 3) stellate myoepithelial cells which envelope the secretory units. Acini can be comprised of serous cells, which secrete a watery fluid, or mucous cells, which produce a mucus-rich secretion. These acini are connected to the oral cavity via branched ductal cells in order to secrete saliva. The branched ductal system is composed of intercalated ducts, striated ducts, and a main excretory duct (Larsen et al. 2010). Myoepithelial cells are the least abundant and most poorly understood salivary gland epithelial cell type. They wrap around each secretory unit and aid them to contract in response to neurotransmitter stimulation to facilitate fluid propagation (Pringle et al., 2011).

In humans and mice, about 90% of the total amount of saliva secreted is from three major salivary glands: the parotid (serous secretions), submandibular (mixed secretions), and sublingual (predominantly mucinous) glands. The rest of the saliva is secreted from minor salivary glands (Miletich, 2010). Saliva performs many protective and physiological functions. It supplies the oral cavity with water, electrolytes, and some essential proteins including lubricants, antimicrobial and remineralization agents, as well as digestive enzymes and growth factors (Brosky, 2007). Consequently, hyposalivation due to salivary gland dysfunction leads to xerostomia, mucositis, dysphagia, dental caries, and malnutrition, which lead to significant deterioration of patient quality of life (de Almeida et al., 2008; Dodds et al., 2005).

Very little is known about salivary gland anomalies in clefting populations. Hypoplasia or aplasia of major salivary gland usually detected by chance, have been reported in a few reports of patients with non-syndromic CLP but are not generally examined in this population (Matsuda et al., 1999; Reija et al., 2013). A change in saliva composition, including increased total antioxidant levels, which are known to increase in response to an infection, and an increase in salivary clearance time have also been reported in cleft children (Ahluwalia et al., 2004; Aizenbud et al., 2008). The coexistence of these craniofacial abnormalities is suggestive of a common underlying genetic etiology.

In a similar way, previous studies have revealed that *Irf6,* arguably the most significant clefting gene*,* is also expressed in tooth and submandibular salivary gland at embryonic stages of mouse

development (Blackburn et al., 2012; Laugel-Haushalter et al., 2012). However, its role in salivary gland organogenesis and importance for salivary gland function is unknown. The Cre-driver line (described in the earlier chapters) which conditionally inactivates *Irf6* in the dental epithelium of mice also inactivtes the gene in salivary gland epithelia, therefore also permitting investigation of the role of *Irf6* in salivary gland development.

Salivary glands provide an outstanding *in vivo* system for studying morphogenetic events (i.e., epithelial proliferation, differentiation, and movement), as salivary gland development continues after birth, and final differentiation does not occur until sexual maturation. If Irf6 is involved in salivary gland development, then the knowledge gained from this study will in turn lead to a better understanding of the oral consequences of cleft lip and palate and the cellular and molecular mechanisms involved. Moreover, this study also investigated the consequences of the absence of *Irf6* on the functions of saliva (i.e., protection against caries development). The resultant findings shed light on the pathogenic mechanisms leading to dental caries in the CLP population.

## 4.2 Results

### *4.2.1 Expression of Irf6 during postnatal stages of salivary gland development*

To delineate the role of *Irf6* in postnatal salivary gland development, paraffin-embedded salivary gland samples from WT mice at 3 and 60 days of age (P03, and P60) were evaluated by immunohistochemistry for expression of Irf6 (figure 4.1.A). At P03, strong expression of Irf6

protein was found in the nuclei of myoepithelial and basal ductal epithelial cells. The level of Irf6 protein expression appeared lower in the older animals although it still followed the same restricted expression in the ductal and myoepithelial cells. The absence of Irf6 protein from salivary glands of knockout mice was confirmed by the absence of immunohistochemical staining (figure 4.1.B).

### *4.2.2 Loss of Irf6 caused severe dysplastic growth in the SMG and SLG*

I first investigated the gross morphology and measured the wet weight of the right and left sublingual and submandibular glands of groups of P60 mice from each genotype; wild type*, Irf6 Null-E*, *Irf6 Het-E*, *Irf6 Het-U*, and *Pitx2 Cre* mice (n = 10/genotype; 5 males and 5 females). The gross anatomy of salivary glands from *Irf6 Null-E* mice displayed significant dysplastic changes with signs of salivary gland fibrosis (figure 4.2.A), whereas all other genotypes had a grossly normal appearance. The wet salivary gland weight was not significantly different between males and females within each genotype but did vary with body size. Accordingly, Sexes within each genotype were combined for average and salivary gland weight was standardized by dividing by body weight.

The mean salivary gland weighted weight of *Irf6 Null-E* mice (1.75±0.07 mg/min/g body weight) was significantly greater than that of WT (1.05±0.11 mg/min/g body weight), *Irf6 Het-E* (1.19±0.10 mg/min/g body weight), *Pitx2 Cre* (1.12±0.1 mg/min/g body weight), and *Irf6 Het-U* (1.00±0.06 mg/min/g body weight) ($P<0.0001$). Salivary glands from wild type mice, *Irf6*

heterozygotes, and *Pitx2 Cre* mice were not significantly different from each other (figure 4.2.B).

To further investigate the effect of the loss of *Irf6* in the oral epithelium on salivary gland morphology, salivary glands from wild type and *Irf6 Null-E* mice at 3 and 60 days of age (P03 and P60) were dissected and fixed for histological analysis. Salivary glands from both wild type and *Irf6 Null-E* mice from the experimental dental caries group (i.e. those infected with *S.mutans* and fed a high sugar diet, see chapter 5) at 70 days of age (P70) were also collected for histological analysis. In mice, the salivary gland ductal system is completely formed although not mature by P03, while the acinar cells are still proliferating, and sexual dimorphism is not yet evident. At puberty, ~ 6 weeks postnatal, the final differentiation of the granular convoluted tubules is completed and the sexual dimorphism is evident (Tucker, 2007). Histological analysis of Haematoxylin and Eosin-stained sections of *Irf6 Null-E* mice salivary glands revealed striking consequences of ablation of Irf6 expression. During normal salivary gland development, the increase in glandular tissue is accompanied by a marked decrease in the amount of interlaying connective and adipose tissue. By comparison, in *Irf6 Null-E* mice, the epithelial structures of the salivary glands (ducts and acini) appeared less developed while the mesenchymal fraction was significantly increased in size. Glandular ducts were sparse, completely disorganized, and mostly blocked, and most acini appeared atrophied and were surrounded by dense connective tissue (Figure 4.3).

The gland morphology was investigated at P60 (figure 4.3) and P70 (figure 4.4) to determine whether the observed phenotype were still present when the glands are fully mature. Histologically, the occluded ducts and atrophied acini were a persistent and permanent phenotype at both mature ages, with the presence of cystic spaces (asterisks, figure 4.4) and fatty changes within the glands. Intriguingly, only salivary glands from the *S.mutans* infected null mice showed inflammatory cell infiltration (figure 4.4).

To investigate mucin content of salivary glands, I performed double staining with periodic acid Schiff and alcian blue at pH 2.5. This stains acidic mucin blue, neutral mucin pink, and the combination of both a purple color. Wild type glands showed the normal appearance of acini (purple) and ductal (pink) cells of submandibular glands, and of acini (blue) and ductal (pink) cells of sublingual glands. In contrast, glands from *Irf6 Null-E* mice exhibited changes in the distribution of neutral and acidic mucin with dramatically increased amount of acidic mucin in both the submandibular and sublingual glands (figure 4.5).

### *4.2.3 Cell adhesion, polarity and proliferation are altered as consequences of Irf6 ablation*

In the *Irf6 Null-E* mice, the glandular epithelium was disorganized, suggesting a loss of cell–cell adhesion and a disruption of polarity. Loss of apical–basal cell polarity and disruption of cell–cell junctions can lead to dysregulation of normal proliferation and differentiation programs in cells, and ultimately cancer formation (Martin et al., 2000; Royer et al., 2011). To examine whether *Irf6* ablation disrupts membrane localization of adhesion molecules, the distribution of

both E-cadherin, a main component of adherens junctions, and NME2, an important regulator of epithelial adhesion (Otsuki et al., 2001) was investigated by IHC. In both the submandibular and sublingual glands, the WT duct and acinar cells exhibited well-defined cell–cell junctions as indicated by classic lateral membrane localization of E-cadherin. By contrast, in the *Irf6* Null-E mice, acini exhibited reduced expression and disorganized localization of E-cadherin (figure 4.6). Interestingly, the localization of NME2 protein was distributed differently depending on the cell type and the proliferative state of the cells in wild type tissue (figure 4.7). A distinct basolateral and nuclear localization of NME2 in duct and serous-type acinar cells (P03) was replaced with cytoplasmic and membranous localization in these cells of the mature gland (P60). In contrast, in SMG of *Irf6* Null-E mice, the amount of NME2 staining was notably weaker and staining was exclusively in the cytoplasm of both P03 and P60 duct and serous-type acinar cells. Likewise, duct and mucous-type acinar cells of WT SLG exhibited mostly basolateral membranous NME2 staining. In contrast, duct and mucous acinar cells of the SLG of *Irf6* Null-E mice showed reduced and only patchy cytoplasmic staining of NME2. Interestingly, in the mature SMG and SLG of the *Irf6* null mice but not in equivalent wild type glands, very distinctive scattered round cells that showed an intense NME2 staining were observed (arrows, figure 4.7).

To examine the effect of *Irf6* ablation on cell proliferation, immunostaining for proliferating cell nuclear antigen (PCNA) was performed in serial sections of salivary glands from WT and *Irf6* Null mice (figure 4.8). At P03 and P60 in WT salivary glands, PCNA-positive nuclei were mainly located in the same group of cells that showed nuclear Irf6 expression, consistent with the

previously described role for Irf6 in regulating epithelial cells proliferation (Ingraham et al., 2006; Richardson et al., 2006). At P03 there was an increase in PCNA staining in salivary glands from *Irf6 Null-E* mice compared to WT controls. At P60, in WT animals, PCNA expression was almost undetectable in the duct and acinar cells, and strong staining was evident mainly restricted to myoepithelial cells, indicating minimal or no proliferative activity of ductal and acinar cells. This was in contrast to the strong expression seen in ductal cells of *Irf6 Null-E* mice indicating that the tissue was continuing to proliferate and terminal differentiation had not yet been initiated.

P63 is a master regulator of epithelial development and morphogenesis. P63 has been used as a cell proliferative and basal cell marker in skin and other epithelial cell types (Romano et al., 2012). A regulatory loop between *Irf6* and *P63* has been proposed in keratinocytes (Gritli-Linde, 2010). Therefore, the consequence of *Irf6* ablation on P63 expression/localization was investigated (figure 4.9). P63 staining was found to exhibit a restricted pattern in WT salivary gland cells. At P03 an intense P63 nuclear localization in the basal layer of duct and myoepithelial cells was observed, whereas the cells lining the glandular lumen showed no detectable staining. At P60, a gradual diminution of nuclear intensity in the terminally differentiated basal ductal cell layers was observed, whereas the myoepithelial cells still stained positive for P63 levels. In contrast, in the *Irf6 Null-E* mice, P63 staining was no longer limited to the basal region. It was detected in the entire population of duct cells at both P03 and P60. This may indicate that apico-basal cell polarity of the glandular ductal cells is disrupted in the *Irf6*

null mice.

Aquaporin 5 (AQP5) is a water channel protein that is crucial to fluid secretion in salivary glands (Ishibashi et al., 2009). The temporo-spatial AQP5 expression pattern in both acini and intercalated ducts has been previously well documented in the mouse submandibular gland (Aure et al., 2014; Larsen et al., 2011). Therefore, immunostaining for AQP5 was utilized to further examine the effect of *Irf6* ablation on the function of the salivary glands and the organization of the cells within the salivary glands (figure 4.10). In WT SMG, strong AQP5 staining was located in the apical and basolateral membrane of both serous type acinar cells and intercalated duct cells as expected. At P60, the AQP5 localization pattern was consistent with that found at P03. In contrast, the *Irf6* null mice exhibited aberrant and mislocalized AQP5 expression. At P03, weak AQP5 immunostaining was detected only in the apical membrane of the serous-type acinar cells and intercalated duct cells of the SMG, at P60 *Irf6* deficient mice, weak immunostaining was localized in both apical and basolateral membranes of the serous acini.

Taken together, these IHC data suggest that Irf6 is required for proper cell adhesion and polarity and thus in the maintenance of the organization of salivary epithelial cells during postnatal stages of gland development. The associated marked increase in cell proliferation also suggests that Irf6 is important for maintaining the balance between the proliferation and differentiation. Moreover, given the altered AQP5 expression, compromised salivary function was expected and further

investigated.

### *4.2.4 Irf6 Null mice exhibited severely altered salivary gland function*

Saliva washes and lubricates oral mucosal surfaces, buffers acids, provides antimicrobial protection, protects the tooth surface, initiates the digestion of carbohydrates, and insures the proper functioning of taste buds by solubilizing food (Dodds et al., 2005). Therefore we aimed to investigate the effect of *Irf6* ablation on salivary gland function. A pilocarpine- induced normalized salivary flow (saliva weight/ minute/ body weight), pH and buffering capacity (the ability to neutralize the acids) were all measured. (All results summarized in table 3).

Saliva pH was within normal range (pH >8) for all genotypes (figure 4.11.A). However, flow rate and buffering capacity (changes in pH when strong acid is added) were significantly lower in the *Irf6 null-E* mice compared to each of the other genotypes ($P < 0.0001$) (figure 4.11.B and C). Both male and female *Irf6 null* mice showed markedly impaired saliva production. The average volume of whole saliva collected in *Irf6 null* mice was as low as 0.70 mg/ min/ g of body weight compared to 1.15mg/ min/ g of body weight in the WT control mice. This was associated with low buffering capacity (as low as pH =2.9) in the *Irf6* null mice compared to normal buffering capacity in the control mice (pH>7.5), measured 20 minutes after the addition of HCL (0.005M/L). *Irf6 Het –E* mice showed a trend toward lower salivary gland hypofunction compared to all other genotypes with a flow rate of 0.97 mg/ min/ g of body weight and buffering capacity of pH=7, but this did not reach statistical significance with the numbers of

animals tested. Wild type, *Irf6 Het-U,* and *Pitx2 Cre* mice showed no significant differences in the salivary function.

These results collectively demonstrate that hypo-functional salivary glands characterized by low pilocarpine-induced salivary flow and buffering capacity observed in *Irf6* null mice are due to altered gland morphology (fewer acinar cells and occluded ducts, as well as AQP5 down regulation) resulting from defects in ductal and acinar cell adhesion, proliferation and differentiation.

## 4.3 Discussion:

Clefting is associated with various complications including cosmetic deformities, dental abnormalities, speech, hearing, swallowing, and growth difficulties, and an increase in caries prevalence in some studies (Al Jamal et al., 2010; Wells, 2014). Salivary gland secretions (i.e., saliva) and saliva composition are key factors in determining the health of the oral tissue and the prevalence of dental caries (Leone et al., 2001). Although abnormalities in the same molecular pathway could underlie clefting, tooth and salivary gland birth defects, given their shared epithelial origin, salivary gland development in cleft lip and palate populations has not been previously studied. In the previous chapter, *Irf6* was shown to be important for regulating tooth morphogenesis, as evident by the disruptions in cusp and root morphology, and ameloblast polarity and organization in *Irf6 Null-E mice* teeth. In this chapter, the role of *Irf6*, as a major

clefting gene, in salivary gland morphology and function was investigated using the same animal model.

Irf6 is highly expressed in the ductal system of the submandibular gland during prenatal stages of development (Fakhouri et al., 2012; Laugel-Haushalter et al., 2012). Here I show strong expression of Irf6 protein in the nuclei of myoepithelial and basal duct cells, the same expression pattern as seen with proliferating cell nuclear antigen (PCNA). Saliva secreted by the acinar cells is NaCl-rich fluid. However, during its passage through the ducts, the ductal cells reabsorb NaCl and secrete $KHCO_3$ to form the hypotonic final saliva (Lee et al., 2012). Myoepithelial cells, located between the acinar epithelium and basement membrane that covers the lumina of the acini and ducts, are packed with alpha-smooth muscle actin and support stimulation of salivary secretion by contraction. Myoepithelial cells also play a role in metabolite transportation to and from the secretory cells (Garrett et al., 1973). The strong expression of Irf6 in these cells, along with the similar localization of the proliferation marker, is suggestive of a prominent role for *Irf6* in postnatal stages of salivary gland development, particularly ductal epithelial cell turnover and differentiation. *Irf6* is also likely to be physiologically relevant to the mechanism of saliva secretion.

The data showed that ablation of Irf6 in oral epithelium leads to an increase in salivary gland weight. Further investigation revealed that *Irf6* null mice exhibited disrupted salivary gland development and function most likely due to the dysplastic changes, as well as an increased

amount of interlobular connective tissue, all of which are traits similar to those observed in mice with terminal duct ligation and patients who have experienced irradiation therapy or Sjögren's syndrome (an auto-immune disease causing loss of saliva producing cells)(Hai et al., 2010; McCartney-Francis et al., 1996; Nagai et al., 2014; Tzioufas et al., 2007). Increased expression of TGFβ1, TGFβ3, alteration in E-cadherin expression, and decreased Wnt1 expression are the main contributors to the dysplastic and fibrotic changes observed in ligated ducts and in irradiated or impaired human salivary glands (Hakim et al., 2011; McCartney-Francis et al., 1996; Woods et al., 2015).

In mice, overexpression of *TGFβ1* leads to glandular atrophy and fibrosis (Hall et al., 2010), whereas both global and conditional knockout of *TGFβ1* result in glandular atrophy, inflammatory cell infiltration, and increased cell proliferation within the salivary glands (Dang et al., 1995; McCartney-Francis et al., 1996). In a parallel way, inhibition of mesenchymal Wnt/ß-catenin signaling or activation of epithelial Wnt/ß-catenin signaling blocks salivary gland branching morphogenesis (Hai et al., 2010; Patel et al., 2011). The Eda/Edar/NF-κB pathway, which is induced by the Wnt pathway, is an essential regulator of salivary gland morphogenesis (Häärä et al., 2011). The Tabby mouse, which carries a mutation in Eda, and phenotypically mimics patients with anhidrotic ectodermal dysplasia, has delayed postnatal development of SMG, fewer ductal structures, fewer granular convoluted tubules, and a permanent dysfunction in saliva production (Blecher et al., 1983). A regulatory loop between Irf6 and the Wnt signaling has been reported to regulate epithelial morphogenesis required for fusion of the primary palate (Ferretti et al., 2011). Moreover, Irf6 has been also shown to act as a mediator of Tgfβ3 signaling

to regulate the epithelial changes required for fusion of the primary palate (Ke et al., 2015). Thus, similar mechanism could reasonably explain the morphological defects observed in the salivary glands of the *Irf6* null mice.

One of the very striking features observed in the salivary glands of *Irf6* null mice is the failure of canalization of the lumen and its occlusion by proliferating cells, confirmed by the PCNA staining of these cells (figure 4.8). Creating the luminal space to allow the passage and modification of saliva into the oral cavity is a fundamental feature of salivary gland morphogenesis. The steps initiating lumen formation are poorly understood, but it has been suggested that two processes form it: 1) apoptosis to create the luminal space, and 2) polarization of the epithelial cell layer lining the lumen (Patel et al., 2011; Wells et al., 2010).

Adherens and tight junctions proteins are expressed in salivary gland epithelium from early stages of salivary gland development until adulthood (Hieda et al., 1996; Menko et al., 2002). These proteins are crucial for lumen formation during salivary gland development (Walker et al., 2008). The outer cells that strongly attach to each other via adherens junctions and to the ECM through integrin are protected from apoptotic activity while the inner cells that loosely attach to each other via tight junctions are more likely to be removed by apoptosis (Wells et al., 2010). This prompts an examination of the expression of adhesion proteins involved in cell- cell and cell-matrix adhesions. *Irf6* ablation in both mice and chicks leads to altered E-cadherin distribution, altered epithelial shape, and a hyperproliferative epidermis (Ingraham et al., 2006;

Parada Sanchez, 2012; Richardson et al., 2006). Likewise, the expression of E-cadherin was disorganized in the ductal and acinar cells in SMGs and SLGs of the *Irf6* Null mice. Few acinar cells showed strong expression of E cadherin while the majority of the acinar cells lost the membranous staining of this adhesion protein. Interestingly, similar expression has been reported in the salivary glands of mice after irradiation (Hakim et al., 2011). The irradiated gland goes through atrophic processes, including epithelial–mesenchymal transition (EMT) in which acinar cells undergoing EMT do not express E cadherin, whereas intact acini still show strong membranous E cadherin expression (Hakim et al., 2011). Thus the reduction in E-cadherin observed following knockout of Irf6 could also explain the increased amount of connective tissue observed in the Irf6 null mice. Mouse SMG explants, lacking the adherens junction protein E cadherin function, exhibited an increase in apoptosis of the ductal cells and a dilated lamina (Walker et al., 2008). E cadherin binds to its key regulator, p120-catenin, to strengthen cell-cell adhesion and to β-catenin to mediate its physical association with the actin cytoskeleton. Similar to the phenotypes observed in the *Irf6* null mice, SMG of the p120 conditional knockout mice exhibited blocked ductal lumens that were occluded by epithelial masses (Kurley et al., 2012). In mice, the inhibition of epithelial β-catenin signaling also led to the development of poorly differentiated acini and less granular convoluted tubules (Hai et al., 2010), somewhat similar to the phenotypes observed in the *Irf6* null mice.

During cytodifferentiation, E-cadherin and β-catenin interact with Rho GTPases, such as Rac1 and RhoA, to maintain salivary cell polarity. This interaction is required for the stabilization of the E-cadherin complexes and the formation of mature acini and ducts (Menko et al., 2002;

Pirraglia et al., 2006, 2013). Previous data from the Cox lab showed that NME1 and NME2, two closely related regulators of epithelial cell adhesion, and negative regulators of RhoA and Rac1 activation respectively (Otsuki et al., 2001), physically interact with Irf6 in epithelial cells (Parada Sanchez, 2012). Consistent with this, HEK293 epithelial cells that ectopically expressed mutant IRF6, which was unable to bind NME2, displayed increased levels of active Rac1 (Chu, 2015). Furthermore, in *Irf6* null mice, the localization of NME2 in secretory-phase ameloblasts was perturbed, changing from a cytoplasmic and nuclear distribution to a distinct localization at the apical/apicolateral surface of the polarized ameloblasts (Chu, 2015), supporting the notion of localized increase in Rac1 activation at the junctional complexes leading to their remodeling. Rac1 has been implicated in the reorganization of junctional complexes and the cytoskeleton as well as pro-apoptotic and anti-apoptotic processes (Harrington et al., 2002; Jiang et al., 2003). During salivary gland development, Rac1 is highly expressed in epithelial cells at the beginning of differentiation and then gradually declines as the lumen is formed. In the Drosophila embryonic salivary gland, selective inhibition of Rac1 led to reduced lumen size and length and failure of the gland cells to migrate (Pirraglia et al., 2013). In line with this, NME2 expression was also mislocalized in the duct and acinar cells of the salivary glands of *Irf6* null mice.

During salivary gland morphogenesis, stabilization of the E-cadherin complex is a prerequisite for proper maturation of both ductal cells and acinar cells (Walker et al., 2008). Moreover, *Irf6* homozygous null embryos have an expanded spinous layer, which lacks the normally formed granular and cornified layers of the epidermis. This expansion was determined to be the result of an increase in proliferation and defective terminal keratinocyte differentiation (Ingraham et al.,

2006). This urged investigation of whether the growth abnormality of the salivary glands in *Irf6* null mice is associated with a shift from the differentiation process to a prolonged proliferation status. Using immunostaining of PCNA, a proliferation marker, at P60, strong nuclear expression of PCNA was observed in the duct cells of SMG and SLG of the *Irf6* null mice in contrast to WT mice. An increased level of PCNA expression has been associated with poor differentiation and more invasive growth of tumor cells (Lan et al., 1996; Poosarla et al., 2015). Thus Irf6 ablation in the salivary glands led to increased proliferative activity and a delay in the terminal differentiation of the ductal and acinar cells, in turn causing some of the morphological defects observed in the *Irf6* null mice.

Parallel to this, loss of *Irf6* function resulted in changes in expression of markers of the basal layer. P63 was no longer limited to the basal ductal cells. The same observation was reported in skin from *Irf6* null embryos where the basal cell markers, P63 and K14, were expressed in the spinous layer of the epidermis compared to the basal layer expression in WT embryos (Ingraham et al., 2006). Remarkably, similar to the ducts of the salivary glands of the *Irf6* null mice, loss of exclusive P63 basal expression in mammary glands results in blocked ducts and blocked luminal cell differentiation, leading to a failure of lactation (Forster et al., 2014).

To examine whether the disorganized and atrophied acinar cells retained their function, immunostaining with AQP5, a functional marker, was utilized. In rats, AQP5 localization and expression levels in submandibular glands follows the variation of the saliva secretion rate. In

animals with normal saliva flow rate, high levels of AQP5 are found at the apical, basal and lateral membrane of acinar cells, whereas in animals with lower saliva flow rate, low levels of AQP5 were found and confined to the apical or lateral membrane of acinar cells (Murdiastuti et al., 2002). AQP5 has shown diffuse cytoplasmic expression in salivary gland acini of human SS patients (Steinfeld et al., 2001). In a very similar way, low levels and mislocalized expression of AQP5 was observed in the SMG of the *Irf6* null mice. Moreover, a substantial reduction of AQP5 expressing acinar cells was evident. Defects in branching and cell differentiation could lead to a lower number of secreting cells and lower glandular surface area, thus reducing saliva volume. *Irf6* ablation leads to changes of acinar and duct structure as well as the disorganization of AQP5 in the salivary gland, which can reasonably cause salivary gland dysfunction, thus salivary gland function was further investigated.

An established pilocarpine-induction procedure was used to investigate salivary flow and composition. These investigations found that *Irf6 Null-E* animals of both sexes had a significantly lower saliva secretion volume compared to all other included genotypes. Parallel with the reduction in saliva flow rate, saliva composition was also altered in these mice. Normal salivary excretion is made up of both serosal and mucosal saliva. The composition of mucosal saliva features the highly glycosylated mucin protein. This protein can hold water via several negatively charged (hydrophilic) groups to form gel-like, sticky saliva. On the other hand, serous saliva lacks mucin but contains amylase enzyme that helps in food digestion (Furness et al., 2011). Changes in the distribution of mucin content within the salivary glands were evident in both the submandibular and sublingual glands of *Irf6 Null-E* mice with a dramatic increase in the

staining of acidic mucin. The main role of AQP5 in saliva secretion is to increase intercalated duct and acinar cell permeability to water (Krane et al., 2001). Similar to the *Irf6* null E mice, mice lacking AQP5 exhibit reduced, hypertonic and viscous saliva secretion (Ma et al., 1999). In patients with cystic fibrosis (CF), mucus secretion is abnormally thick and viscous, leading to the plugging of lumins and crypts of different organs with mucoid secretions (Oppenheimer et al., 1975). Failure to secrete bicarbonate ($HCO3^{-}$) is one of the common pathogenic mechanisms in abnormal mucus release in CF (Garcia et al., 2009). In a similar way, the observed alteration in mucus content of the *Irf6* null mice could be in part due to altered $HCO3^{-}$ content leading to more acidic mucin and reduced buffering capacity.

Salivary pH and buffering capacity are usually used for general assessment of saliva chemistry. Low salivary flow rates have been found to be associated with low carbonate secretion rates, leading to low salivary buffering capacity (Sánchez et al., 2003). In the *Irf6* null mice, salivary pH was within the normal range. This could be explained by the fact that stimulated saliva was measured around 10 am -11 am. Since mice are nocturnal, this increases the chances that mice were sleeping rather than eating just before saliva collection. Given that salivary glands are not completely atrophied in these mice, this could provide enough time for the pH level to return to the normal range. However, when saliva was subjected to 20 minutes of an acidic challenge (i.e., buffering capacity test), the salivary pH of samples collected from the *Irf6 Null-E* mice dropped significantly.

The factors that affect the resting pH levels of saliva include the buffering capacity, the diffusion of acids from plaque into saliva, and the production of bases in plaque. It has been reported that an increase in plaque weight is associated with a decrease in microbial acid production activity (Borgström et al., 2000). In heavy plaque formation, a more complex composition of microorganisms exists, including acid fermentatives, acid consumers, saccharolytic bacteria, and degenerated and dead microorganisms. These microorganisms, through different biochemical processes, will have a significant influence on the acidity in dental plaque. For example, ammonia from the deamination of amino acids and breakdown of urea in saliva can make plaque pH less acidic (Shu et al., 2007). The bacterial genus Veillonella uses lactate as a substrate, processing it to less acidic products such as propionic acid and acetic acid (Marsh et al., 2015). An association between salivary contents and plaque composition has been previously reported (Rudney et al., 1991, 1993). In a similar way, the salivary hypofunction found in the Irf6 null mice may alter the commensal microorganisms in the oral cavity leading to an increased load of oral microbiota, specifically acid fermentative and acid consumer bacteria hindering the ability to detect the lower pH of the salivary secretions.

## 4.4 Figures and tables

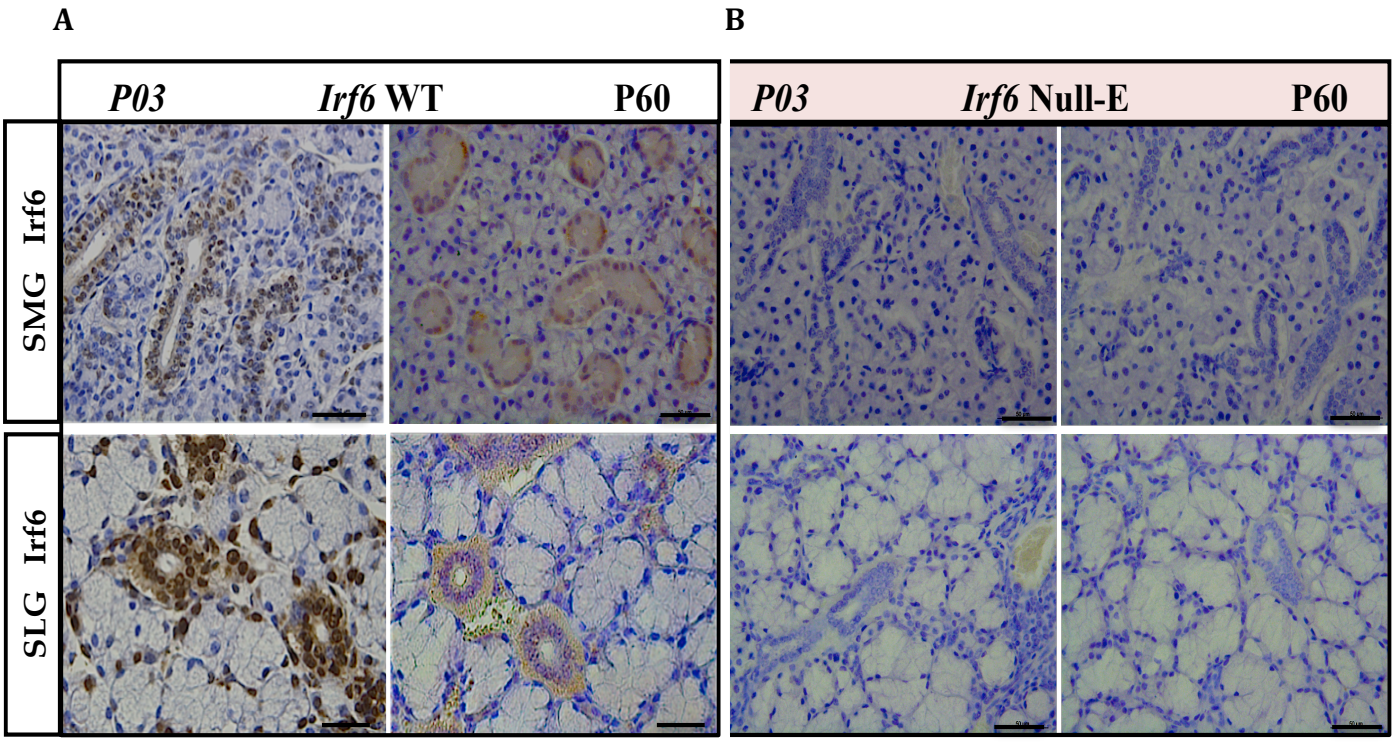


**Figure 4.1: Irf6 expression in salivary glands from *Irf6 Null-E* and *WT* animals.** At P3 and P60. A) At P03, strong Irf6 expression is localized in the ductal cells (arrow) and on the subpopulation of myoepithelial cells surrounding the acini and duct cells (arrowheads). At P60, both SMG and SLG have a weaker but the same restricted expression in the ductal and myoepithelial cells. B) Expression of Irf6 was completely absent in glands from knockout animals.

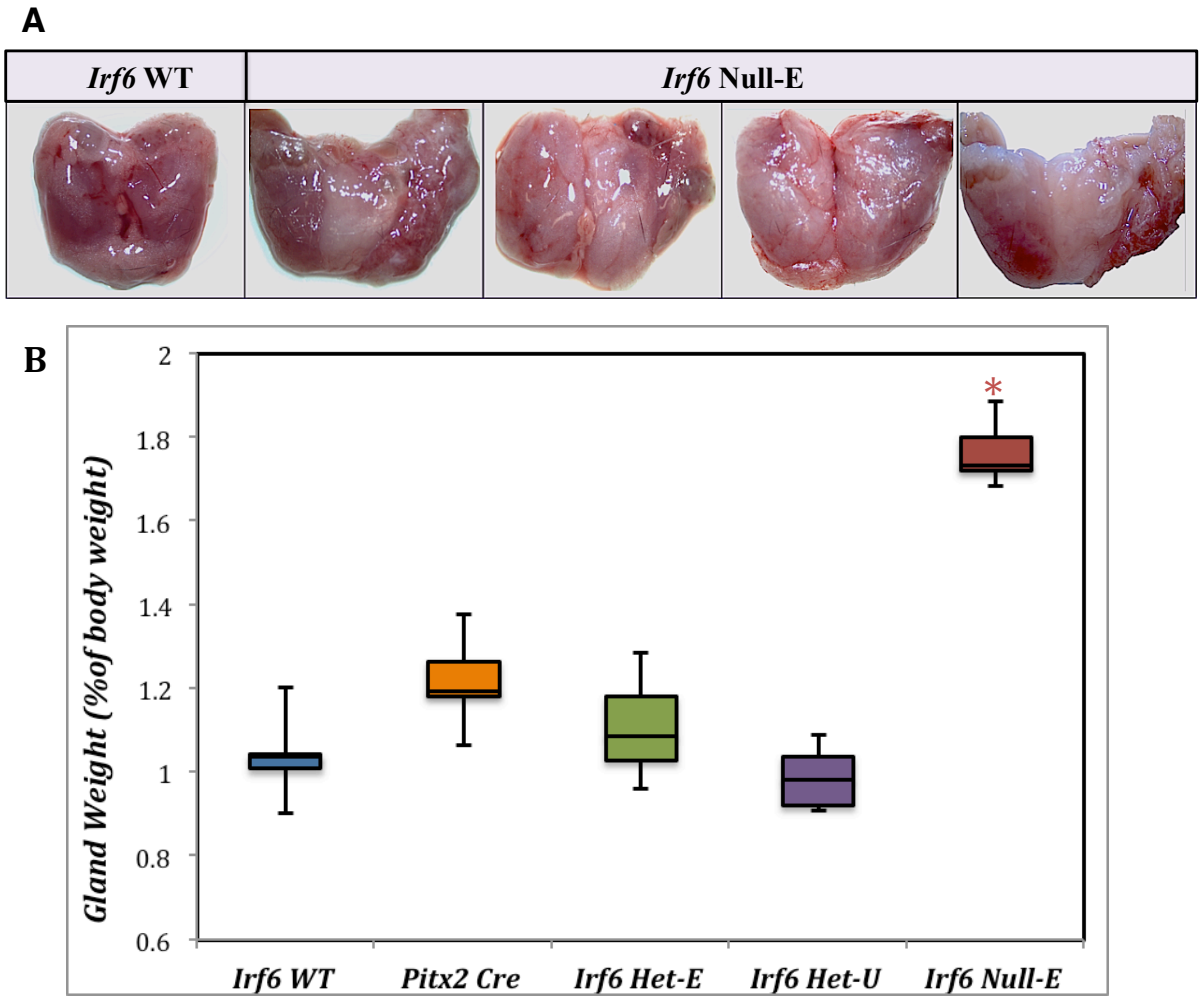


**Figure 4.2: Morphological, and weight alterations in salivary gland of *Irf6* mutants.** (A) The gross anatomy of female submandibular and sublingual glands in *Irf6* Null-E mice display morphological defects compared to WT salivary glands at P70. (B) Wet salivary gland weight (salivary gland weight/body weight ratio) was significantly increased in the *Irf6 null-E* mice (*$P < 0.0001$) compared to all other genotypes. (n= 10 mice/genotype)

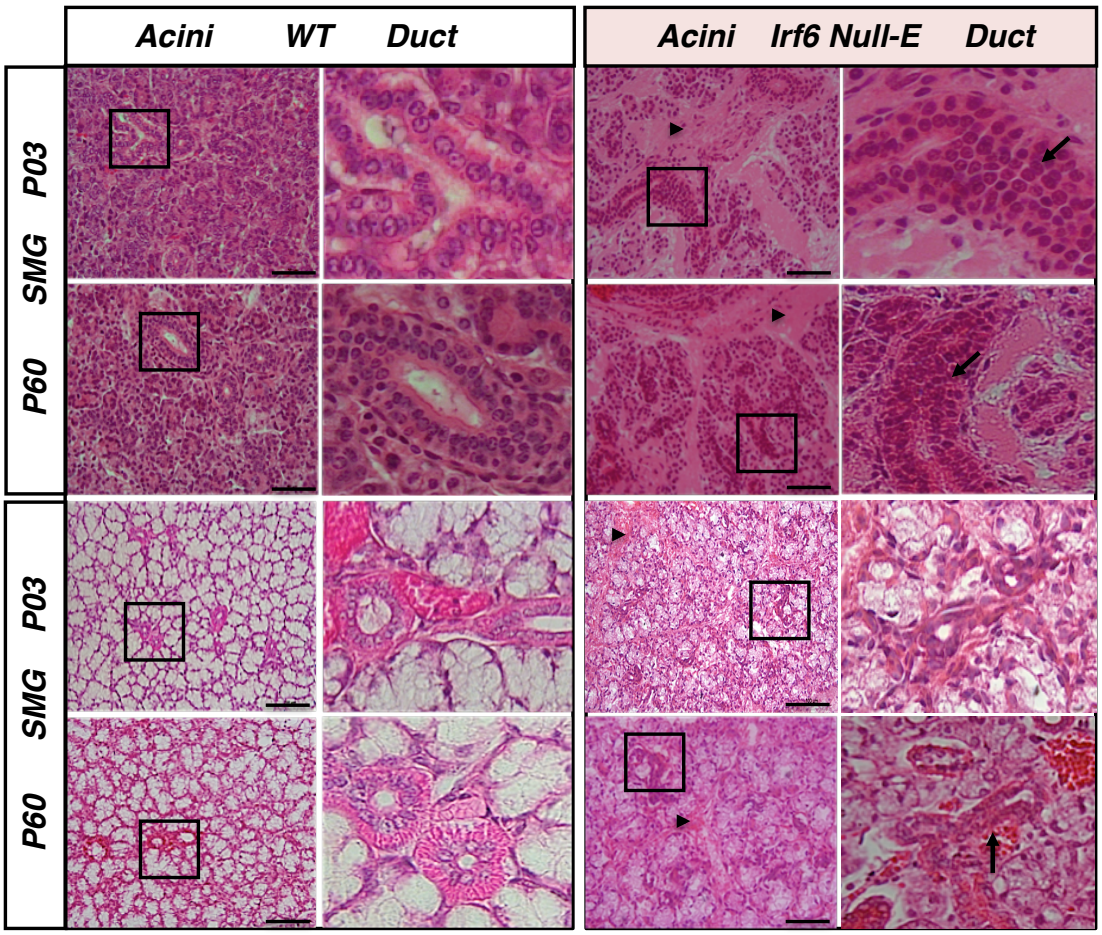


**Figure 4.3: Histological defects in salivary gland of *Irf6* mutants.** Hematoxylin and eosin staining of submandibular and lingual gland sections from 3 and 60 days female WT and *Irf6* null mice. The small boxes under Acini indicate the area magnified under Duct a magnification of the ductal structure within the glands. Arrowheads point to areas indicative of fibrosis, and arrows point to occluded ducts in the *Irf6 null* mice.

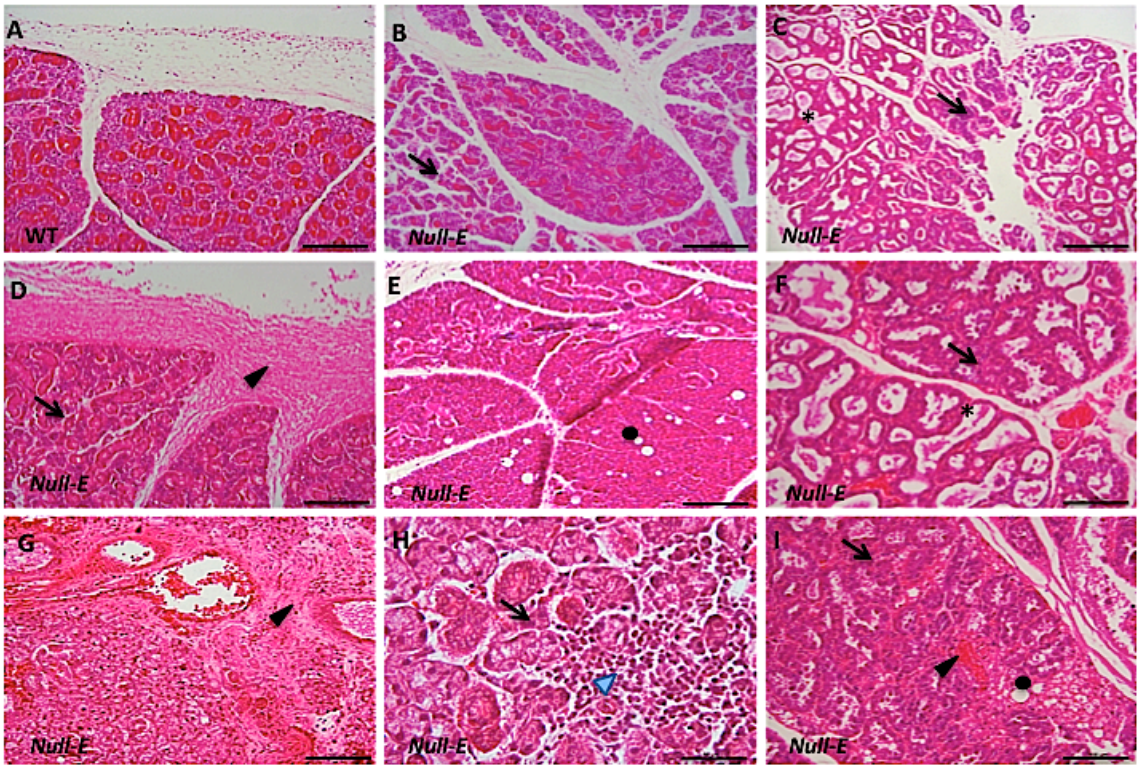


**Figure 4.4: Histological defects in SMG of S. *mutans* infected mutant mice.** (A-I) H&E-stained sections show the normal appearance of wild-type (WT) submandibular salivary glands (A) with a thin fibrous capsule surrounding the gland. (B-I) Submandibular salivary glands of *Irf6* null mice frequently showed ductal and acinar atrophy (black arrows), which was gradually replaced by fibrous tissue (black arrowheads). Inflammatory cell infiltration (blue arrowhead; H), the presence of cystic spaces (asterisks; C,F), and fatty changes (black circles; E,I) were also evident in *Irf6* null mice. Scale bar=(A-E) 200 $\mu$m and (F-I) 100 $\mu$m.

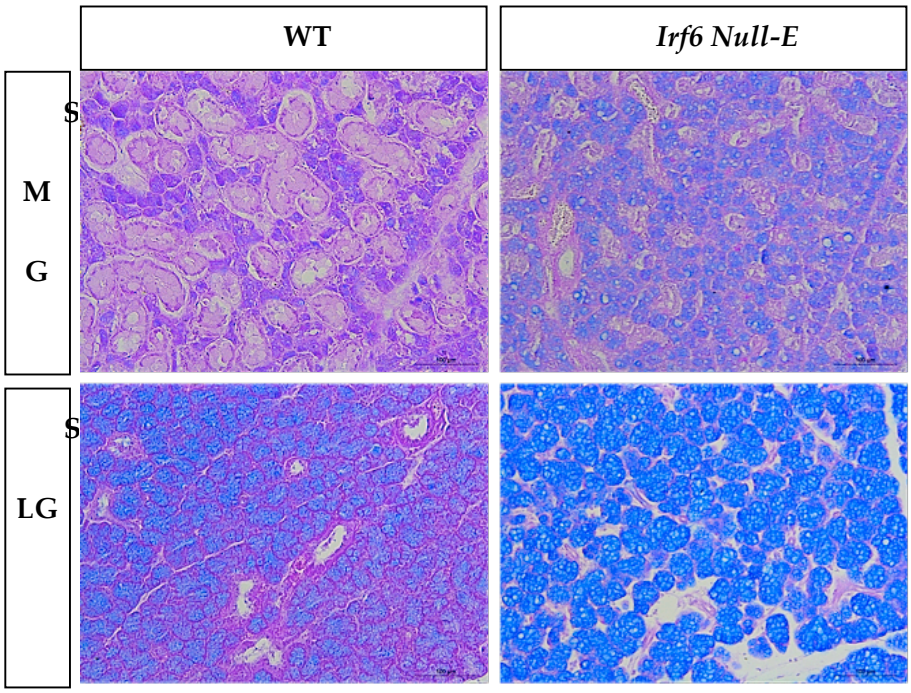


**Figure 4.5: Disturbance in Mucin staining in salivary glands of *Irf6* mutants.** WT glands show the normal appearance of acini (purple) and ductal (pink) cells of SMG and of acini (blue) and ductal (pink) cells of sublingual glands. Changes in the distribution of neutral (purple) and acid mucin (blue) was evident in both SLG and SMG of *Irf6* Null-E mice compared to the WT, with a dramatic increase in the amount of positively stained cells for alcian blue (acidic mucin) in the null mice. Scale bar=100 $\mu$m

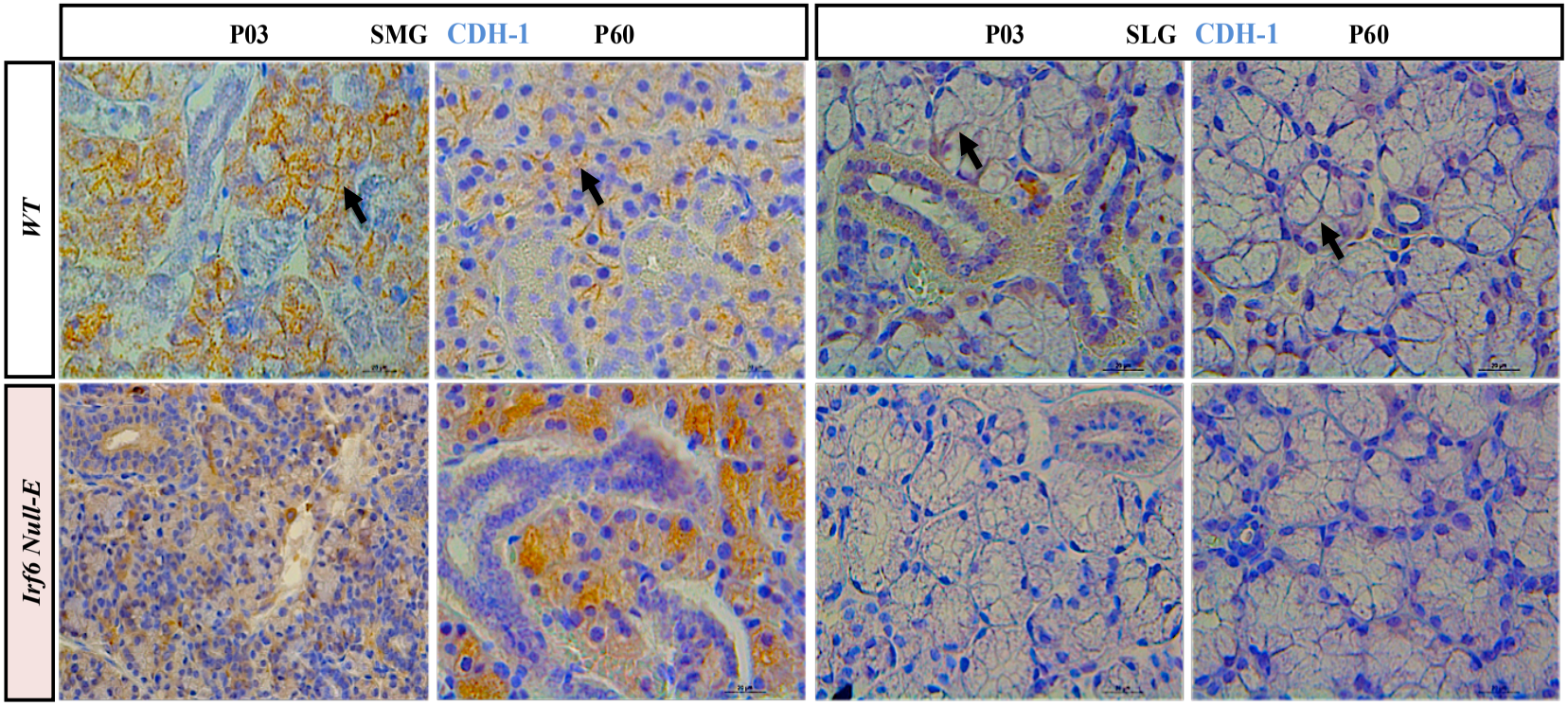


**Figure 4.6: Immunohistochemical localization of E-cadherin (cell adhesion protein).** At P03, *Irf6* ablation induced disorganization of E-cadherin in both SMG and SLG of the *Irf6* null mice compared to the normal basolateral expression in the WT glands (black arrows). This disorganized expression is still persistence as the glands mature at P60.

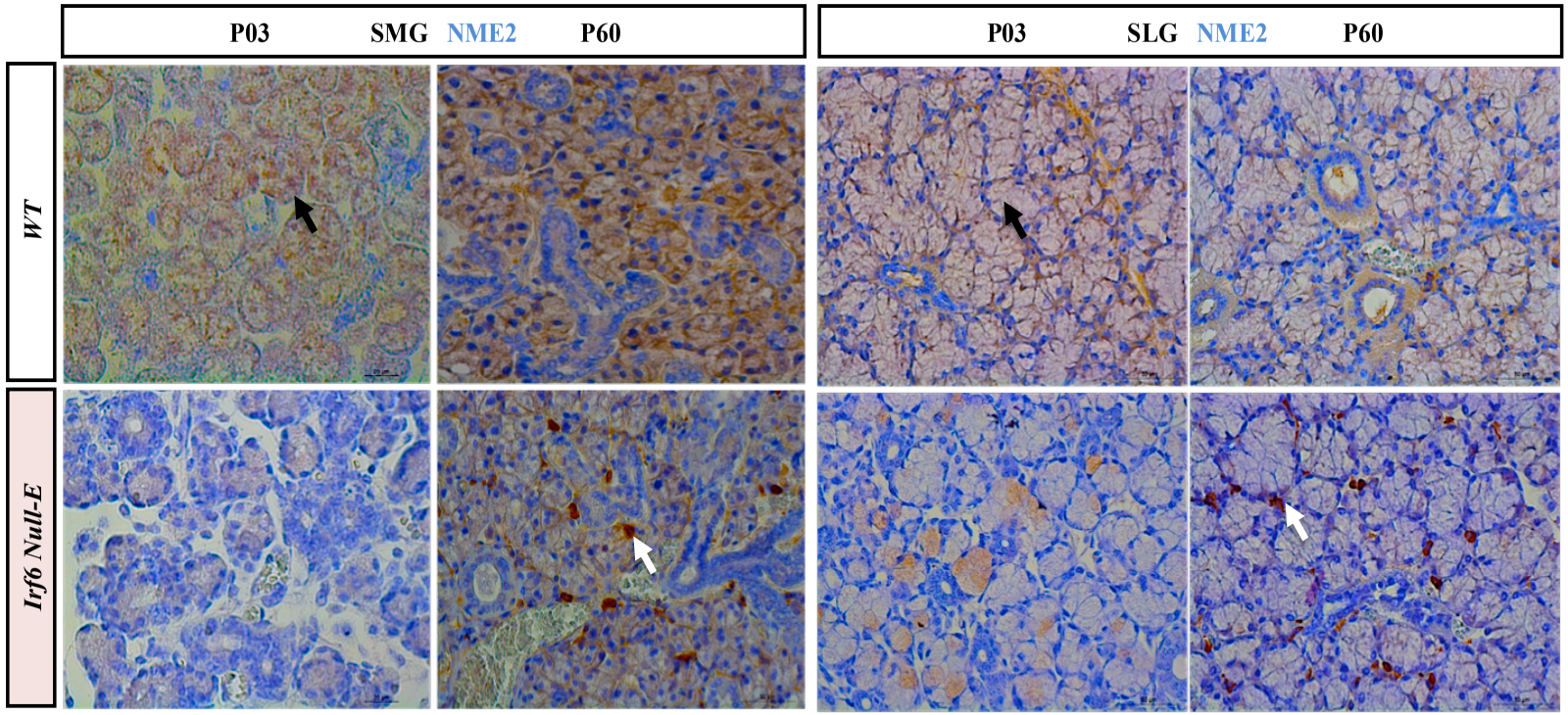


**Figure 4.7: Immunohistochemical localization of NME2, adhesion and Rac1 regulator.** In SMG, the distinct basolateral and nuclear localization of NME2 in duct and serous-type acinar cells of WT samples (P03, black arrows) was replaced with exclusive cytoplasmic localization in these cells as the gland mature (P60). In contrast, the *Irf6* null mice exhibited low levels of NME2 staining that was exclusively in the cytoplasm of both proliferative (P03) and mature ductal and serous-type acinar cells (P60). In SLG, WT duct and mucous-type acinar cells exhibited basolateral membranous staining of NME2. In contrast, ductal and mucous acinar cells of *Irf6* null mice exhibited reduced and patchy cytoplasmic staining of NME2. Interestingly, in the mature SMG and SLG of the *Irf6* null mice, very distinctive scattered round cells that showed an intense NME2 staining were observed (white arrows).

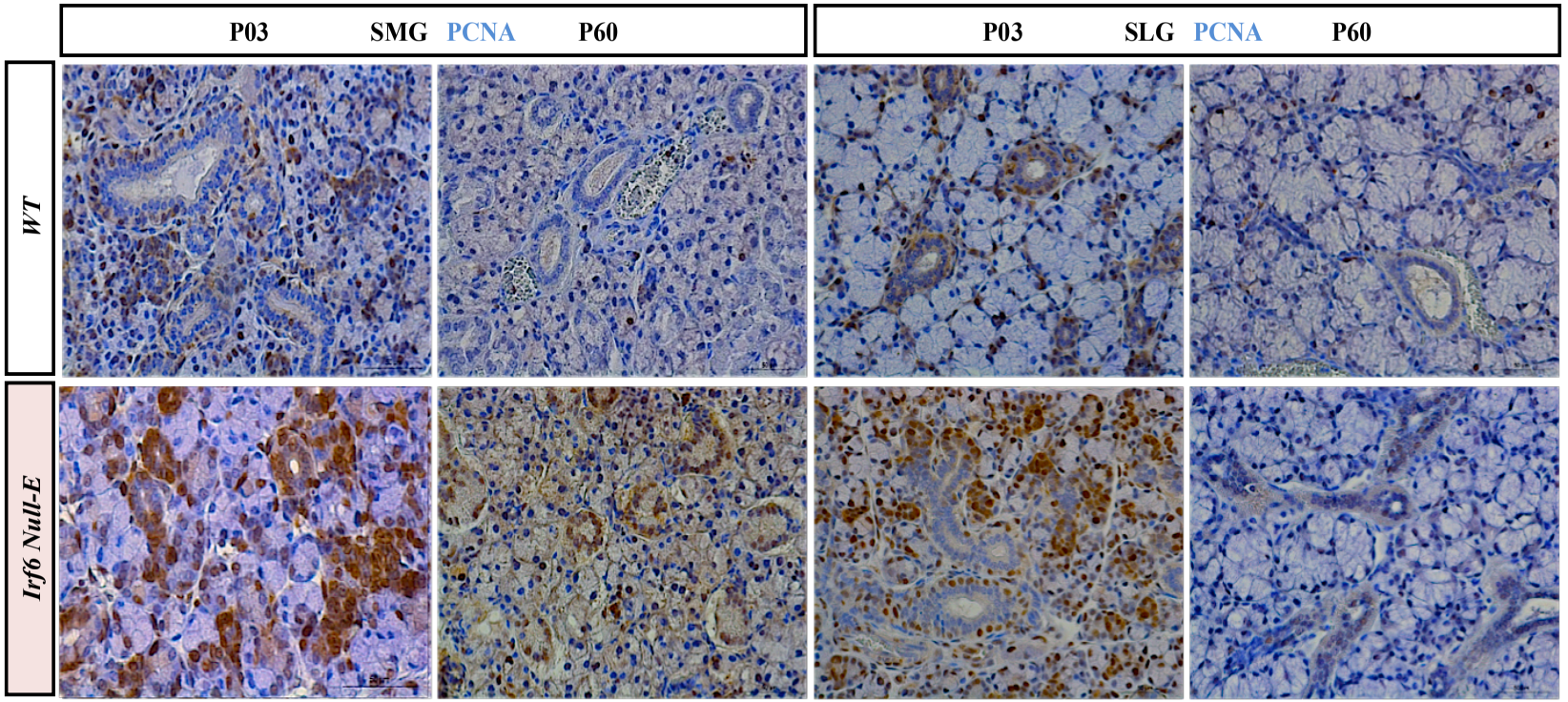


**Figure 4.8: Immunohistochemical localization of PCNA, a marker for cell proliferation.** At P03, loss of Irf6 increased the expression of PCNA. At P60, the *Irf6* null mice displayed persistent and elevated nuclear staining for PCNA compared to the salivary glands from WT animals. PCNA-positive cells were also found within the occluded ducts (arrows).

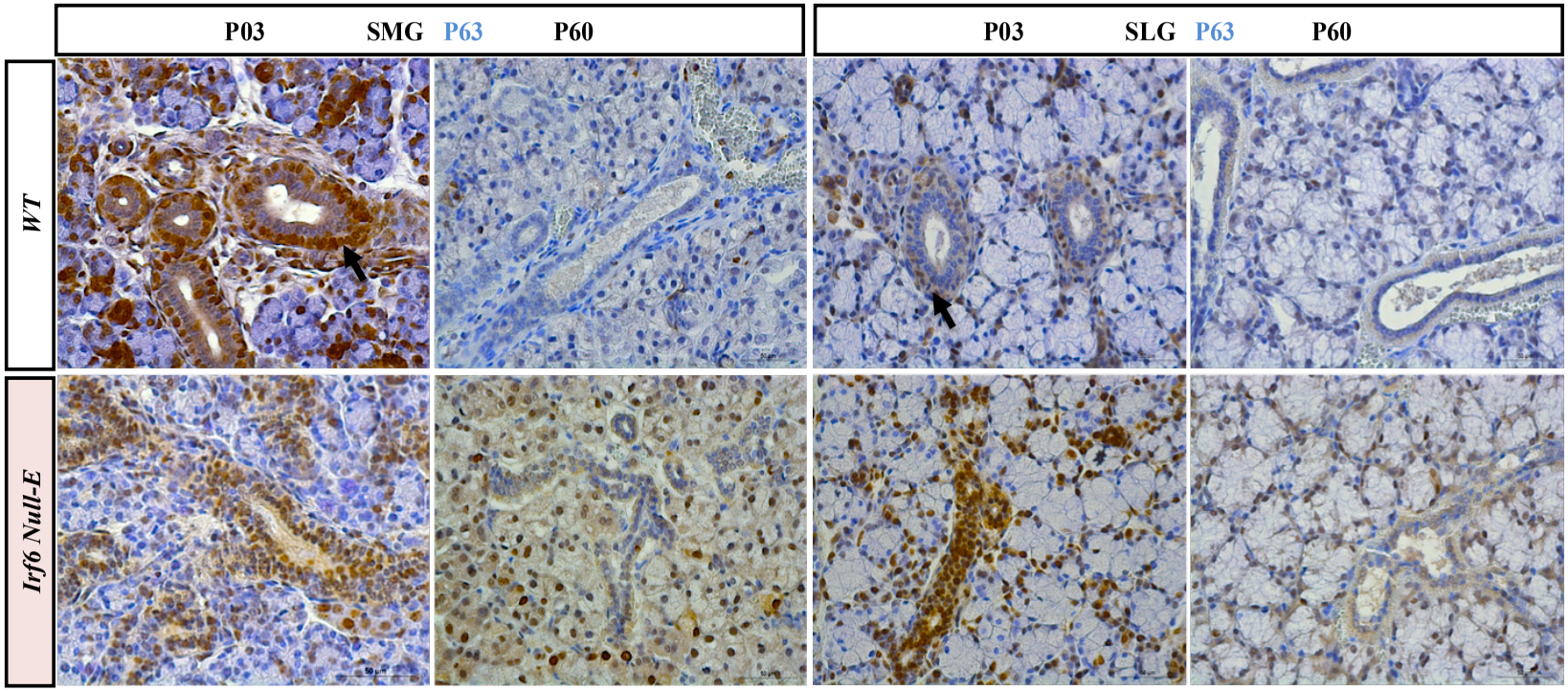


**Figure 4.9: Immunohistochemical localization of P63, a proliferative and basal cell marker.** Ductal cells of SMG and SLG of the *Irf6 Null-E* mice showed increases in P63 expression compared to the basal cell expression in the WT glands. Arrows identify the basal ductal cell layer.

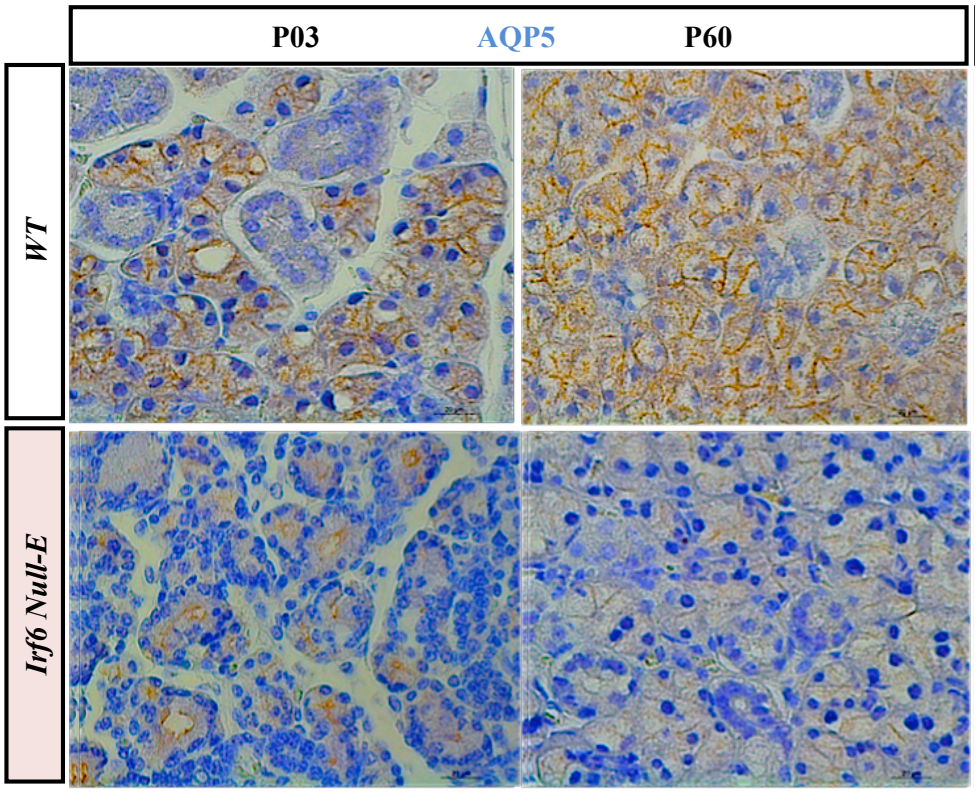


**Figure 4.10: Immunohistological staining of AQP5 as a function and differentiation marker.** AQP5 is expressed on the apical and basolateral membrane of WT serous acinar cells, whereas *Irf6* null acinar cells have reduced apical membrane expression of AQP5 at P03, and reduced and disorganized expression at P60.

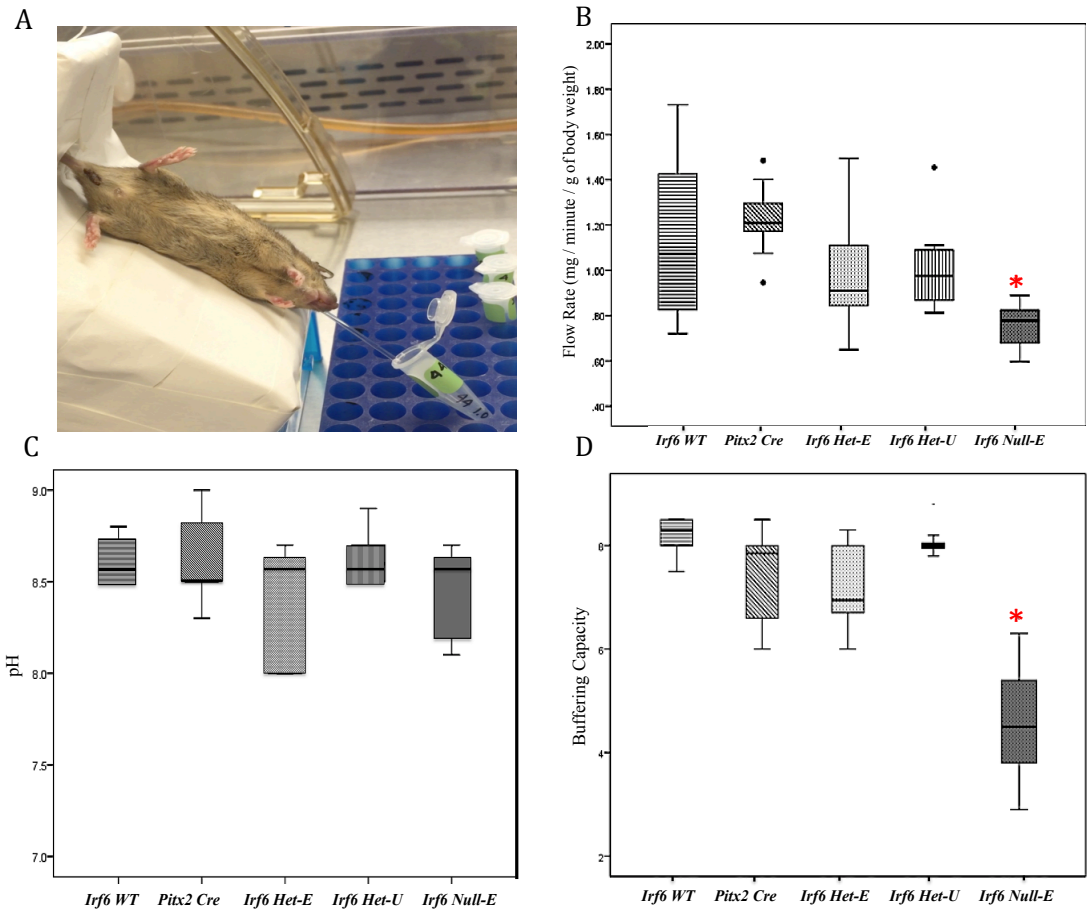


**Figure 4.11: Saliva collection method and salivary function parameters.** (A) Pilocarpine-stimulated saliva collection using gravity-mediated capillary action. Normalized stimulated salivary flow rates (B) and buffering capacity (D) were significantly lower in the *Irf6* null-E mice compared to each of the other genotypes (wildtype (WT) and heterozygotes,*$P < 0.001$). However, saliva pH (C) was within normal range (8 to 9) for all genotypes. n=10 mice/group.

**Table 3: Median, mean and range for salivary gland variables within each genotype.**

| Variables | *WT* | *Pitx2 Cre* | *Irf6 Het-E* | *Irf6 Het-U* | *Irf6 Null* | *P-value* |
|---|---|---|---|---|---|---|
| ***Flow Rate (Mg/min/g)*** | | | | | | |
| **Median** | 1.07 a | 1.21a | 0.97a | 0.98 a | 0.78 b | |
| **Mean±SD** | 1.14±0.34 | 1.22±0.15 | 0.97±0.23 | 1.02±0.21 | 0.75±0.10 | <0.0001 |
| **Range** | 1.01 | 0.54 | 0.85 | 0.64 | 0.29 | |
| ***pH*** | | | | | | |
| **Median** | 8.55 a | 8.50 a | 8.55 a | 8.60 a | 8.60 a | |
| **Mean±SD** | 8.58±0.26 | 8.55±0.29 | 8.32±0.53 | 8.58±0.24 | 8.45±0.25 | 0.79 |
| **Range** | 1.00 | 1.00 | 1.70 | 0.80 | 0.60 | |
| ***Buffering Capacity (pH)*** | | | | | | |
| **Median** | 8.30 a | 7.85 a | 6.95 a | 8.00 a | 4.50 b | |
| **Mean±SD** | 8.22±0.33 | 7.49±0.90 | 7.12±0.81 | 8.10±0.31 | 4.57±1.11 | <0.0001 |
| **Range** | 1.00 | 2.50 | 2.30 | 1.00 | 3.40 | |

T

he medians were compared using the Kruskal-Wallis method. Lower case letters (a and b) indicate the pairwise comparison between groups among the values at the same horizontal line, based on Bonferroni correction for multiple comparison tests. Groups that have a different letter indicate a median value that differs significantly from the others (P>0.01). n= 10 mice/ge

# 5 Chapter 5: The influence of Irf6 ablation on dental caries development and bacterial viability.

## 5.1 Introduction

Cleft lip and palate is one of the most common birth defects and has been found to be associated with multiple dento-facial anomalies, including hypoplastic teeth, supernumerary teeth, microdontia and defects of the orbicularis oris muscle (Jugessur et al., 2009; Walker et al., 2009). Despite this strong association, there have been few studies directly investigating a common etiologic or pathologic mechanism. Nevertheless, in view of this associated spectrum of anomalies, numerous studies have investigated the risk of caries development in the CLP population, with the vast majority reporting an increase in caries incidence and severity (Ahluwalia et al., 2004; Wells, 2014). However, the cause of the observed increase in caries is largely unknown, making it difficult to manage and prevent.

Maintaining good oral health in children with clefting is essential to the success of the treatment outcomes, especially orthodontic treatment. However, the challenges in establishing and maintaining good oral health in this population are numerous and include decreased access to dental brushing as a consequence of the anatomy of the cleft area, malpositioned teeth, limited mobility of the upper lip, and the use of pre and post surgical appliances (Ahluwalia et al., 2004; Gaudilliere et al., 2014; Shashni et al., 2015).

Caries is a multifactorial, principally microbial disease, the susceptibility of which can be impacted by numerous host systems, including oral bacterial load, enamel integrity, and salivary gland physiology. Oral bacterial loads have been found to differ in children with orofacial clefts, possibly due to the open communication between the nasal cavity and any remaining defects in the palate (Chuo et al., 2009; Weiss et al., 2005). A genetic contribution to dental caries has been also described in individuals with CLP. Associations between polymorphisms in the transforming growth factor beta (TGFB3) and the defensin beta 1 (DEFB1) genes and high caries scores in children with cleft lip and palate have been reported (Akota et al., 2014; Antunes et al., 2014). These genes have been implicated in biological mechanisms that when disrupted could lead to increase risk of dental caries. For example, TGFB3 is the main regulator of the morphogenesis of many developing organs such as palate, tooth and salivary gland (Hall et al., 2010; Huang et al., 2010).

Oral colonization by Streptococcus mutans and caries development is reduced upon deletion of carbonic anhydrase VI expression in saliva. The DEFB1 gene, which encodes beta 1 defensin salivary antimicrobial peptide, has been implicated in the resistance of epithelial surfaces to microbial colonization (Polesello et al., 2015). However, it is not clearly understood whether poor oral hygiene as a consequence of clefting or other biological mechanisms is responsible for predisposing this population to dental caries.

The complex multifactorial nature of dental caries necessitates a tractable in vivo model system. The conditionally targeted mice for the cleft gene, *Irf6*, causes an array of tooth anomalies (as

described in patients with CLP; Chu 2015 and Chapter 3) and salivary gland hypofunction (Chapter 4). In the *Irf6* tissue-specific knockout, deletion occurs only in the oral epithelium after the maxillary and medial nasal processes have fused to form the lip / primary palate, and consequently, a cleft lip/palate phenotype does not occur. Therefore, these mice provide an ideal system with which to investigate the risk factors for caries progression in CLP population.

Given the possible role for *Irf6* in innate immunity (Kwa et al., 2014; Ramnath et al., 2015), bacterial viability will also be assessed to investigate if the colonization of the oral cavity by different strains of bacteria may be enhanced in the *Irf6* mouse model. These results would ultimately translate into more effective caries prevention in a population of cleft lip and palate patients.

## 5.2 Results

### *5.2.1 S. mutans colonizes and persists in the mouse oral cavity following an oral dose of ~1x10$^8$ cells.*

In a pilot study of eight female animals (2 x *Irf6 WT*, 2 x *Irf6 Het-E*, 2 x *Irf6 Het-U*, and *2 x Irf6 Null-E*), I tested the susceptibility of *Irf6* conditional knockout mice and their controls to infection by *S. mutans*. The bacterial strain *Streptococcus mutans UA159* was selected for the experiment, which was performed using oropharyngeal swabbing method (Paper et al., 2005). This method involves inoculation with the bacteria on three consecutive days starting at 17 days of age. Two days prior to the inoculation, all animals were swabbed to test for indigenous *S.*

*mutans* in their oral flora. Only mice that tested negative were included in the study. Mice were screened for infection at five days and also at eight weeks after the initial inoculation by streaking oral swabs on Mitis Salivarius Agar (MSA) containing streptomycin. All animals tested positive for the infection at both time points. These data confirm that a single species of oral bacteria can colonize the mouse oral cavity and allowed the inoculation experiment to be performed as described in Chapter 2.

### *5.2.2 Dental caries develop in the absence of cariogenic diet in the inoculated mutant but not WT mice*

The second aim of the pilot study was to assess if any caries would be detectable after *S. mutans* inoculation, in the absence of the cariogenic diet. The same eight mice used in the previous experiment were fed regular diet (5053, PicoLab Rodent Diet 20) and water, and followed up for eight weeks from the initial inoculation. At eight weeks, the mice were euthanized and subjected to assessment for caries detection using a dissecting microscope. Occlusal surface caries were visible mainly in the maxillary, and to a lesser degree in the mandibular, teeth of the *Irf6 Null-E* mice. Occlusal surface caries were also visible, albeit to a noticeably lesser extent, in the *Irf6 Het-E* mice, but not evident in the *Irf6 Het-U* or wild-type animals (figure 5.1). These data are consistent with a gene dosage effect for the loss of *Irf6*, and exacerbated by reduced *Pitx2* expression (from Pitx2-Cre allele). However, it is unclear if the effects were due to altered tooth morphology and reduced mineral density (Chapter 3), abnormal salivary gland development / function (Chapter 4) or related to the role of Irf6 in innate oral immunity. Nevertheless, the data do indicate that *Irf6* ablation in the oral epithelia increases the animal's susceptibility to dental

caries even in the absence of high levels of fermentable carbohydrates in the diet.

### *5.2.3 Massively increased caries incidence and severity in the Irf6 null mouse model*

To further determine whether the ablation of *Irf6* alters the severity and incidence of dental caries, animals of each of the different genotypes were inoculated with *S.mutans* bacteria at 15 days of age, to avoid the earlier colonization of endogenous *S.mutans* observed in the pilot study. Starting from the first day of inoculation, mice were fed a soft cariogenic powder diet (56% sucrose). The soft diet minimizes the tooth wear .The powdered diet did not constrain the eating behavior of any of the mice included in the study, as their mean weight gain was comparable to matched genotype control animals fed on regular standard rodent chow.

Caries examination was performed blind to the mouse's genotype. A determination of the number of surfaces involved in carious teeth was evaluated under a dissecting microscope (figure 5.2). A score of 0 was given for an intact surface, 1 for carious lesion(s) affecting the occlusal surface only, and 2 for carious lesion(s) affecting one smooth surface only. Scores of 3, 4, and 5 were assigned for carious lesion(s) affecting occlusal surfaces and one, two, or more than two smooth surfaces, respectively.

In addition, the severity of carious lesions was evaluated following microCT imaging (figure 5.3) using the DataViewer software (Bruker) according to Keyes' scoring system with modification (Keyes, 1958). This second scoring system was employed in which a score of 1 was given for radiolucency within the enamel but not reaching the dentino-enamel junction, 2 for

radiolucency within the dentin but just below the dentino-enamel junction, 3 for radiolucency half way below the dentino-enamel junction, and 4 for radiolucency reaching the pulp. Each molar tooth was evaluated utilizing the two scoring systems, after which the total caries scoring was calculated, compared by Kruskal-Wallis with Bonferroni correction for multiple comparison tests. The number of teeth presenting with dental caries on different surfaces and at varying degrees of severity in mandibular and maxillary molars is shown in figure 5.4 (A, A') and figure 5.4 (B, B'), respectively.

Individual tooth surfaces have been reported as exhibiting different susceptibilities to caries. This is thought to be mainly due to different tooth surface morphologies, with occlusal surfaces (due to the pits and fissures) being the most susceptible and the smooth (labial and lingual) surfaces being the least susceptible ( Chestnutt et al., 1996; Hannigan et al., 2000). In the *Irf6 Null-E* mice, 32% of the teeth have occlusal caries, compared to 33%, 28%, 8% and 8% in the *Pitx2 Cre, Irf6 Het-E*, *Irf6 Het-U,* and WT mice, respectively. In contrast, 60% of the *Irf6 Null-E* mice molars have a combination of occlusal and smooth surface caries, compared to 7%, 8%, 0%, and 0% in the *Pitx2 Cre, Irf6 Het-E*, *Irf6 Het-U,* and WT mice respectively. In the *Irf6* null mice, the massive increase in smooth-surface caries also correlated with increased caries severity, with 53% of teeth from the *Irf6 Null-E* animals exhibiting dental caries that extensively destroyed enamel and dentin and reached the pulp. The first and second maxillary and mandibular molars were nearly completely disintegrated, and almost all of the dental roots had been lost. Moreover, alveolar bone resorption of the mandible and maxilla was evident as shown in figure 5.3.

When the two scoring systems were combined, the mean total caries score of *Irf6 Null-E* mice

(71.7; Figure 5.5) was more than 35 fold higher than that of *Irf6 Het-U* and WT controls (2; $P < 0.0001$; Figure 5.5) and over 4 fold more severe that both the *Irf6 Het-E* and *Pitx2 Cre* mice (17.1; Figure 5.5). Notably, both the *Irf6 Het-E* and *Pitx2 Cre* mice showed an average 8 fold greater severity of caries than the WT and *Irf6 Het-U* mice. However, because of the marked variability in presentation in the *Irf6 Het-E* and *Pitx2 Cre* mice, this was not found to be significant after Bonferroni correction. It is possible that with inclusion of a larger number of specimens that this could become significant for these genotypes. Nevertheless, this tendency towards an increase in caries severity in the *Irf6 Het-E* and *Pitx2 Cre* mice could be explained by the enamel mineralization defects that were also observed in these mice (Chapter 3).

### *5.2.4 Blood glucose levels*

To determine whether the mice that were fed high-sucrose diet developed diabetes, blood glucose level was measured from the tail vein using a digital glucometer (Accu-Chek Advantage). All animals showed values within normal ranges (blood glucose level less than 120 mg/dL) throughout the experimental period.

### *5.2.5 Irf6 null mice exhibited a significant increases in total and S. mutans bacteria populations*

Mutans streptococci are acidogenic bacteria that, when adhered to tooth surfaces, utilize carbohydrates to produce acids, leading to a breakdown in the normal homeostasis of commensal microorganisms. The acidity leads to a shift toward more pathogenic bacteria and ultimately

results in the initiation of dental caries. A laboratory technique to estimate total oral bacterial colonies growing on BA media and *S. mutans* colonies growing on MSA media was used. Two blinded investigators did the bacterial colony counting, and the average of the two readings was been utilized. Significant loads of total and *S.mutans* bacteria were detected in all animals observed in our study up to eight weeks after initial inoculation. The number of total bacterial and *S.mutans* colony forming units was significantly higher ($P<0.001$) in *Irf6* Null mice compared to their respective heterozygotes, Pitx2 Cre and wild-type (WT) littermates (table5.1 and figure 5.6), suggesting that *Irf6* ablation enhances the bacterial colonization in the oral cavity.

## 5.3 Discussion

Given the altered tooth morphology, delayed mineralization, and the altered salivary gland structure and function in the *Irf6* conditional mouse model, the consequence of *Irf6* ablation on caries development were assessed. As dental caries do not naturally develop in rodents, a common caries induction protocol using cariogenic bacteria and high carbohydrate diet was employed.

Interestingly, in the pilot study, *Irf6 Null-E* and to lesser degree *Irf6 Het-E* mice developed occlusal caries when infected with *S. mutans* even when fed a non-cariogenic, standard laboratory diet. Deep pits and fissures on the occlusal surfaces of molars are more prone to carious lesions because these regions provide an excellent site for food impaction and bacterial stagnation (Konig, 1963; Wang et al., 2012a). In a similar way, the altered morphology of the

*Irf6* null mice, where the buccal and lingual cusps were fused together partially or completely leaving a deep groove and sometimes a fossa in the center of the crown (figure 3.3) may have enhanced the caries susceptibility. This could also explain the location of the caries, in which only the deep pits and fissure of the *Irf6* null mice and to lesser degree the *Irf6 Het-E* mice showed carious lesion (figure 5.1). Moreover, earlier acquisition of endogenous *S. mutans* was observed in the *Irf6* null animals compared to all other genotypes. Association between the earlier acquisition of *S. mutans* and increased caries risk is well documented in the literature (Law et al., 2007; Nogueira et al., 2005), An early appearance of *S. mutans* was reported in the mouth of toothless infants when obturators were inserted to fix cleft palates compared to those that were not obturated (van Loveren et al., 1998). In the pilot study, I showed that even in the absence of overt clefting or a cariogenic diet, the ablation of the clefting gene *Irf6* in mice increases the risk of dental caries and alters the commensal oral microbiota.

Next, caries development was assessed in animals of the same genotypes under a high cariogenic diet. The incidence and severity of both smooth and occlusal surface caries of mandibular and maxillary molars were massively elevated in the *Irf6 Null-E mice*. Significant increases in caries incidence and severity have been observed in *Aqp5* deficient mice with a 60% reduction in salivary flow rate and decreased water content of saliva (Paper et al., 2005) and in a mouse model of cystic fibrosis with low saliva buffering capacity (Catalán et al., 2011). A combination of salivary hypofunction and enamel mineralization defects was associated with excessive wear and higher caries experience in a mouse model of hyperglycemia (Akita-/-) (Yeh et al., 2012). In a similar way the enamel mineralization defects, decreased salivary flow rate and salivary

buffering capacity, may all be influencing caries in the *Irf6 Null-E* mice.

One possible mechanism for the increase in caries susceptibility and severity in the *Irf6 Null-E mice* is the enamel mineralization defects observed in these mice. In human studies, positive associations between genetic variation in genes involved in enamel formation and increased caries susceptibility have been reported, including amelogenin (Deeley et al., 2008; Jeremias et al., 2013), tuftelin (Patir et al., 2008; Slayton et al., 2005), and enamelin (Jeremias et al., 2013). However, although both *Pitx2 Cre* mice and mice doubly heterozygotes for the *Pitx2 Cre* and the *Irf6* floxed allele also present with significantly reduced enamel mineralization, the mean caries score of these mice was considerably lower compared to that observed in the null mice. Therefore the salivary glandular hypofunction and saliva compositional changes, rather than the mineralization defect, are more likely as mechanisms for the massive caries severity observed in the *Irf6 Null-E mice*.

Saliva has an essential role in protection against dental caries, through its cleaning, diluting, and buffering capacity, demineralization and remineralization control, and its antimicrobial activity (Brosky, 2007; de Almeida et al., 2008). Interfering with any of these processes may compromise the protective functions of saliva and enhance caries. For example, *Irf6* null mice have significantly reduced stimulated salivary flow and buffering capacity. In patients with reduced salivary flow rate, oral clearance and buffering capacity are also reduced. Impaired salivary clearance has been associated with high caries incidence in both the elderly and 'dry mouth' patients, and it was previously reported in cleft lip and palate population (Ahluwalia et al., 2004; Gati et al., 2011; Risheim et al., 1992). A high correlation between reduced buffering

capacity and increase in prevalence of dental caries is well documented in the literature (Cunha-Cruz et al., 2013; Featherstone, 2000; Sánchez et al., 2003). The inability of saliva to clear bacteria and food particles, leads to increased bacterial loads reduced buffering capacity and potentially lower local pH. The acidic environment favors demineralization rather than remineralization, leading to lesion progression from initial demineralization to non-cavitated lesions, and eventually to severely cavitated lesions (Carounanidy et al., 2009; Leone et al., 2001), similar to what was seen in the *Irf6* null mice.

Saliva is also a key player in remineralization by acting as calcium and phosphate reservoir that can replace lost minerals in hard tooth structures (Cunha-Cruz et al., 2013). The relative concentrations of the organic salivary constituents are known to depend on salivary flow rate (Rudney, 1989). Therefore, reduced flow rate could be combined with altered mineral content to enhance tooth decalcification, and increase caries susceptibility.

Maintaining the stability of the microbial composition of the oral cavity is crucial for caries prevention. This stability (microbial homeostasis) can be disturbed by either change in the local environment or decreased host immunity elements, mainly controlled by saliva. It is well known that *S.mutans* bacteria are capable of initiating changes in the plaque ecology to support the growth of acid- producing and acid-tolerant species leading to dental decay in both human and animal models (Culp et al., 2011; Kristoffersson et al., 1985; Sundell et al., 2015). The level of *S.mutans* bacteria in plaque and saliva has been used as an indicator of caries risk (Kristoffersson et al., 1985; Parisotto et al., 2010). A variety of other bacterial species can also produce acids from a high-sucrose diet and could contribute to caries initiation, including non-mutans

streptococci such as *S. gordonii, S. mitis, S. oralis* and *S. anginosus* (van Houte et al., 1996). The *Irf6 Null-E* mice exhibit enhanced susceptibility to *S.mutans* infection. This was clearly reflected in the higher bacterial burdens in null mice as opposed to the other genotypes and wildtype mice. A significant increase in the mean total oral bacterial abundance in the *Irf6* Null mice compared to all other genotypes was also found.

Changes in the quantity and the quality of the saliva lead to a rise in bacterial adherence and generation of plaque forming bacteria on the tooth surfaces. As a result, patients with xerostomia (dry mouth) have extensive dental caries, rampant levels of *S. mutans* and increased risk of oral candidal infection (Furness et al., 2011; Risheim et al., 1992).

Saliva also contains several innate and adaptive immune mediators that function to restrict microbial growth and colonization of microorganisms in the oral cavity. For example, antimicrobial peptides in the saliva provide non-specific innate immune defense. These include α-defensins, β-defensins, cathelicidin LL37 and calprotectin. A positive correlation between the concentrations of the defensins in the saliva of adolescents and Mutans Streptococci counts from plaque has been previously reported (Phattarataratip et al., 2011). In further support of this is the correlation between genetic variation in the promoter region of DEFB1 (encoding β-defensin), β-defensin concentration in saliva, and susceptibility to dental caries have been reported in children with cleft lip and palate (Akota et al., 2014). Lower levels of salivary defensins have also been found to be indicators of salivary gland hypofunction (Tanida et al., 2003). Thus, the association

between salivary gland hypofunction and low secretory antimicrobial peptide secretion rates is one mechanism suspected of influencing susceptibility to infections in the *Irf6* null mice. Further knowledge of the properties of different components of salivary secretions may permit a better understanding and assessment of dental caries susceptibility in these mice and ultimately in the cleft lip and palate population.

## 5.4 Figures and tables

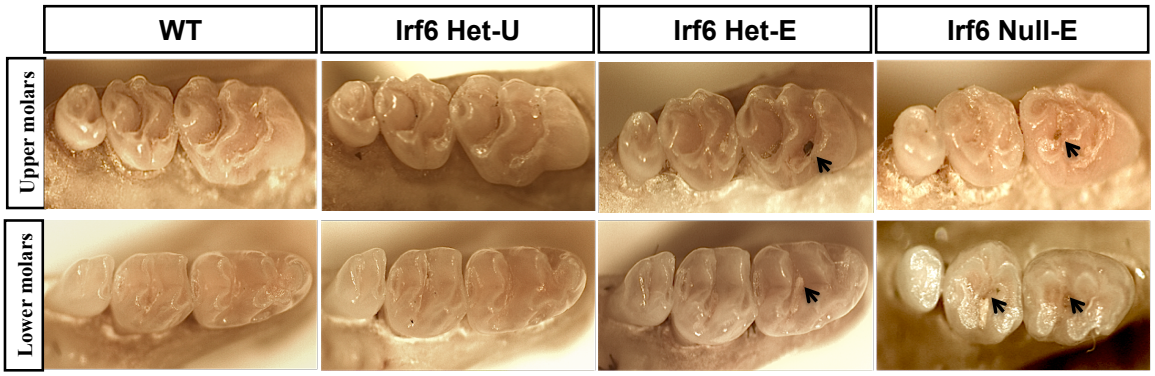


**Figure 5.1: Dental caries develop in the absence of cariogenic diet in *Irf6* mutants.** Occlusal views of representative mandibular and maxillary jaws from wild type and mutant mice, showing occlusal caries (black arrows) in the epithelial null and heterozygote mice.

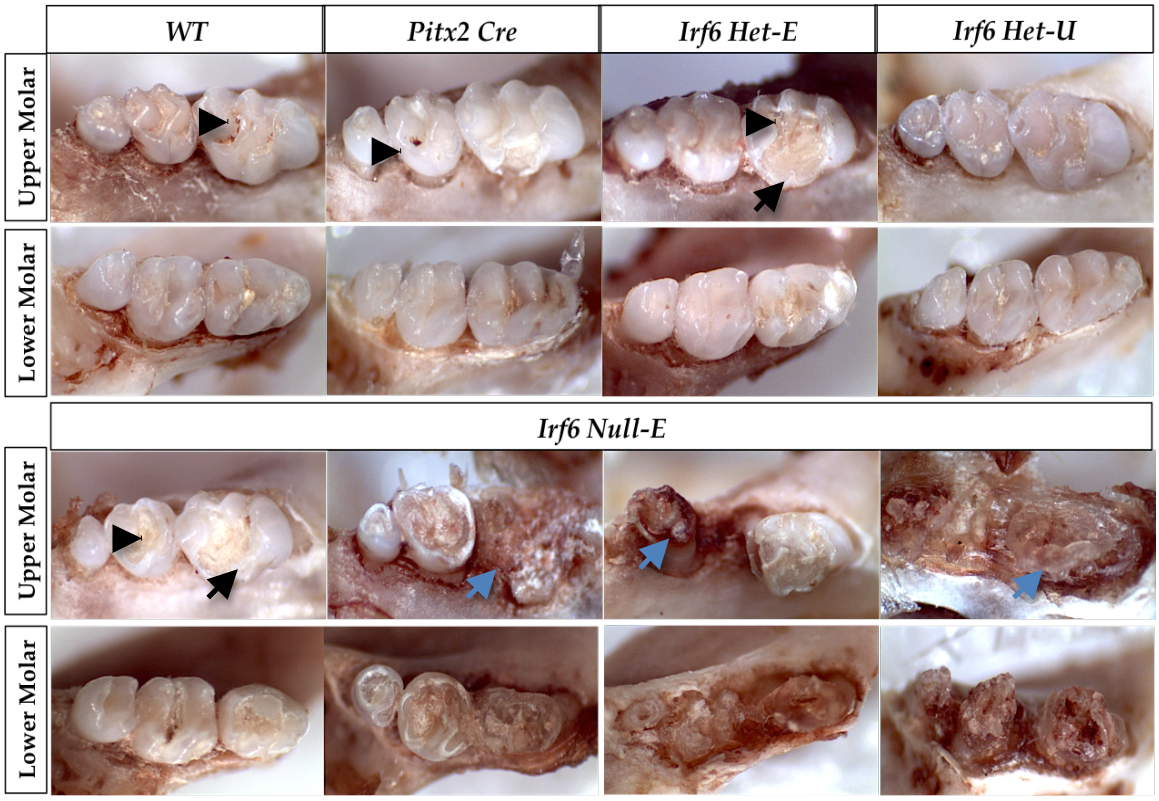


**Figure 5.2: *Irf6* mutants showed a massive increase in the incidence of caries.** Dissecting microscope images of caries in mandibular and maxillary molars of *Irf6 Null-E* mice, *Irf6* heterozygotes, and WT and *Pitx2 Cre* controls. Normal intact molars/very mild occlusal caries (arrowhead) in the wild type and Irf6 Het-U mice. Occlusal caries (arrowhead) and smooth surface caries (black arrow) mainly in the first molar of *Irf6 het-E* and *Pitx2 Cre* mice. Whereas, Severe carious lesions where caries expands to the dental root, resulting in a completely decayed crown (blue arrow) was the main presentation of dental caries in the *Irf6 Null- E* mice.

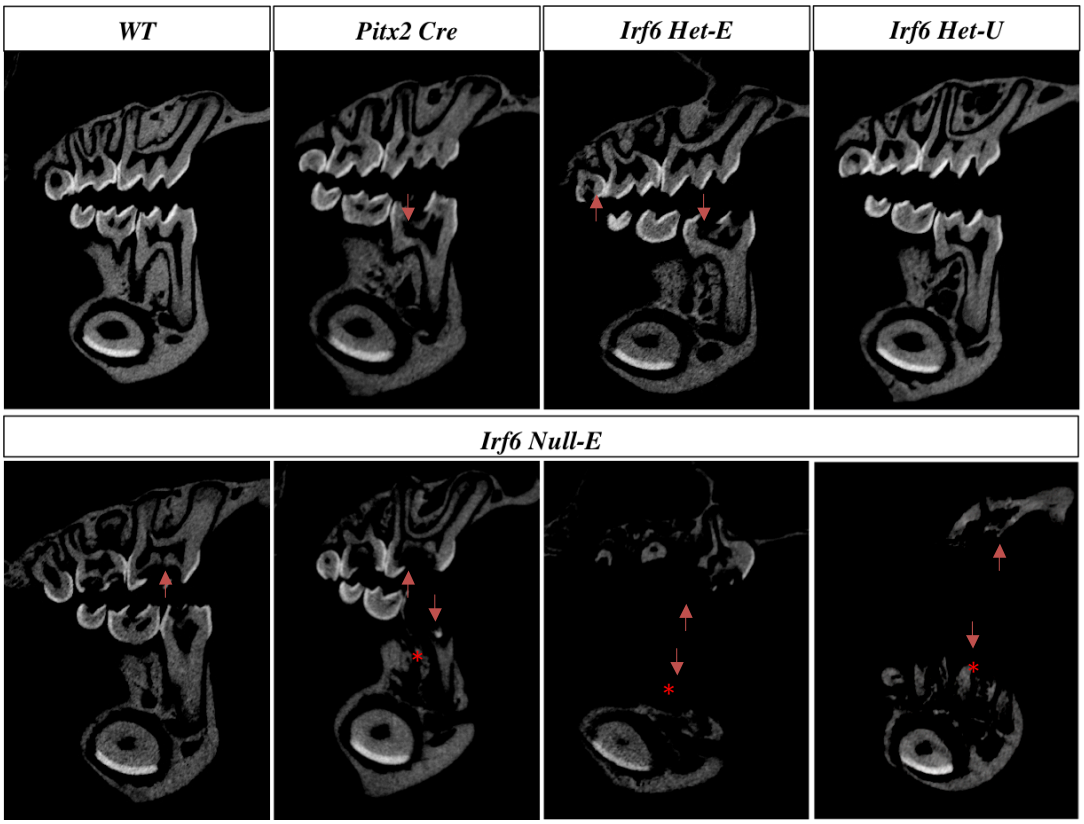


**Figure 5.3: *Irf6* mutants showed a massive increase in the severity of dental caries.** Micro-CT images of caries in mandibular and maxillary molars of *Irf6 Null-E* mice, *Irf6* heterozygotes, and WT and *Pitx2 Cre* controls. Upper panel showed healthy intact molars in WT and *Irf6 Het-U*. Dental caries with a focal radiolucent areas (arrow) in the crown were observed in Irf6 Het-E and *Pitx2 Cre* mice. Consistent with the macroscopic observation, extensive carious lesions with a completely decayed crown and root caries were the main presentation in the *Irf6 Null- E* mice. Alveolar bone resorption of the mandible (asterisks) was only observed in the *Irf6* Null mice.

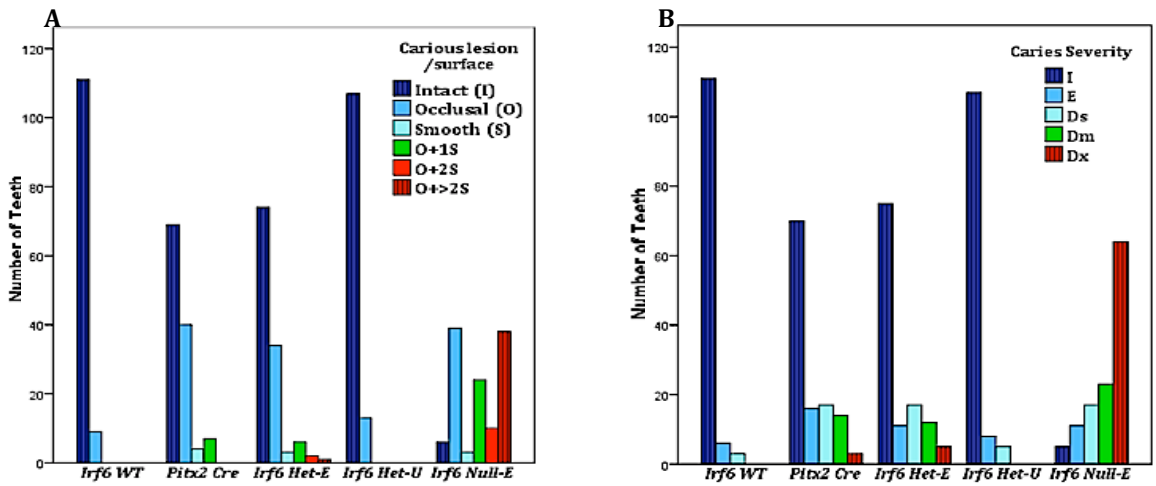


A B'

| Carious Lesion/ surface | Irf6 WT | Pitx2 Cre | Irf6 Het-E | Irf6 Het-U | Irf6 Null-E |
|---|---|---|---|---|---|
| | | | n=120 teeth/group | | |
| Sound | 111 (92.5) | 69 (57.5) | 74 (61.7) | 107 (90.6) | 6 (6.00) |
| Occlusal Surface (OS) | 9 (7.50) | 40 (33.3) | 34 (28.3) | 13 (9.40) | 39 (32.5) |
| Smooth Surface (SS) | 0 (0) | 4 (3.30) | 3 (2.50) | 0 (0) | 3 (1.70) |
| OS+1 SS | 0 (0) | 7 (5.80) | 6 (5.00) | 0 (0) | 24 (20.8) |
| OS+2 SS | 0 (0) | 0 (0) | 2 (1.70) | 0 (0) | 10 (4.20) |
| OS+>2 SS | 0 (0) | 0 (0) | 1 (0.80) | 0 (0) | 38 (35.8) |

| Caries Severity | Irf6 WT | Pitx2 Cre | Irf6 Het-E | Irf6 Het-U | Irf6 Null-E |
|---|---|---|---|---|---|
| | | | n=120 teeth/group | | |
| Sound | 111 (92.5) | 70 (58.3) | 75 (62.5) | 101(90.6) | 5 (4.17) |
| Enamel | 6 (5) | 16 (13.3) | 11 (9.17) | 14 (4.20) | 11 (9.17) |
| Slight Dentin | 3 (2.5) | 17 (14.2) | 17 (14.2) | 5 (5.20) | 17 (14.2) |
| Moderate Dentin | 0 (0) | 14 (11.7) | 12 (10.0) | 0 (0) | 23 (19.2) |
| Sever dentin | 0 (0) | 3 (2.50) | 5 (4.17) | 0 (0) | 64 (53.3) |

**Figure 5.4: The number of teeth present with dental caries on different surfaces and severity.** *Irf6* null teeth showed an increase in incidence and severity of dental caries compared to all other matched genotypes. Both *Irf6 Het-E* and *Pitx2 Cre* showed a tendency toward an increase in caries incidence and severity compared to WT and *Irf6 Het-U* mice. (A, A'). A determination of the number of surfaces involved in carious teeth were evaluated under dissecting microscope and expressed as Intact surface (I), occlusal surface only (O), one smooth surface only (1S), occlusal and one smooth surface (O+1S), occlusal and two smooth surfaces (O+2S), and occlusal and more than two Smooth surfaces (O+ >2S). (B, B') Severity of carious lesions was evaluated following microCT imaging and expressed as enamel involvement only (E), slight dentin involvement (Ds), moderate dentin involvement (Dm), and extensive dentin involvement that reaching the pulp (Dx). Values in A' and B' are given as the number of teeth (percentage).

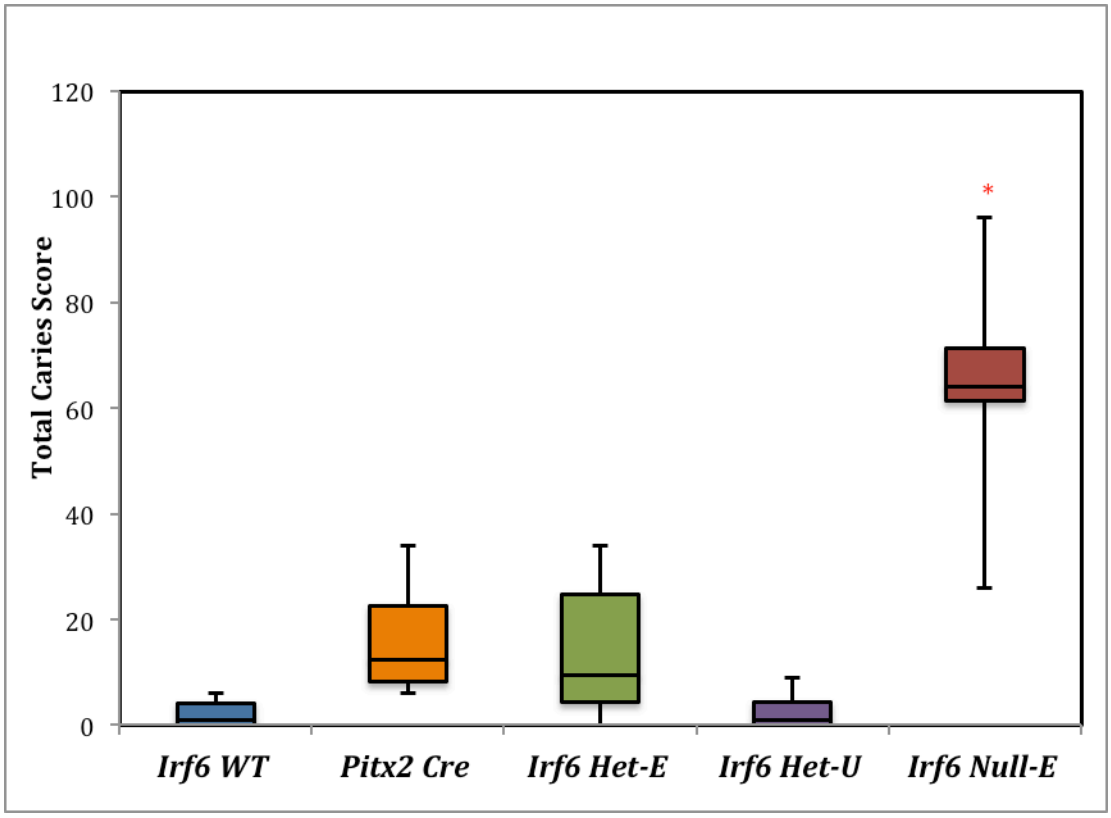


**Figure 5.5: The mean total caries score.** *Irf6* null teeth showed a significant increase in incidence and severity of dental caries (indicated by asterisks, P<0.0001) compared to all other genotypes. The differences in the total caries scores between heterozygote littermates, Pitx2 Cre and WT controls were not statistically different after Bonferroni correction. * Means significant difference at P<0.01. n= 10 mice/genotype.

**Table 4: Median, mean and range for the number of viable bacterial colonies (cfu x $10^5$)**

| Variables | *WT* | *Pitx2 Cre* | *Irf6 Het-E* | *Irf6 Het-U* | *Irf6 Null* | *P-value* |
|---|---|---|---|---|---|---|
| ***Total bacteria*** | | | | | | |
| **Median** | 2.66 a | 3.60 a | 3.60 a | 2.50 a | 4.92 b | <0.0001* |
| **Mean±SD** | 2.60±0.2 | 3.58±0.83 | 3.58±0.20 | 2.51±0.13 | 5.17±0.14 | |
| **Range** | 2.00-2.9 | 2.00-2.90 | 3.30-3.90 | 2.30-2.70 | 3.30-8.10 | |
| ***S. mutans*** | | | | | | |
| **Median** | 2.36 ac | 3.24 ac | 3.36 a | 2.33 c | 4.83 b | <0.0001* |
| **Mean±SD** | 2.73±0.7 | 3.21±0.40 | 3.25±0.43 | 2.36±0.11 | 4.93±0.62 | |
| **Range** | 1.80-3.4 | 2.90-3.60 | 2.50-3.40 | 2.30-2.60 | 4.00-5.70 | |

The medians were compared by Kruskal-Wallis method. Lower case letters indicate the pairwise comparison between groups among the values at the same horizontal line, based on Bonferroni correction for multiple comparison tests. Groups that share even one letter indicate a median value that does not differ significantly from the others (P>0.01). * Means significant difference at P<0.05, n= 10 mice/genotype.

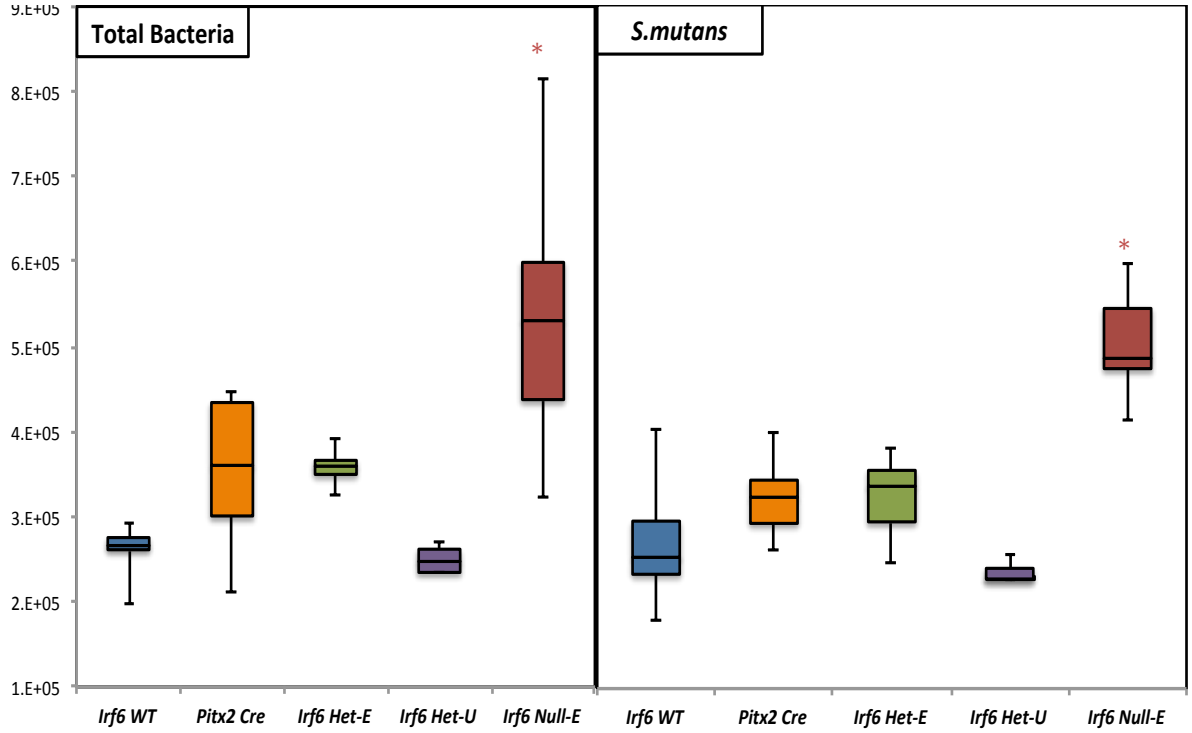


**Figure 5.6: Median, mean and range for bacterial viability within each genotype.** The medians were compared by the Kruskal-Wallis method. *Irf6* null mice showed a significant increase in the total and *s. mutans* bacterial count (indicated by asterisks, P<0.0001) compared to all other genotypes.

# 6 Chapter 6: General Discussion

## 6.1 Summary and future directions

Clefting of the lip and palate (CLP) is the most common birth defect of the face, occurring globally with an incidence of approximately 1 out of every 700 live births. CLP is a complex disease with both genetic and environmental risk factors contributing to its etiology (Dixon et al., 2011; Murray, 2002). Patients with CLP can present with a wide spectrum of subclinical defects that could be considered part of the normal phenotypic spectrum. These include various dental anomalies, often involving hypoplasia of the enamel, as well as discontinuities of the orbicularis oris muscle (Eerens et al., 2001; Jugessur et al., 2009; Tan et al., 2012). Salivary gland aplasia, a very rare developmental defect, as well as changes in saliva composition, have been reported in patients with non-syndromic CLP (Aizenbud et al., 2008; Matsuda et al., 1999; Reija et al., 2013). Individuals with CLP seem to be at increased risk for dental caries (Antunes et al., 2014; Shashni et al., 2015; Wells, 2014). Despite this association, there have been few studies directly investigating a common etiologic or pathobiologic mechanism mainly because of the perinatal mortality seen with most mouse CLP models. Mutations in the *IRF6* gene represent the greatest genetic contribution to both isolated and syndromic CLP (Cobourne, 2004; Rutledge et al., 2010). Defects in IRF6 are also known to cause VWS featuring CLP and dental defects (Kondo et al., 2002). Thus, we here focused on *IRF6* as the most prominent CLP gene.

The overall goal of this research was to assess the function of *Irf6* in oral epithelia during morphogenesis of teeth and salivary glands, and in particular, how it later impacts tooth structure, salivary function and caries susceptibility. To this end, I employed a knockout mouse with targeted ablation of *Irf6* in oral epithelium. Not only did these mice show an array of tooth abnormalities resembling those observed in CLP populations (i.e., hypodontia, taurodontism and abnormally shaped teeth; see Chapter 3), but by bypassing the cleft phenotype, they permit investigation of the gene's other roles in caries-associated biological risks and the actual development of dental caries.

In Chapters three and four, I analyzed the role of *Irf6* in the organogenesis of two ectodermal organs, the tooth and major salivary glands. Chapter three revealed that the full range of CLP-associated dental defects was recapitulated in *Irf6* null mice, including hypodontia, supernumerary teeth, alteration in crown and root morphologies including taurodontism and enamel mineralization defects. Previous studies demonstrated Irf6 is also expressed in the submandibular salivary gland (Fakhouri et al., 2012; Laugel-Haushalter et al., 2012). However, its role in salivary gland organogenesis and importance for salivary gland function was unknown. Thus, Chapter four examined the effect of *Irf6* ablation on salivary gland development. I found that *Irf6* ablation drastically alters the structure of both major salivary glands investigated. Salivary glands from *Irf6* null mice exhibited persistent dysplastic changes, and an overall disorganized structure. Utilizing IHC, salivary glands of the *Irf6* null mice showed reduced and disorganized expression of E-cadherin and NME2, two key regulators of epithelial

adhesion strength and polarity, suggesting that *Irf6* ablation may alter salivary cell polarization and thus cell differentiation through an inability to organize epithelial cell-cell junctions properly. In line with this, *Irf6* null mice showed elevated epithelial proliferation as detected by an increase in PCNA staining and reduced acinar cell differentiation as detected by weaker and disorganized staining of the marker AQP5. As a consequence, salivary gland hypofunction, including a low flow rate, reduced buffering capacity, as well as changes in mucin distribution were observed in the null mice.

Taken together, the results from Chapter 3 and 4, in conjunction with previous data from the Cox lab (Chu, 2015; Parada Sanchez, 2012), support a role for *Irf6* during tooth and salivary gland development that is likely due to a functional role of *Irf6* in organization of the epithelial cell junctions and epithelial cell polarity. When this function is perturbed, the epithelia fail to organize and undergo the morphogenetic processes necessary to complete development of the respective tissues properly. Deconstruction of cell-cell junctions, in turn, leads to increases in proliferation (a well-known phenomenon tied to reduced epithelial adhesion), and altered epithelial cell terminal differentiation.

## 6.2 The role of Irf6 in the establishment of epithelial polarity

Cell polarity, in which cells orient to generate asymmetry along the apical-basal cell axis, is a key feature for proper epithelial tissue organization and function (Royer et al., 2011; Shin et al., 2006) Adhesion receptors, specifically integrins and cadherins, regulate cell-matrix and cell-cell

attachment and polarity and transmit signals between the cells and their environment (Daley et al., 2012; Shin et al., 2006). The Rho family of GTPases, including Rac1 and RhoA, are crucial regulators of both upstream and downstream signaling pathways of cadherin and integrin adhesions (Takaishi et al., 1997). The Rho GTPase family functions in the establishment of cell polarity through the modulation of actin cytoskeleton organization to regulate the assembly and disassembly of E-cadherin complexes (Kuroda et al., 1997; Menko et al., 2002). In addition, proper regulation of RhoA activity is critical to keratinocyte differentiation (Vaezi et al., 2002). For example, matrix focal adhesion was found to be altered and cell proliferation increased when Rho-associated coiled-coil containing protein kinase (ROCK II) was ablated (Adachi et al., 2011; Nakashima et al., 2011).

Cytoskeletal organization in the ameloblast has been proposed as a crucial process in the organized formation of the enamel matrix (Nishikawa et al., 1988). During tooth development, Rac1 and RhoA are expressed in the enamel organ, with higher expression in differentiated ameloblasts (polarized cells) compared to the inner and outer cells of enamel epithelium (non-polarized cells) (Biz et al., 2010). Ameloblasts carry integrin cell receptors which contribute to amelogenesis by mediating cell adhesion with the enamel extracellular matrix proteins (Huang et al., 2008). Integrin α6β4 interacts with laminin α5 and signals through the Rac/cdc42 pathway to regulate cell polarity of inner dental epithelium and initiate ameloblast differentiation (Filipenko et al., 2005). Ameloblasts completely polarize as they mature into the secretory stages, with RhoGDI (an inhibitor of Rac1 and RhoA) being downregulated as this process proceeds (Hatakeyama et al., 2009). Moreover, Rac1 conditionally deleted mice exhibited disorganized

secretory ameloblasts, and reduced amelogenin and ameloblastin expression, whereas amelogenin knockouts express higher levels of RhoGDI (Hatakeyama et al., 2009; Huang et al., 2011).

In line with this integrin-mediated adhesion, Rho GTPase-mediated contraction and E-cadherin down-regulation by the Rac GTPases are required for the proper invagination of Drosophila embryonic salivary gland epithelia, the collective migration of the gland, and the control of lumen length (Harunaga et al., 2011; Pirraglia et al., 2006, 2013). Loss of Rac GTPases during salivary gland development leads to failure of the gland to migrate and reduced lumen length, whereas constitutive activation of Rac1 leads to dispersal of the salivary gland cells and loss of gland integrity (Pirraglia et al., 2006). ROCK activity is also required during initiation of branching in the salivary gland, and for basement membrane placement, and specifically deposition and accumulation of fibronectin and collagen IV (Daley et al., 2009). ROCK1 also mediates epithelial cell polarity through the polarity protein, Par1b, in the columnar outer epithelial layer of the developing submandibular salivary gland (Daley et al., 2012).

Previous data from the Cox lab showed that during primary palatal fusion, Irf6 interacts with the NME complex to regulate pre-fusion oral epithelial polarity, and HEK293T cells ectopically expressing a mutation to disrupt IRF6: NME interaction displayed increased levels of Rac1 and RhoA (Chu, 2015; Parada Sanchez, 2012). Irf6 deficient keratinocytes also express higher RhoA levels (Chu, 2015). Arhgap29, a GTPase activating protein, has been also identified as a

downstream target of Irf6, and Irf6 deficient keratinocytes exhibit lower levels of Arhgap29 (Biggs et al., 2014). In line with this, genetic deletion of *Irf6* in embryonic mouse oral epithelium (Irf6 Null-E) results in down regulation and redistribution of NME2 expression in the ameloblasts of developing tooth (Chu, 2015). In Chapter 4, I show that *Irf6* is also regulating NME2 localization during salivary gland development and that, as a consequence of *Irf6* ablation, NME2 and E cadherin expression is disorganized and substantially reduced. In addition, cell proliferation is remarkably increased in these cells. It has previously been shown that a major role of the NME complex is the direct binding to and regulation of the activating complexes for Rac1 and RhoA. It is therefore expected that the role of the IRF6: NME complex is to modulate Rho GTPase family activity including Rac1 and RhoA to permit proper epithelial morphogenesis and differentiation.

Further studies should be pursued to examine changes in the cellular distribution of members of the Rho GTPase family and E-cadherin and its associated partners during different stages of tooth and salivary gland development in the absence of Irf6 to better understand the contribution of the regulation of adhesion complexes and the cytoskeleton to the developmental defects observed as a consequence of Irf6 ablation. This would shed more light on the mechanisms by which alteration of IRF6 function could lead to a wide spectrum of subclinical defects associated with CLP.

## 6.3 Integration of *Irf6* with other signaling pathways during craniofacial morphogenesis

Formation of ectodermal organs involves multiple signaling pathways, such as Wnt, Shh, and Notch signaling, which establish apical-basal membrane domains, shape cell morphology for invagination, and regulate cell proliferation. During palatogenesis, crosstalk between Irf6 and other signaling pathways has been proposed, in which SHH regulates WNT signaling and expression of the transcription factor, TFAP2A, via a P63/IRF6 regulatory module, and disruption of any component of this cascade can lead to cleft lip/palate (Kurosaka et al., 2014). Indeed, *Irf6* homozygous null mouse embryos exhibit altered expression of Wnt, Shh, Notch1 and Notch2 during the prenatal stages of tooth development (Blackburn et al., 2012). Similar pathways and responses are also likely to be acting during salivary gland morphogenesis. For example, in a duct ligation model of salivary gland wounding, atrophy of the gland occurs with enhanced fibrosis and acinar cell loss (Nagai et al., 2014; Woods et al., 2015). This is similar to the phenotype observed in the *Irf6* null mice. Interestingly, subsequent de-ligation of ducts can be used to induce salivary gland progenitor/stem cells proliferation and lead to the upregulation of Wnt, and Notch signaling pathways and several components of the Hh (Hedgehog) pathway, including Gli1 and Ptch1 simultaneously (Hai et al., 2010). Given these consideration and phenotype-genotype correlations observed in the present study, it is hypothesized that crosstalk exists between *Irf6* and other signaling pathways during both tooth and salivary gland morphogenesis. Future studies should be pursued to confirm this genetic interaction; this can be done through the generation of compound heterozygous mice and assessment of any phenotypic enhancement compared to mice heterozygous for each individual mutant allele.

### *6.3.1 Interaction of Irf6 and canonical WNT signaling during craniofacial development*

Mouse and human mutations in the Wnt10a and *Wnt* signaling activated pathway have been

shown to result in small teeth with reduced cusp number and hypodontia as well as taurodontic teeth and short roots, similar to these observed in the *Irf6 Null-E* mice (Ahn et al., 2010; Blackburn et al., 2015; J Laurikkala et al., 2001; Pispa et al., 1999; Boogaard et al., 2012; Yang et al., 2014). During salivary gland development, the WNT pathway is activated initially in the mesenchyme and later in the ductal epithelium cells at the time of lumen formation (Patel et al., 2011). Mesenchymal Wnt/ß-catenin signaling induces expression of ectodysplasin-A (Eda) to trigger the activation of the Edar/NF-êB pathway in the epithelium (Häärä et al., 2011). Inhibition of mesenchymal Wnt/ß-catenin signaling blocks SMG branching morphogenesis (Häärä et al., 2011). Eda overexpressing mice show larger lumina (Nordgarden et al., 2004). On the other hand, the Tabby mouse, carrying a mutation in *Eda* gene, showed a delay in postnatal SMG development, with fewer ductal structures and less granular convoluted tubules, as well as permanent dysfunction in saliva production (Blecher et al., 1983). These defects are similar to those observed in the *Irf6* null mice.

A regulatory loop between the WNT pathway, Irf6, and P63 has been proposed in facial epithelia during palatogenesis. WNT signaling functions as a positive regulator of P63, which in turn directly regulates *Irf6* expression. This was in part based on the finding of lower levels of Irf6 and P63 in the junction between MXP, MNP, and LNP of *Wnt9b* null mice. P63 mutant mice show a failure of tooth epithelial thickening ( Laurikkala et al., 2006). Moreover, RhoA, a downstream effector of Wnt signaling, has been linked to craniofacial development through an Irf6 mediated regulatory network via Arhgap29 – a member of the Rho GTPase activating protein family in the palatal epithelium of *Irf6* deficient mice (Schlessinger et al. 2009).

Remarkably, *Irf6* homozygous null mutant mice exhibited altered expression and displacement of the enamel knot marker genes (*Shh and Wnt*) from their normal location within the center of the invaginated incisor epithelium to the outermost part of the abnormally evaginated incisor epithelium (Blackburn et al., 2012). In line with this, data from Cox lab has revealed transiently decreased Wnt10b mRNA expression in *Irf6 Null-E* P4 molars (Chu, 2015). Aberrant expression of P63 in *Irf6 Null-E* ductal cells was also noted (Chapter 4).

### *6.3.2 Interaction of Irf6 and canonical SHH signaling during craniofacial development*

SHH plays a role in cellular differentiation and polarization during tooth morphogenesis. During embryonic stages of tooth development, *Shh* acts as a negative-feedback regulator of Wnt signaling to control tooth pattern and number (Ahn et al., 2010). Interestingly, alterations in the Shh pathway have caused phenotypic alterations similar to these observed in teeth and salivary glands of the *Irf6* null mice. Conditional removal of Shh activity after the invagination of the dental epithelium leads to massive alteration of the shape and size of the teeth and severe disruptions in the polarity and organization of the ameloblasts and odontoblasts (Dassule et al., 2000). Moreover, mice carrying an abnormal C-terminus of Patched1, a Shh receptor protein, show shorter roots as a result of reduced cell proliferation around the HERS, suggesting that Shh signaling is also important in tooth root development (Nakatomi et al., 2006). Hedgehog signaling also is known to play a role in salivary gland morphogenesis. Hh signaling promotes cell polarization and acinar lumen formation in developing submandibular gland epithelia during embryonic salivary gland branching morphogenesis. It also modulates proliferation and differentiation of salivary gland epithelial cells (Jaskoll et al., 2004). Activating Hh signaling in

GLI1 knockout mouse salivary glands leads to increased proliferation of the ductal and acinar cells, blocked acinar cell differentiation, and cystic duct formation (Fiaschi et al., 2011).

Similar to *Wnt* expression, canonical *Shh* expression is also altered in *Irf6* homozygote-null mutant mice (Blackburn et al., 2012). *Irf6* is required for proper Shh (Hh ligand) expression in the lingual epithelium (Goudy et al., 2013).The expression of Shh in embryonic salivary gland epithelium is also induced by the Edar/NF-kB pathway, downstream of the mesenchymal Wnt-Eda pathways (Häärä et al., 2011).

### *6.3.3 Interaction of Irf6 and NOTCH signaling during craniofacial development*

The Notch signaling pathway plays an essential role during differentiation of the dental epithelium, morphogenesis of teeth, and determination of cusp patterns (Mitsiadis et al., 2005). Disruption in Notch signaling leads to altered desmosome formation at the ameloblast-SI interface, leading to defective enamel formation (Jheon et al., 2016). Mice deficient in Jagged2, a ligand for Notch receptors, showed altered tooth morphogenesis, with misshapen crown morphology, alterations in enamel knot markers, and altered apoptosis (Mitsiadis et al., 2010). Expression of an activated Notch transgene in mouse salivary glands was also noted to disrupt glandular cell differentiation and lead to the accumulation of proliferating immature ductal cells and poorly differentiated adenocarcinomas (Jhappan et al., 1992).

MCS9.7, an upstream enhancer element of Irf6, contains a conserved binding site for the

transcription factor P63 and Notch (Rahimov et al., 2008; Restivo et al., 2011; Thomason et al., 2010). Moreover, Irf6 has been shown to be a primary Notch target in keratinocytes, in which Irf6 induces terminal differentiation and suppresses pro-proliferative genes like P63 (Restivo et al., 2011). A significant reduction of Irf6 expression is observed in the epidermis of mice with keratinocyte-specific deletion of *Notch1* and *Notch2* (Dumortier et al., 2010). Further evidence of the interaction between Irf6 and Notch has come from mice that are heterozygous for both the $Irf6^{R84C}$ allele and the Notch1 receptor ligand, Jagged1. These mice exhibit fully penetrant orofacial clefting and oral adhesions (Richardson et al., 2009). P63 mutant mice also show downregulation of Notch1 expression in the dental epithelium (Laurikkala et al., 2006). Moreover, Notch1 and Notch2 expression were also downregulated in incisor tooth germs of *Irf6* null mice, supporting the notion of a regulatory loop ( Blackburn et al., 2012).

## 6.4 The consequence of Irf6 ablation on caries development and bacterial colonization

Dental caries is a highly prevalent and costly microbial disease. In CLP populations, dental caries is usually assumed to be due to inadequate oral self-care (due to the physical presence of the cleft, as well as malpositioned teeth) and high sugar-containing diets, rather than biological factors (such as tooth and salivary gland defects)(Wells, 2014). Current management of CLP is costly and entails the blend of an extensive series of treatments from various healthcare providers, most of which require the maintenance of good oral health. Thus, it is imperative to know whether patients with CLP are at elevated risk for dental caries. Utilizing the *Irf6* conditional knockout mouse model, in Chapter 5, the consequences of *Irf6* ablation on caries

incidence and severity, as well as oral bacterial colonization, was pursued.

In light of the tooth mineralization defect and the massive alteration of structure and function of salivary glands observed in the *Irf6* null mice, it was hypothesized that the *Irf6* null mice would show an increase in caries experience, as well as enhanced bacterial colonization, when inoculated with *S.mutans* and fed a highly cariogenic diet. That said, the massive increase in caries severity in *Irf6* null mice teeth compared to all other matched controls was remarkable and unexpected. This was also associated with a significant increase in bacterial colonization. The severity of dental caries in *Irf6* null mice after only eight weeks of exposure to a high sugar diet was interestingly greater than what was reported in mice with salivary gland hypofunction ($AQP5^{-/-}$), and mice with defective enamel mineralization (Irf6 Het), as well as mice with a combination of both risk factors ($Akita^{-/-}$, and cystic fibrosis mouse model) (Catalán et al., 2011; Paper et al., 2005; Yeh et al., 2012). None of these studies/models reported the complete disintegration of molars, a presentation we observed in ~50% of the 120 teeth scored for caries in the *Irf6* null mice. Furthermore it is noteworthy that we found that *Irf6* null mice developed dental caries even in the absence of the cariogenic diet, and only after 8 weeks of bacterial colonization. Neither presentation has ever been reported in any rodent model.

Dental caries susceptibility is determined by several host factors such as tooth form, saliva function, bacterial colonization of the oral cavity, as well as the level of oral immune response. Saliva has a crucial role in protection against dental caries, via eliminating of bacteria

(lubrication, clearance, and antimicrobial activity), buffering acids, and facilitating the tooth reparative process by reversing the diffusion rate of calcium and phosphate towards the tooth surface (Brosky, 2007). In both human and mouse models, compromising the protective quantity and quality of saliva leads to increases in caries experience, and stimulating salivary flow through the chewing of sugar free gum was found to reduce the incidence of dental caries (Catalán et al., 2011; Paper et al., 2005; Ribelles et al., 2010; Stookey, 2008; X. P. Wang et al., 2012) .

The studies described in this thesis document for the first time an alteration in salivary gland structure and function as a consequence of *Irf6* ablation. *Irf6* null mice have a significantly low salivary flow rate and buffering capacity, as well as changes in the distribution of neutral and acidic mucins. The buffering capacity of the stimulated whole saliva is mainly due to its bicarbonate content (~90%), whereas the rest arises from phosphate and protein content (de Almeida et al., 2008). Thus, one can speculate that the composition of saliva is also altered in the *Irf6* null mice. It must be noted that *Irf6* null mice also have an enamel mineralization defect, which likely intensified the caries susceptibility of these animals. Moreover, deep pits and fissures on the occlusal surfaces of molars are more prone to carious lesions because these regions provide excellent sites for food impaction and bacterial stagnation (Konig, 1963; Wang et al., 2012a). In a similar way, the altered tooth morphology of the *Irf6* null mice, where the buccal and lingual cusps were fused together - either partially or completely - leaving a deep groove, and sometimes a fossa in the center of the crown (figure 3.3), may have enhanced the caries susceptibility. This could also explain the location of the caries observed in the pilot study

(mice received bacterial inoculation, and fed regular diet), in which only the deep pits and fissures of the *Irf6* null mice, and to lesser degree the *Irf6 Het-E* mice, showed carious lesions (figure 5.1).

The host immune response has an important role in protecting the body against invading pathogens. The oral immune response to *S. mutans* has been reported to protect against dental caries (Challacombe et al., 1984). Studies demonstrate that the production of salivary IgA after local injection of *S.mutans* antigen protects rats from dental caries (Katz et al., 1993; Michalek et al., 1978). Moreover, a positive correlation between the concentrations of salivary antimicrobial peptides and counts of *S.mutans* recovered from plaque in the teeth of children has been previously reported (Phattarataratip et al., 2011). Lower levels of salivary defensins have been found to be indicators of salivary gland hypofunction (Tanida et al., 2003). Thus, the association between salivary gland hypofunction and low salivary antimicrobial peptide secretion rates is one mechanism suspected of influencing susceptibility to infections and thus caries progression in the *Irf6* null mice.

## 6.5 A possible role for the oral epithelium role in bacterial colonization in the *Irf6* Null mice

The initiation of an adaptive immune response begins with antigen recognition. Pattern recognition receptors such as Toll Like Receptors (TLRs) allow the innate system to recognize self from non-self and respond to pathogens. Recognition of foreign antigens activates cells of

the innate system such as neutrophils, macrophages and dendritic cells, which in turn initiate the adaptive immune responses. TLR2 is a key mediator of host defenses that recognizes molecular epitopes associated with Gram-positive and Gram-negative bacteria. TLR3 is also a major participant in detecting damaged cells and initiating cell repair (Mogensen, 2009). IRF6 has been found to regulate TLR2-elicited chemokine responses in epithelial cells and TLR3 responses in human keratinocytes (Kwa et al., 2014; Ramnath et al., 2015). Moreover, Irf6 is strongly expressed in neutrophils and macrophages, suggesting that it is required for proper functioning of these cells (Dunnwald, 2014).

The oral epithelium also plays an active role in orchestrating innate immune defenses in two separate ways; first, by acting as an effective physical antimicrobial barrier at mucosal surfaces, and second by serving as a source of antimicrobial peptides including the defensins and several cytokines such as IL-8 (Dutzan et al., 2016). The *Pitx2 Cre* line used to generate our *Irf6* null mice is tissue specific; it expresses Cre in the developing oral and tooth epithelia. Therefore, Irf6 null mice were lacking the expression of Irf6 in these tissues. In mice deficient for *Irf6*, barriers like the cornified layer of the skin and the superficial layer of the oral epithelium fail to differentiate properly (Ingraham et al., 2006; Richardson et al., 2009). In line with this, *Irf6* null mice showed intraoral soft tissue changes, such as a plaque-like pattern and erythematous areas distributed across the dorsum of the tongue, were observed (figure 6.1). It seems that these erythematous areas had lost the superficial epithelium, suggesting the surface tissue sloughed possibly due to a weak adhesion of the tongue epithelia. Taken together, the enamel mineralization defects, salivary gland hypofunction, diminished innate immunity and epithelial

integrity due to *Irf6* ablation likely aid the colonization of *S. mutans* within the oral biofilm and subsequent contribution to dental caries (figure 6.2). It is currently difficult to assess which risk factors are most important. However, in the future, we plan to use a Cre driver line that is under the control of different tissue-specific promoters (i.e., promoter expressing only in the tooth or only in the salivary gland tissue). This would allow us to separate the impact of different biological risk factors (i.e., tooth defects, salivation, and immune function) on caries susceptibility.

## 6.6 Figures and tables

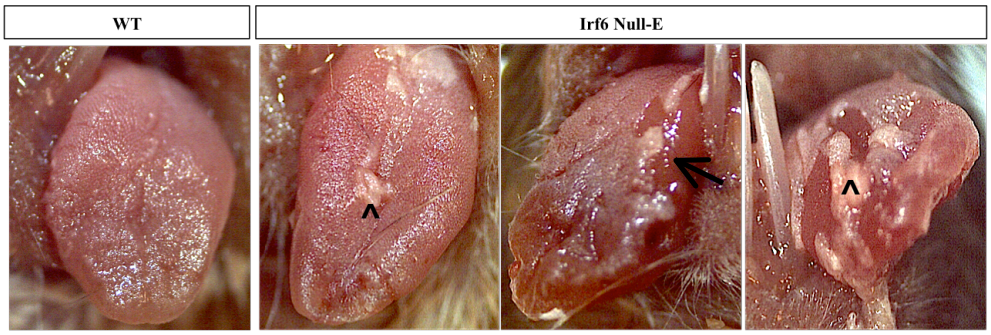


**Figure 6.1: Intraoral soft tissue changes in the Irf6 null mice.** A plaque-like pattern, and erythematous areas distributed across the dorsum of the tongue in the Irf6 null mice.

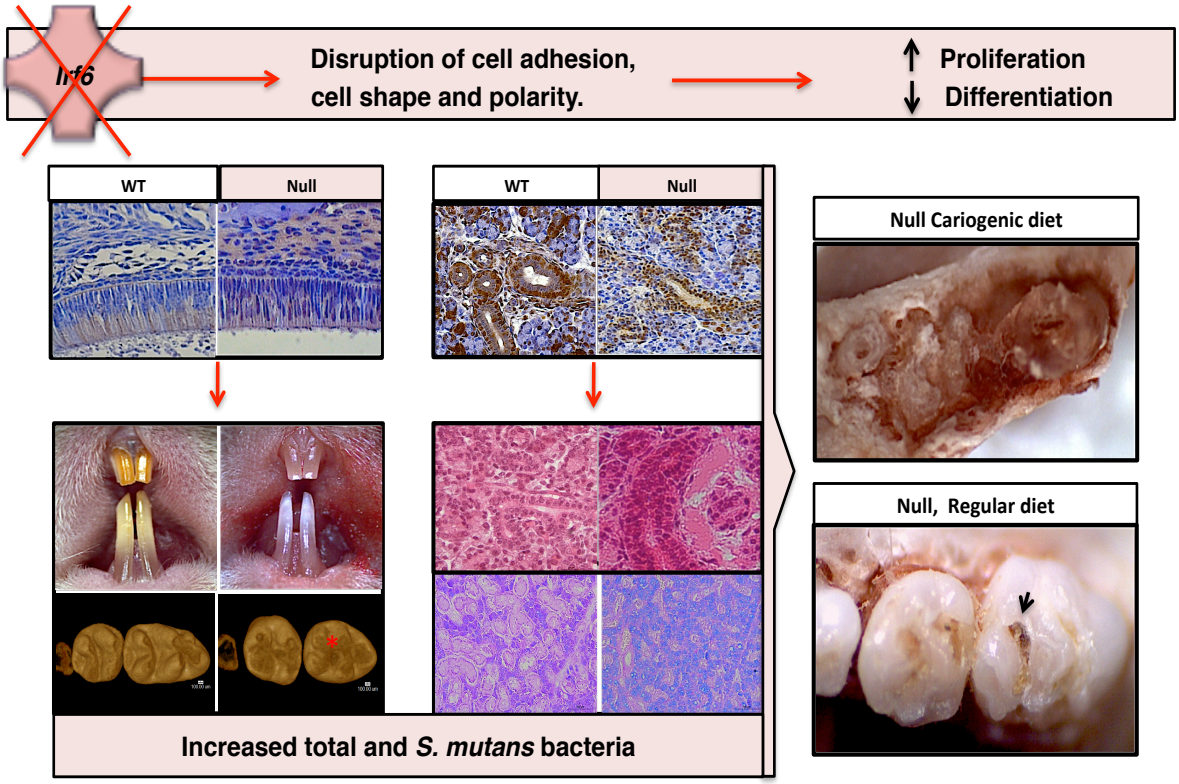


**Figure 6.2: Proposed mechanism to explain the influence of *Irf6* ablation on caries activity.** Alterations in epithelial polarity and disturbances in adhesion proteins due to *Irf6* ablation may account for enamel mineralization defects, and salivary gland hypofunction. These factors as well as diminished innate immunity and epithelial integrity likely aids the colonization of *S. mutans* within the oral biofilm and subsequent contribution to dental caries

# 7 References


Adachi, S., Yasuda, I., Nakashima, M., Yamauchi, T., Yoshioka, T., Okano, Y., … Kozawa, O. (2011). Rho-kinase inhibitor upregulates migration by altering focal adhesion formation via the Akt pathway in colon cancer cells. European journal of pharmacology, 650(1), 145–50.

Ahluwalia, M., Brailsford, S. R., Tarelli, E., Gilbert, S. C., Clark, D. T., Barnard, K., & Beighton, D. (2004). Dental Caries, Oral Hygiene, and Oral Clearance in Children with Craniofacial Disorders. Journal of Dental Research, 83(2), 175–179.

Ahn, Y., Sanderson, B. W., Klein, O. D., & Krumlauf, R. (2010). Inhibition of Wnt signaling by Wise (Sostdc1) and negative feedback from Shh controls tooth number and patterning. Development, 137(19), 3221–3231.

Aizenbud, D., Peri-Front, Y., & Nagler, R. M. (2008). Salivary analysis and antioxidants in cleft lip and palate children. Archives of Oral Biology, 53(6), 517–522.

Akota, I., Uta, R., Deeley, K., Küchler, E. C., & Vieira, A. R. (2014). Genetic variation in the promoter region of beta-defensin 1 ( DEFB 1 ) is associated with high caries experience in children born with cleft lip and palate, 1(February 2013), 235–240.

Al Jamal, G. a, Hazza'a, A. M., & Rawashdeh, M. a. (2010). Prevalence of dental anomalies in a population of cleft lip and palate patients. The Cleft palate-craniofacial journal : official publication of the American Cleft Palate-Craniofacial Association, 47(4), 413–420.

Alves Pereira, K. M., do Amaral, B. A., dos Santos, B. R. M., Galvão, H. C., Freitas, R. de A., & de Souza, L. B. (2010). Immunohistochemical expression of E-cadherin and beta-catenin in ameloblastomas and tooth germs. Oral surgery, oral medicine, oral pathology, oral radiology, and endodontics, 109(3), 425–31.

Amendt, B. A., Sutherland, L. B., & Russo, A. F. (1999). Multifunctional role of the Pitx2 homeodomain protein C-terminal tail. Molecular and cellular biology, 19(10), 7001–10.

Antunes, L. S., Tannure, P. N., Antunes, L. A. A., Reis, M. F., Costa, M. C., Gouvêa, C. V. D., … Küchler, E. C. (2014). Genetic association for caries susceptibility among cleft lip and/or palate individuals. The journal of contemporary dental practice, 15(3), 288–93.

Aure, M. H., Ruus, A.-K., & Galtung, H. K. (2014). Aquaporins in the adult mouse submandibular and sublingual salivary glands. Journal of molecular histology, 45(1), 69–80.

Bailey, C. M., & Hendrix, M. J. C. (2008). IRF6 in development and disease: a mediator of quiescence and differentiation. Cell cycle (Georgetown, Tex.), 7(13), 1925–30.

Barnes, B. J., Kellum, M. J., Pinder, K. E., Frisancho, J. A., & Pitha, P. M. (2003). Interferon regulatory factor 5, a novel mediator of cell cycle arrest and cell death. Cancer research, 63(19),

6424–31.

Bartlett, J. D. (2013). Dental enamel development: proteinases and their enamel matrix substrates. ISRN dentistry, 2013, 684607.

Bartlett, J. D., Dobeck, J. M., Tye, C. E., Perez-Moreno, M., Stokes, N., Reynolds, A. B., … Skobe, Z. (2010). Targeted p120-catenin ablation disrupts dental enamel development. PloS one, 5(9), e12703.

Bartlett, J. D., & Smith, C. E. (2013). Modulation of cell-cell junctional complexes by matrix metalloproteinases. Journal of dental research, 92(1), 10–7.

Beanan, M. J., & Sargent, T. D. (2000). A PEER REVIEWED FORUM Regulation and Function of Dlx3 in Vertebrate, 553(June), 545–553.

Bei, M. (2009). Molecular genetics of tooth development. Current opinion in genetics & development, 19(5), 504–10.

Biggs, L. C., Naridze, R. L., DeMali, K. A., Lusche, D. F., Kuhl, S., Soll, D. R., … Dunnwald, M. (2014). Interferon regulatory factor 6 regulates keratinocyte migration. Journal of cell science, 127(Pt 13), 2840–8.

Biz, M. T., Marques, M. R., Crema, V. O., Moriscot, A. S., & dos Santos, M. F. (2010). GTPases RhoA and Rac1 are important for amelogenin and DSPP expression during differentiation of ameloblasts and odontoblasts. Cell and tissue research, 340(3), 459–70.

Blackburn, J., Kawasaki, K., Porntaveetus, T., Kawasaki, M., Otsuka-Tanaka, Y., Miake, Y., … Ohazama, A. (2015). Excess NF-κB induces ectopic odontogenesis in embryonic incisor epithelium. Journal of dental research, 94(1), 121–8.

Blackburn, J., Ohazama, A., Kawasaki, K., Otsuka-Tanaka, Y., Liu, B., Honda, K., … Sharpe, P. T. (2012). The role of Irf6 in tooth epithelial invagination. Developmental biology, 365(1), 61–70.

Blecher, S. R., Debertin, M., & Murphy, J. S. (1983). Pleiotropic effect of Tabby gene on epidermal growth factor-containing cells of mouse submandibular gland. The Anatomical record, 207(1), 25–9.

Bokhout, B., Hofman, F. X., van Limbeek, J., Kramer, G. J., & Prahl-Andersen, B. (1997). Incidence of dental caries in the primary dentition in children with a cleft lip and/or palate. Caries research, 31(1), 8–12.

Bokhout, B., van Loveren, C., Hofman, F. X., Buijs, J. F., van Limbeek, J., & Prahl-Andersen, B. (1996). Prevalence of Streptococcus mutans and lactobacilli in 18-month-old children with cleft lip and/or palate. The Cleft palate-craniofacial journal : official publication of the American Cleft Palate-Craniofacial Association, 33(5), 424–8.

Borgström, M. K., Edwardsson, S., Sullivan, A., & Svensäter, G. (2000). Dental plaque mass and

acid production activity of the microbiota on teeth. European journal of oral sciences, 108(5), 412–7.

Brosky, M. E. (2007). The role of saliva in oral health: strategies for prevention and management of xerostomia. The journal of supportive oncology, 5(5), 215–25.

C. B. Chuo, & M. J. Timmons. (2009). The Bacteriology of Children Before Primary Cleft Lip and Palate Surgery.

Carounanidy, U., & Sathyanarayanan, R. (2009). Dental caries: A complete changeover (Part II)-Changeover in the diagnosis and prognosis. Journal of conservative dentistry : JCD, 12(3), 87–100.

Catalán, M. A., Scott-Anne, K., Klein, M. I., Koo, H., Bowen, W. H., & Melvin, J. E. (2011). Elevated incidence of dental caries in a mouse model of cystic fibrosis. PloS one, 6(1), e16549.

Catón, J., & Tucker, A. S. (2009). Current knowledge of tooth development: patterning and mineralization of the murine dentition. Journal of anatomy, 214(4), 502–15.

Chai, Y., & Maxson, R. E. (2006). Recent advances in craniofacial morphogenesis. Developmental dynamics : an official publication of the American Association of Anatomists, 235(9), 2353–75.

Challacombe, S. J., Bergmeier, L. A., & Rees, A. S. (1984). Natural antibodies in man to a protein antigen from the bacterium Streptococcus mutans related to dental caries experience. Archives of oral biology, 29(3), 179–84.

Chestnutt, I. G., Schafer, F., Jacobson, A. P., & Stephen, K. W. (1996). Incremental susceptibility of individual tooth surfaces to dental caries in Scottish adolescents. Community dentistry and oral epidemiology, 24(1), 11–6.

Choi, S. J., Song, I. S., Feng, J. Q., Gao, T., Haruyama, N., Gautam, P., … Hart, T. C. (2010). Mutant DLX 3 disrupts odontoblast polarization and dentin formation. Developmental biology, 344(2), 682–92.

Chu, E. Y. (2015). © 2015 Emily Y. Chu.

Cobourne, M. T. (2004). The complex genetics of cleft lip and palate. European journal of orthodontics, 26(1), 7–16.

Cox, C. J., Espinoza, H. M., McWilliams, B., Chappell, K., Morton, L., Hjalt, T. A., … Amendt, B. A. (2002). Differential regulation of gene expression by PITX2 isoforms. The Journal of biological chemistry, 277(28), 25001–10.

Cox, T. C. (2004). Taking it to the max: the genetic and developmental mechanisms coordinating midfacial morphogenesis and dysmorphology. Clinical genetics, 65(3), 163–76.

Cuervo, R., Valencia, C., Chandraratna, R. A. S., & Covarrubias, L. (2002). Programmed cell

death is required for palate shelf fusion and is regulated by retinoic acid. Developmental biology, 245(1), 145–56.

Culp, D. J., Robinson, B., Parkkila, S., Pan, P.-W., Cash, M. N., Truong, H. N., … Gullett, S. L. (2011). Oral colonization by Streptococcus mutans and caries development is reduced upon deletion of carbonic anhydrase VI expression in saliva. Biochimica et biophysica acta, 1812(12), 1567–76.

Cunha-Cruz, J., Scott, J., Rothen, M., Mancl, L., Lawhorn, T., Brossel, K., & Berg, J. (2013). Salivary characteristics and dental caries: evidence from general dental practices. Journal of the American Dental Association (1939), 144(5), e31–40.

Daley, W. P., Gervais, E. M., Centanni, S. W., Gulfo, K. M., Nelson, D. A., & Larsen, M. (2012). ROCK1-directed basement membrane positioning coordinates epithelial tissue polarity. Development (Cambridge, England), 139(2), 411–22.

Daley, W. P., Gulfo, K. M., Sequeira, S. J., & Larsen, M. (2009). Identification of a mechanochemical checkpoint and negative feedback loop regulating branching morphogenesis. Developmental biology, 336(2), 169–82.

Dang, H., Geiser, A. G., Letterio, J. J., Nakabayashi, T., Kong, L., Fernandes, G., & Talal, N. (1995). SLE-like autoantibodies and Sjögren's syndrome-like lymphoproliferation in TGF-beta knockout mice. Journal of immunology (Baltimore, Md. : 1950), 155(6), 3205–12.

Dassule, H. R., Lewis, P., Bei, M., Maas, R., & McMahon, A. P. (2000). Sonic hedgehog regulates growth and morphogenesis of the tooth. Development (Cambridge, England), 127(22), 4775–85.

Davis, M. A., & Reynolds, A. B. (2006). Blocked Acinar Development, E-Cadherin Reduction, and Intraepithelial Neoplasia upon Ablation of p120-Catenin in the Mouse Salivary Gland. Developmental Cell, 10(1), 21–31.

de Almeida, P. D. V., Grégio, A. M. T., Machado, M. A. N., de Lima, A. A. S., & Azevedo, L. R. (2008). Saliva composition and functions: a comprehensive review. The journal of contemporary dental practice, 9(3), 72–80.

De Groote, P., Tran, H. T., Fransen, M., Tanghe, G., Urwyler, C., De Craene, B., … Declercq, W. (2015). A novel RIPK4-IRF6 connection is required to prevent epithelial fusions characteristic for popliteal pterygium syndromes. Cell death and differentiation, 22(6), 1012–24.

Deeley, K., Letra, A., Rose, E. K., Brandon, C. A., Resick, J. M., Marazita, M. L., & Vieira, A. R. (2008). Possible association of amelogenin to high caries experience in a Guatemalan-Mayan population. Caries research, 42(1), 8–13.

Dixon, M. J., Marazita, M. L., Beaty, T. H., & Murray, J. C. (2011). Cleft lip and palate: understanding genetic and environmental influences. Nature reviews. Genetics, 12(3), 167–78.

Dodds, M. W. J., Johnson, D. A., & Yeh, C.-K. (2005). Health benefits of saliva: a review.

Journal of dentistry, 33(3), 223–33.

Dressler, S., Meyer-Marcotty, P., Weisschuh, N., Jablonski-Momeni, A., Pieper, K., Gramer, G., & Gramer, E. (2010). Dental and Craniofacial Anomalies Associated with Axenfeld-Rieger Syndrome with PITX2 Mutation. Case reports in medicine, 2010, 621984.

Dumortier, A., Durham, A.-D., Di Piazza, M., Vauclair, S., Koch, U., Ferrand, G., … Radtke, F. (2010). Atopic dermatitis-like disease and associated lethal myeloproliferative disorder arise from loss of Notch signaling in the murine skin. PloS one, 5(2), e9258.

Dunnwald, M. (2014). IRF6 in the Inflammatory Phase of Cutaneous Wound Healing.

Dupin, E., Creuzet, S., & Le Douarin, N. M. (2006). The contribution of the neural crest to the vertebrate body. Advances in experimental medicine and biology, 589, 96–119.

Dutzan, N., Konkel, J. E., Greenwell-Wild, T., & Moutsopoulos, N. M. (2016). Characterization of the human immune cell network at the gingival barrier. Mucosal immunology.

Duverger, O., Zah, A., Isaac, J., Sun, H.-W., Bartels, A. K., Lian, J. B., … Morasso, M. I. (2012). Neural crest deletion of Dlx3 leads to major dentin defects through down-regulation of Dspp. The Journal of biological chemistry, 287(15), 12230–40.

Eerens, K., Vlietinck, R., Heidbüchel, K., Van Olmen, A., Derom, C., Willems, G., & Carels, C. (2001). Hypodontia and tooth formation in groups of children with cleft, siblings without cleft, and nonrelated controls. The Cleft palate-craniofacial journal : official publication of the American Cleft Palate-Craniofacial Association, 38(4), 374–8.

Ericson, D., & Bratthall, D. (1989, October). Simplified method to estimate salivary buffer capacity. Scandinavian journal of dental research.

Fakhouri, W. D., Rhea, L., Du, T., Sweezer, E., Morrison, H., Fitzpatrick, D., … Schutte, B. C. (2012). MCS9.7 enhancer activity is highly, but not completely, associated with expression of Irf6 and p63. Developmental dynamics : an official publication of the American Association of Anatomists, 241(2), 340–9.

Featherstone, J. D. (2000). The science and practice of caries prevention. Journal of the American Dental Association (1939), 131(7), 887–99.

Ferretti, E., Li, B., Zewdu, R., Wells, V., Hebert, J. M., Karner, C., … Selleri, L. (2011). A conserved Pbx-Wnt-p63-Irf6 regulatory module controls face morphogenesis by promoting epithelial apoptosis. Developmental cell, 21(4), 627–41.

Fiaschi, M., Kolterud, A., Nilsson, M., Toftgård, R., & Rozell, B. (2011). Targeted expression of GLI1 in the salivary glands results in an altered differentiation program and hyperplasia. The American journal of pathology, 179(5), 2569–79.

Filipenko, N. R., Attwell, S., Roskelley, C., & Dedhar, S. (2005). Integrin-linked kinase activity regulates Rac- and Cdc42-mediated actin cytoskeleton reorganization via alpha-PIX. Oncogene,

24(38), 5837–49.

Fleischmannova, J., Matalova, E., Tucker, A. S., & Sharpe, P. T. (2008). Mouse models of tooth abnormalities. European journal of oral sciences, 116(1), 1–10.

Forster, N., Saladi, S. V., van Bragt, M., Sfondouris, M. E., Jones, F. E., Li, Z., & Ellisen, L. W. (2014). Basal cell signaling by p63 controls luminal progenitor function and lactation via NRG1. Developmental cell, 28(2), 147–60.

Frebourg, T., Oliveira, C., Hochain, P., Karam, R., Manouvrier, S., Graziadio, C., … Seruca, R. (2006). Cleft lip/palate and CDH1/E-cadherin mutations in families with hereditary diffuse gastric cancer. Journal of medical genetics, 43(2), 138–42.

Furness, S., Worthington, H. V, Bryan, G., Birchenough, S., & McMillan, R. (2011). Interventions for the management of dry mouth: topical therapies. The Cochrane database of systematic reviews, (12), CD008934.

Garcia, M. A. S., Yang, N., & Quinton, P. M. (2009). Normal mouse intestinal mucus release requires cystic fibrosis transmembrane regulator-dependent bicarbonate secretion. The Journal of clinical investigation, 119(9), 2613–22.

Garrett, J. R., & Parsons, P. A. (1973). Alkaline phosphatase and myoepithelial cells in the parotid gland of the rat. The Histochemical journal, 5(5), 463–71.

Gati, D., & Vieira, A. R. (2011). Elderly at greater risk for root caries: a look at the multifactorial risks with emphasis on genetics susceptibility. International journal of dentistry, 2011, 647168.

Gaudilliere, D., Thakur, Y., Ku, M., Kaur, A., Shrestha, P., & Girod, S. C. (2014). Caries management by risk assessment in a cleft and craniofacial center. The Journal of craniofacial surgery, 25(6), e529–36.

Goudy, S., Angel, P., Jacobs, B., Hill, C., Mainini, V., Smith, A. L., … Schutte, B. C. (2013). Cell-autonomous and non-cell-autonomous roles for IRF6 during development of the tongue. PloS one, 8(2), e56270.

Gritli-Linde, A. (2010). p63 and IRF6: brothers in arms against cleft palate. The Journal of clinical investigation, 120(5), 1386–9.

Häärä, O., Fujimori, S., Schmidt-Ullrich, R., Hartmann, C., Thesleff, I., & Mikkola, M. L. (2011). Ectodysplasin and Wnt pathways are required for salivary gland branching morphogenesis. Development (Cambridge, England), 138(13), 2681–91.

Hai, B., Yang, Z., Millar, S. E., Choi, Y. S., Taketo, M. M., Nagy, A., & Liu, F. (2010). Wnt/β-catenin signaling regulates postnatal development and regeneration of the salivary gland. Stem cells and development, 19(11), 1793–801.

Hakim, S. G., Ribbat, J., Berndt, A., Richter, P., Kosmehl, H., Benedek, G. A., … Rades, D. (2011). Expression of Wnt-1, TGF-β and related cell-cell adhesion components following

radiotherapy in salivary glands of patients with manifested radiogenic xerostomia. Radiotherapy and oncology : journal of the European Society for Therapeutic Radiology and Oncology, 101(1), 93–9.

Hall, B. E., Zheng, C., Swaim, W. D., Cho, A., Nagineni, C. N., Eckhaus, M. A., … Kulkarni, A. B. (2010). Conditional overexpression of TGF-beta1 disrupts mouse salivary gland development and function. Laboratory investigation; a journal of technical methods and pathology, 90(4), 543–55.

Hannigan, A., O'Mullane, D. M., Barry, D., Schäfer, F., & Roberts, A. J. (2000). A caries susceptibility classification of tooth surfaces by survival time. Caries research, 34(2), 103–8.

Harrington, A. W., Kim, J. Y., & Yoon, S. O. (2002). Activation of Rac GTPase by p75 is necessary for c-jun N-terminal kinase-mediated apoptosis. The Journal of neuroscience : the official journal of the Society for Neuroscience, 22(1), 156–66.

Harris, E. F., & Hullings, J. G. (1990). Delayed dental development in children with isolated cleft lip and palate. Archives of oral biology, 35(6), 469–73.

Harris, T. J. C., & Tepass, U. (2010). Adherens junctions: from molecules to morphogenesis. Nature Reviews Molecular Cell Biology, 11(7), 502–514.

Harunaga, J., Hsu, J. C., & Yamada, K. M. (2011). Dynamics of salivary gland morphogenesis. Journal of dental research, 90(9), 1070–7.

Hasslöf, P., & Twetman, S. (2007). Caries prevalence in children with cleft lip and palate--a systematic review of case-control studies. International journal of paediatric dentistry / the British Paedodontic Society [and] the International Association of Dentistry for Children, 17(5), 313–9.

Hatakeyama, J., Fukumoto, S., Nakamura, T., Haruyama, N., Suzuki, S., Hatakeyama, Y., … Kulkarni, A. B. (2009). Synergistic roles of amelogenin and ameloblastin. Journal of dental research, 88(4), 318–22.

Heymann, R., About, I., Lendahl, U., Franquin, J.-C., Obrink, B., & Mitsiadis, T. A. (2002). E- and N-cadherin distribution in developing and functional human teeth under normal and pathological conditions. The American journal of pathology, 160(6), 2123–33.

Hieda, Y., Iwai, K., Morita, T., & Nakanishi, Y. (1996). Mouse embryonic submandibular gland epithelium loses its tissue integrity during early branching morphogenesis. Developmental dynamics : an official publication of the American Association of Anatomists, 207(4), 395–403.

Hu, J. C.-C., Chun, Y.-H. P., Al Hazzazzi, T., & Simmer, J. P. (2007). Enamel formation and amelogenesis imperfecta. Cells, tissues, organs, 186(1), 78–85.

Huang, X., Bringas, P., Slavkin, H. C., & Chai, Y. (2009). Fate of HERS during tooth root development. Developmental biology, 334(1), 22–30.

Huang, X. F., & Chai, Y. (2010). TGF-ß signalling and tooth development. The Chinese journal of dental research : the official journal of the Scientific Section of the Chinese Stomatological Association (CSA), 13(1), 7–15.

Huang, Z., Kim, J., Lacruz, R. S., Bringas, P., Glogauer, M., Bromage, T. G., … Snead, M. L. (2011). Epithelial-specific knockout of the Rac1 gene leads to enamel defects. European journal of oral sciences, 119 Suppl , 168–76.

Huang, Z., Sargeant, T. D., Hulvat, J. F., Mata, A., Bringas, P., Koh, C.-Y., … Snead, M. L. (2008). Bioactive nanofibers instruct cells to proliferate and differentiate during enamel regeneration. Journal of bone and mineral research : the official journal of the American Society for Bone and Mineral Research, 23(12), 1995–2006.

Hunt, O., Burden, D., Hepper, P., & Johnston, C. (2005). The psychosocial effects of cleft lip and palate: a systematic review. European journal of orthodontics, 27(3), 274–85.

Idrees, F., Bloch-Zupan, A., Free, S. L., Vaideanu, D., Thompson, P. J., Ashley, P., … Sowden, J. C. (2006). A novel homeobox mutation in the PITX2 gene in a family with Axenfeld-Rieger syndrome associated with brain, ocular, and dental phenotypes. American journal of medical genetics. Part B, Neuropsychiatric genetics : the official publication of the International Society of Psychiatric Genetics, 141B(2), 184–91.

Ingraham, C. R., Kinoshita, A., Kondo, S., Yang, B., Sajan, S., Trout, K. J., … Schutte, B. C. (2006). Abnormal skin, limb and craniofacial morphogenesis in mice deficient for interferon regulatory factor 6 (Irf6). Nature genetics, 38(11), 1335–1340.

Ishibashi, K., Hara, S., & Kondo, S. (2009). Aquaporin water channels in mammals. Clinical and experimental nephrology, 13(2), 107–17.

Itoh, M., & Bissell, M. J. (2003). The organization of tight junctions in epithelia: implications for mammary gland biology and breast tumorigenesis. Journal of mammary gland biology and neoplasia, 8(4), 449–62.

Iwata, J., Suzuki, A., Pelikan, R. C., Ho, T.-V., Sanchez-Lara, P. A., Urata, M., … Chai, Y. (2013). Smad4-Irf6 genetic interaction and TGFβ-mediated IRF6 signaling cascade are crucial for palatal fusion in mice. Development (Cambridge, England), 140(6), 1220–30.

Janebodin, K., Buranaphatthana, W., Ieronimakis, N., Hays, A. L., & Reyes, M. (2013). An in vitro culture system for long-term expansion of epithelial and mesenchymal salivary gland cells: role of TGF-β1 in salivary gland epithelial and mesenchymal differentiation. BioMed research international, 2013, 815895.

Jaskoll, T., Leo, T., Witcher, D., Ormestad, M., Astorga, J., Bringas, P., … Melnick, M. (2004). Sonic hedgehog signaling plays an essential role during embryonic salivary gland epithelial branching morphogenesis. Developmental dynamics : an official publication of the American Association of Anatomists, 229(4), 722–32.

Jaskoll, T., & Melnick, M. (1999). Submandibular gland morphogenesis: stage-specific

expression of TGF-alpha/EGF, IGF, TGF-beta, TNF, and IL-6 signal transduction in normal embryonic mice and the phenotypic effects of TGF-beta2, TGF-beta3, and EGF-r null mutations. The Anatomical record, 256(3), 252–68.

Jeremias, F., Koruyucu, M., Küchler, E. C., Bayram, M., Tuna, E. B., Deeley, K., … Vieira, A. R. (2013). Genes expressed in dental enamel development are associated with molar-incisor hypomineralization. Archives of oral biology, 58(10), 1434–42.

Jhappan, C., Gallahan, D., Stahle, C., Chu, E., Smith, G. H., Merlino, G., & Callahan, R. (1992). Expression of an activated Notch-related int-3 transgene interferes with cell differentiation and induces neoplastic transformation in mammary and salivary glands. Genes & development, 6(3), 345–55.

Jheon, A. H., Prochazkova, M., Meng, B., Wen, T., Lim, Y.-J., Naveau, A., … Klein, O. D. (2016). Inhibition of Notch Signaling During Mouse Incisor Renewal Leads to Enamel Defects. Journal of bone and mineral research : the official journal of the American Society for Bone and Mineral Research, 31(1), 152–62.

Jiang, K., Zhong, B., Ritchey, C., Gilvary, D. L., Hong-Geller, E., Wei, S., & Djeu, J. Y. (2003). Regulation of Akt-dependent cell survival by Syk and Rac. Blood, 101(1), 236–44.

Jiang, R., Bush, J. O., & Lidral, A. C. (2006). Development of the upper lip: morphogenetic and molecular mechanisms. Developmental dynamics : an official publication of the American Association of Anatomists, 235(5), 1152–66.

Johnston, M. C., & Bronsky, P. T. (1995). Prenatal craniofacial development: new insights on normal and abnormal mechanisms. Critical reviews in oral biology and medicine : an official publication of the American Association of Oral Biologists, 6(1), 25–79.

Jugessur, A., Farlie, P. G., & Kilpatrick, N. (2009). The genetics of isolated orofacial clefts: from genotypes to subphenotypes. Oral diseases, 15(7), 437–53.

Kangas, A. T., Evans, A. R., Thesleff, I., & Jernvall, J. (2004). Nonindependence of mammalian dental characters. Nature, 432(7014), 211–4.

Karsten, A., Larson, M., & Larson, O. (2005). Length of the cleft in relation to the incidence of hypodontia of the second premolar and to inheritance of cleft lip and palate in children with isolated cleft palate. Scandinavian journal of plastic and reconstructive surgery and hand surgery / Nordisk plastikkirurgisk forening [and] Nordisk klubb for handkirurgi, 39(5), 283–6.

Kassai, Y., Munne, P., Hotta, Y., Penttilä, E., Kavanagh, K., Ohbayashi, N., … Itoh, N. (2005). Regulation of mammalian tooth cusp patterning by ectodin. Science (New York, N.Y.), 309(5743), 2067–70.

Katz, J., Harmon, C. C., Buckner, G. P., Richardson, G. J., Russell, M. W., & Michalek, S. M. (1993). Protective salivary immunoglobulin A responses against Streptococcus mutans infection after intranasal immunization with S. mutans antigen I/II coupled to the B subunit of cholera

toxin. Infection and immunity, 61(5), 1964–71.

Ke, C.-Y., Xiao, W.-L., Chen, C.-M., Lo, L.-J., & Wong, F.-H. (2015). IRF6 is the mediator of TGFβ3 during regulation of the epithelial mesenchymal transition and palatal fusion. Scientific Reports, 5, 12791.

Keyes, P. R. (1958). McClure's, (score C).

Kioussi, C., Briata, P., Baek, S. H., Rose, D. W., Hamblet, N. S., Herman, T., … Rosenfeld, M. G. (2002). Identification of a Wnt/Dvl/β-Catenin → Pitx2 Pathway Mediating Cell-Type-Specific Proliferation during Development. Cell, 111(5), 673–685.

Kirchberg, A., Treide, A., & Hemprich, A. (2004). Investigation of caries prevalence in children with cleft lip, alveolus, and palate. Journal of cranio-maxillo-facial surgery : official publication of the European Association for Cranio-Maxillo-Facial Surgery, 32(4), 216–9.

Klein, O. D., Minowada, G., Peterkova, R., Kangas, A., Yu, B. D., Lesot, H., … Martin, G. R. (2006). Sprouty genes control diastema tooth development via bidirectional antagonism of epithelial-mesenchymal FGF signaling. Developmental cell, 11(2), 181–90.

Knight, A. S., Schutte, B. C., Jiang, R., & Dixon, M. J. (2006). Developmental expression analysis of the mouse and chick orthologues of IRF6: the gene mutated in Van der Woude syndrome. Developmental dynamics : an official publication of the American Association of Anatomists, 235(5), 1441–7.

Kondo, S., Schutte, B. C., Richardson, R. J., Bjork, B. C., Knight, A. S., Watanabe, Y., … Murray, J. C. (2002). Mutations in IRF6 cause Van der Woude and popliteal pterygium syndromes. Nature genetics, 32(2), 285–9.

Konig, K. G. (1963). Dental Morphology in Relation to Caries Resistance with Special Reference to Fissures as Susceptible Areas. Journal of Dental Research, 42(1), 461–476.

Kouskoura, T., Fragou, N., Alexiou, M., John, N., Sommer, L., Graf, D., … Mitsiadis, T. A. (2011). The genetic basis of craniofacial and dental abnormalities. Schweizer Monatsschrift für Zahnmedizin = Revue mensuelle suisse d'odonto-stomatologie = Rivista mensile svizzera di odontologia e stomatologia / SSO, 121(7-8), 636–46.

Krane, C. M., Melvin, J. E., Nguyen, H. V, Richardson, L., Towne, J. E., Doetschman, T., & Menon, A. G. (2001). Salivary acinar cells from aquaporin 5-deficient mice have decreased membrane water permeability and altered cell volume regulation. The Journal of biological chemistry, 276(26), 23413–20.

Krapels, I. P., Vermeij-Keers, C., Müller, M., de Klein, A., & Steegers-Theunissen, R. P. (2006). Nutrition and genes in the development of orofacial clefting. Nutrition reviews, 64(6), 280–8.

Kristoffersson, K., Gröndahl, H. G., & Bratthall, D. (1985). The more Streptococcus mutans, the more caries on approximal surfaces. Journal of dental research, 64(1), 58–61.

Küchler, E. C., Gomes Da Motta, L., Vieira, A. R., & Granjeiro, J. M. (2011). Side of dental anomalies and taurodontism as potential clinical markers for cleft subphenotypes. Cleft Palate-Craniofacial Journal, 48(1), 103–108.

Kumakami-Sakano, M., Otsu, K., Fujiwara, N., & Harada, H. (2014). Regulatory mechanisms of Hertwig′s epithelial root sheath formation and anomaly correlated with root length. Experimental cell research, 325(2), 78–82.

Kurley, S. J., Bierie, B., Carnahan, R. H., Lobdell, N. A., Davis, M. A., Hofmann, I., … Reynolds, A. B. (2012). p120-catenin is essential for terminal end bud function and mammary morphogenesis. Development, 139(10), 1754–1764.

Kuroda, S., Fukata, M., Fujii, K., Nakamura, T., Izawa, I., & Kaibuchi, K. (1997). Regulation of cell-cell adhesion of MDCK cells by Cdc42 and Rac1 small GTPases. Biochemical and biophysical research communications, 240(2), 430–5.

Kurosaka, H., Iulianella, A., Williams, T., & Trainor, P. a. (2014). Disrupting hedgehog and WNT signaling interactions promotes cleft lip pathogenesis. The Journal of clinical investigation, 124(4), 1660–71.

Kwa, M. Q., Nguyen, T., Huynh, J., Ramnath, D., De Nardo, D., Lam, P. Y., … Scholz, G. M. (2014). Interferon regulatory factor 6 differentially regulates Toll-like receptor 2-dependent chemokine gene expression in epithelial cells. The Journal of biological chemistry, 289(28), 19758–68.

Lages, E. M. B., Marcos, B., & Pordeus, I. A. (2004). Oral health of individuals with cleft lip, cleft palate, or both. The Cleft palate-craniofacial journal : official publication of the American Cleft Palate-Craniofacial Association, 41(1), 59–63.

Lam L. Cheng, B.D.Sc(Hons)., B.Dent.St., Stephen L. Moor, Cert Dent Thy, Academic Upgrade, B.H.Sc., Christopher T.C. Ho, B.D.Sc(Hons)., M. D. S. (2007). Predisposing Factors to Dental Caries in Children With Cleft Lip and Palate: A Review and Strategies for Early Prevention. Cleft Palate–Craniofacial Journal.

Lan, H. A., Zain, R. B., Saitoh, M., Muramatsu, Y., Shrestha, P., & Mori, M. (1996). Proliferating cell nuclear antigen (PCNA) and p53 in epithelial dysplasia and squamous cell carcinoma of oral mucosa--a marker for poor tumor differentiation, increasing nuclear atypia and invasiveness? Anticancer research, 16(5B), 3059–65.

Larsen, H. S., Aure, M. H., Peters, S. B., Larsen, M., Messelt, E. B., & Kanli Galtung, H. (2011). Localization of AQP5 during development of the mouse submandibular salivary gland. Journal of molecular histology, 42(1), 71–81.

Larsen, M., Yamada, K. M., & Musselmann, K. (2010). Systems analysis of salivary gland development and disease. Wiley interdisciplinary reviews. Systems biology and medicine, 2(6), 670–82.

Laugel-Haushalter, V., Langer, a., Marrie, J., Fraulob, V., Schuhbaur, B., Koch-Phillips, M., …

Bloch-Zupan, a. (2012). From the transcription of genes involved in ectodermal dysplasias to the understanding of associated dental anomalies. Molecular Syndromology, 3(4), 158–168.

Laurikkala, J., Mikkola, M. L., James, M., Tummers, M., Mills, A. A., & Thesleff, I. (2006). p63 regulates multiple signalling pathways required for ectodermal organogenesis and differentiation. Development (Cambridge, England), 133(8), 1553–63.

Laurikkala, J., Mikkola, M., Mustonen, T., Aberg, T., Koppinen, P., Pispa, J., … Thesleff, I. (2001). TNF signaling via the ligand-receptor pair ectodysplasin and edar controls the function of epithelial signaling centers and is regulated by Wnt and activin during tooth organogenesis. Developmental biology, 229(2), 443–55.

LAUTERSTEIN, A. M., & MENDELSOHN, M. (1964). AN ANALYSIS OF THE CARIES EXPERIENCE OF 285 CLEFT PALATE CHILDREN. The Cleft palate journal, 29, 314–9.

Law, V., Seow, W. K., & Townsend, G. (2007). Factors influencing oral colonization of mutans streptococci in young children. Australian dental journal, 52(2), 93–100; quiz 159.

Lee, M. G., Ohana, E., Park, H. W., Yang, D., & Muallem, S. (2012). Molecular mechanism of pancreatic and salivary gland fluid and HCO3 secretion. Physiological reviews, 92(1), 39–74.

Leone, C. W., & Oppenheim, F. G. (2001). Physical and chemical aspects of saliva as indicators of risk for dental caries in humans. Journal of dental education, 65(10), 1054–62.

Lézot, F., Thomas, B., Greene, S. R., Hotton, D., Yuan, Z.-A., Castaneda, B., … Berdal, A. (2008). Physiological implications of DLX homeoproteins in enamel formation. Journal of cellular physiology, 216(3), 688–97.

Li, X., Venugopalan, S. R., Cao, H., Pinho, F. O., Paine, M. L., Snead, M. L., … Amendt, B. A. (2014). A model for the molecular underpinnings of tooth defects in Axenfeld-Rieger syndrome. Human molecular genetics, 23(1), 194–208.

Little, H. J., Rorick, N. K., Su, L.-I., Baldock, C., Malhotra, S., Jowitt, T., … Shore, P. (2009). Missense mutations that cause Van der Woude syndrome and popliteal pterygium syndrome affect the DNA-binding and transcriptional activation functions of IRF6. Human molecular genetics, 18(3), 535–45.

Liu, F., Chu, E. Y., Watt, B., Zhang, Y., Gallant, N. M., Andl, T., … Millar, S. E. (2008). Wnt/beta-catenin signaling directs multiple stages of tooth morphogenesis. Developmental biology, 313(1), 210–24.

Liu, W., Selever, J., Lu, M.-F., & Martin, J. F. (2003). Genetic dissection of Pitx2 in craniofacial development uncovers new functions in branchial arch morphogenesis, late aspects of tooth morphogenesis and cell migration. Development (Cambridge, England), 130(25), 6375–85.

Logan, C. Y., & Nusse, R. (2004). The Wnt signaling pathway in development and disease. Annual review of cell and developmental biology, 20, 781–810.

Luan, X., Ito, Y., & Diekwisch, T. G. H. (2006). Evolution and development of Hertwig's epithelial root sheath. Developmental dynamics : an official publication of the American Association of Anatomists, 235(5), 1167–80.

Lucas, V. S., Gupta, R., Ololade, O., Gelbier, M., & Roberts, G. J. (2000). Dental health indices and caries associated microflora in children with unilateral cleft lip and palate. The Cleft palate-craniofacial journal : official publication of the American Cleft Palate-Craniofacial Association, 37(5), 447–52.

Luukko, K., & Kettunen, P. (2014). Coordination of tooth morphogenesis and neuronal development through tissue interactions: lessons from mouse models. Experimental cell research, 325(2), 72–7.

Ma, T., Song, Y., Gillespie, A., Carlson, E. J., Epstein, C. J., & Verkman, A. S. (1999). Defective secretion of saliva in transgenic mice lacking aquaporin-5 water channels. The Journal of biological chemistry, 274(29), 20071–4.

Mamane, Y., Heylbroeck, C., Génin, P., Algarté, M., Servant, M. J., LePage, C., … Hiscott, J. (1999). Interferon regulatory factors: the next generation. Gene, 237(1), 1–14.

Marsh, P. D., Head, D. A., & Devine, D. A. (2015). Dental plaque as a biofilm and a microbial community—Implications for treatment. Journal of Oral Biosciences, 57(4), 185–191.

Martin, T. A., Ye, L., Sanders, A. J., Lane, J., & Jiang, W. G. (2000). Cancer Invasion and Metastasis: Molecular and Cellular Perspective. Landes Bioscience.

Martínez-Alvarez, C., Tudela, C., Pérez-Miguelsanz, J., O'Kane, S., Puerta, J., & Ferguson, M. W. (2000). Medial edge epithelial cell fate during palatal fusion. Developmental biology, 220(2), 343–57.

Matsuda, C., Matsui, Y., Ohno, K., & Michi, K. (1999). Salivary gland aplasia with cleft lip and palateA case report and review of the literature. Oral Surgery, Oral Medicine, Oral Pathology, Oral Radiology, and Endodontology, 87(5), 594–599.

McCartney-Francis, N. L., Mizel, D. E., Redman, R. S., Frazier-Jessen, M., Panek, R. B., Kulkarni, A. B., … Wahl, S. M. (1996). Autoimmune Sjögren's-like lesions in salivary glands of TGF-beta1-deficient mice are inhibited by adhesion-blocking peptides. Journal of immunology (Baltimore, Md. : 1950), 157(3), 1306–12.

Melnick, M., & Jaskoll, T. (2000). Mouse submandibular gland morphogenesis: a paradigm for embryonic signal processing. Critical reviews in oral biology and medicine : an official publication of the American Association of Oral Biologists, 11(2), 199–215.

Meng, L., Bian, Z., Torensma, R., & Von den Hoff, J. W. (2009). Biological mechanisms in palatogenesis and cleft palate. Journal of dental research, 88(1), 22–33.

Menko, A. S., Zhang, L., Schiano, F., Kreidberg, J. A., & Kukuruzinska, M. A. (2002). Regulation of cadherin junctions during mouse submandibular gland development.

Developmental dynamics : an official publication of the American Association of Anatomists, 224(3), 321–33.

Michalek, S. M., McGhee, J. R., & Babb, J. L. (1978). Effective immunity to dental caries: dose-dependent studies of secretory immunity by oral administration of Streptococcus mutans to rats. Infection and immunity, 19(1), 217–24.

Miletich, I. (2010). Introduction to salivary glands: structure, function and embryonic development. Frontiers of oral biology, 14, 1–20.

Milunsky, J. M., Maher, T. A., Zhao, G., Roberts, A. E., Stalker, H. J., Zori, R. T., … Lin, A. E. (2008). TFAP2A mutations result in branchio-oculo-facial syndrome. American journal of human genetics, 82(5), 1171–7.

Mina, M., & Kollar, E. J. (1987). The induction of odontogenesis in non-dental mesenchyme combined with early murine mandibular arch epithelium. Archives of oral biology, 32(2), 123–7.

Mitsiadis, T. A., Graf, D., Luder, H., Gridley, T., & Bluteau, G. (2010). BMPs and FGFs target Notch signalling via jagged 2 to regulate tooth morphogenesis and cytodifferentiation. Development (Cambridge, England), 137(18), 3025–35.

Mitsiadis, T. A., Regaudiat, L., & Gridley, T. (2005). Role of the Notch signalling pathway in tooth morphogenesis. Archives of oral biology, 50(2), 137–40.

Mogensen, T. H. (2009). Pathogen recognition and inflammatory signaling in innate immune defenses. Clinical microbiology reviews, 22(2), 240–73, Table of Contents.

Moretti, F., Marinari, B., Lo Iacono, N., Botti, E., Giunta, A., Spallone, G., … Costanzo, A. (2010). A regulatory feedback loop involving p63 and IRF6 links the pathogenesis of 2 genetically different human ectodermal dysplasias. The Journal of clinical investigation, 120(5), 1570–7.

Mossey, P. (2003). Global strategies to reduce the healthcare burden of craniofacial anomalies. British dental journal, 195(10), 613.

Mossey, P. A., Little, J., Munger, R. G., Dixon, M. J., & Shaw, W. C. (2009). Cleft lip and palate. Lancet, 374(9703), 1773–85.

Murdiastuti, K., Miki, O., Yao, C., Parvin, M. N., Kosugi-Tanaka, C., Akamatsu, T., … Hosoi, K. (2002). Divergent expression and localization of aquaporin 5, an exocrine-type water channel, in the submandibular gland of Sprague-Dawley rats. Pflügers Archiv : European journal of physiology, 445(3), 405–12.

Murray, J. C. (2002). Gene/environment causes of cleft lip and/or palate. Clinical genetics, 61(4), 248–56.

Nagai, K., Arai, H., Okudera, M., Yamamura, T., Oki, H., & Komiyama, K. (2014). Epiregulin is critical for the acinar cell regeneration of the submandibular gland in a mouse duct ligation

model. Journal of oral pathology & medicine : official publication of the International Association of Oral Pathologists and the American Academy of Oral Pathology, 43(5), 378–87.

Nakashima, M., Adachi, S., Yasuda, I., Yamauchi, T., Kawaguchi, J., Hanamatsu, T., … Moriwaki, H. (2011). Inhibition of Rho-associated coiled-coil containing protein kinase enhances the activation of epidermal growth factor receptor in pancreatic cancer cells. Molecular cancer, 10(1), 79.

Nakatomi, M., Morita, I., Eto, K., & Ota, M. S. (2006). Sonic hedgehog signaling is important in tooth root development. Journal of dental research, 85(5), 427–31.

Nawa, H., Oberoi, S., & Vargervik, K. (2008). Taurodontism and Van der Woude syndrome: Is there an association? Angle Orthodontist, 78(5), 832–837.

Nishikawa, S., Fujiwara, K., & Kitamura, H. (1988). Formation of the tooth enamel rod pattern and the cytoskeletal organization in secretory ameloblasts of the rat incisor. European journal of cell biology, 47(2), 222–32.

Nogueira, R. D., Alves, A. C., Napimoga, M. H., Smith, D. J., & Mattos-Graner, R. O. (2005). Characterization of salivary immunoglobulin A responses in children heavily exposed to the oral bacterium Streptococcus mutans: influence of specific antigen recognition in infection. Infection and immunity, 73(9), 5675–84.

Nordgarden, H., Mustonen, T., Berner, H. S., Pispa, J., Ilmonen, M., Jensen, J. L., … Lyngstadaas, S. P. (2004). Ectodysplasin-A1 Promotes Epithelial Branching and Duct Formation in Developing Submandibular Glands.

Olasoji, H. O., Ukiri, O. E., & Yahaya, A. (2005). Incidence and aetiology of oral clefts: a review. African journal of medicine and medical sciences, 34(1), 1–7.

Oppenheimer, E. H., & Esterly, J. R. (1975). Pathology of cystic fibrosis review of the literature and comparison with 146 autopsied cases. Perspectives in pediatric pathology, 2, 241–78.

Otsuki, Y., Tanaka, M., Yoshii, S., Kawazoe, N., Nakaya, K., & Sugimura, H. (2001). Tumor metastasis suppressor nm23H1 regulates Rac1 GTPase by interaction with Tiam1. Proceedings of the National Academy of Sciences of the United States of America, 98(8), 4385–90.

Paper, O., Culp, D. J., Quivey, R. Q., Bowen, W. H., Fallon, M. a, Pearson, S. K., & Faustoferri, R. (2005). A Mouse Caries Model and Evaluation of Aqp5 –/– Knockout Mice. Caries research, 39(6), 448–54.

Parada Sanchez, M. T. (2012, February 25). Dissecting the role of the major cleft gene, IRF6, in primary palatal epithelia.

Pardo V, R. A., Castillo T, S., & Vieira, A. R. (2006). [Genetic studies of a Chilean family with three different dental anomalies]. Revista médica de Chile, 134(12), 1541–8.

Parisotto, T. M., Steiner-Oliveira, C., Duque, C., Peres, R. C. R., Rodrigues, L. K. A., & Nobre-

dos-Santos, M. (2010). Relationship among microbiological composition and presence of dental plaque, sugar exposure, social factors and different stages of early childhood caries. Archives of oral biology, 55(5), 365–73.

Patel, N., Sharpe, P. T., & Miletich, I. (2011). Coordination of epithelial branching and salivary gland lumen formation by Wnt and FGF signals. Developmental Biology, 358(1), 156–167.

Patir, A., Seymen, F., Yildirim, M., Deeley, K., Cooper, M. E., Marazita, M. L., & Vieira, A. R. (2008). Enamel formation genes are associated with high caries experience in Turkish children. Caries research, 42(5), 394–400.

Pegelow, M., Alqadi, N., & Karsten, A. L. A. (2012). The prevalence of various dental characteristics in the primary and mixed dentition in patients born with non-syndromic unilateral cleft lip with or without cleft palate. European Journal of Orthodontics, 34(5), 561–570.

Phattarataratip, E., Olson, B., Broffitt, B., Qian, F., Brogden, K. A., Drake, D. R., … Banas, J. A. (2011). Streptococcus mutans strains recovered from caries-active or caries-free individuals differ in sensitivity to host antimicrobial peptides. Molecular oral microbiology, 26(3), 187–99.

Pirraglia, C., Jattani, R., & Myat, M. M. (2006). Rac function in epithelial tube morphogenesis. Developmental biology, 290(2), 435–46.

Pirraglia, C., Walters, J., Ahn, N., & Myat, M. M. (2013). Rac1 GTPase acts downstream of αPS1βPS integrin to control collective migration and lumen size in the Drosophila salivary gland. Developmental biology, 377(1), 21–32.

Pispa, J., Jung, H. S., Jernvall, J., Kettunen, P., Mustonen, T., Tabata, M. J., … Thesleff, I. (1999). Cusp patterning defect in Tabby mouse teeth and its partial rescue by FGF. Developmental biology, 216(2), 521–34.

Polesello, V., Zupin, L., Di Lenarda, R., Biasotto, M., Ottaviani, G., Gobbo, M., … Segat, L. (2015). Impact of DEFB1 gene regulatory polymorphisms on hBD-1 salivary concentration. Archives of oral biology, 60(7), 1054–8.

Poosarla, C., Ramesh, M., Ramesh, K., Gudiseva, S., Bala, S., & Sundar, M. (2015). Proliferating Cell Nuclear Antigen in Premalignancy and Oral Squamous Cell Carcinoma. Journal of clinical and diagnostic research : JCDR, 9(6), ZC39–41.

Pöyry, M., Nyström, M., & Ranta, R. (1989). Tooth development in children with cleft lip and palate: a longitudinal study from birth to adolescence. European journal of orthodontics, 11(2), 125–30.

Pringle, S., Nanduri, L. S. Y., van der Zwaag, M., van Os, R., & Coppes, R. P. (2011). Isolation of mouse salivary gland stem cells. Journal of visualized experiments : JoVE, (48).

Qiu, M., Bulfone, A., Ghattas, I., Meneses, J. J., Christensen, L., Sharpe, P. T., … Rubenstein, J. L. (1997). Role of the Dlx homeobox genes in proximodistal patterning of the branchial arches: mutations of Dlx-1, Dlx-2, and Dlx-1 and -2 alter morphogenesis of proximal skeletal and soft

tissue structures derived from the first and second arches. Developmental biology, 185(2), 165–84.

Radoja, N., Guerrini, L., Lo Iacono, N., Merlo, G. R., Costanzo, A., Weinberg, W. C., … Morasso, M. I. (2007). Homeobox gene Dlx3 is regulated by p63 during ectoderm development: relevance in the pathogenesis of ectodermal dysplasias. Development (Cambridge, England), 134(1), 13–8.

Rahimov, F., Marazita, M. L., Visel, A., Cooper, M. E., Hitchler, M. J., Rubini, M., … Murray, J. C. (2008). Disruption of an AP-2alpha binding site in an IRF6 enhancer is associated with cleft lip. Nature genetics, 40(11), 1341–7.

Rakian, A., Yang, W.-C., Gluhak-Heinrich, J., Cui, Y., Harris, M. A., Villarreal, D., … Harris, S. E. (2013). Bone morphogenetic protein-2 gene controls tooth root development in coordination with formation of the periodontium. International journal of oral science, 5(2), 75–84.

Ramnath, D., Tunny, K., Hohenhaus, D. M., Pitts, C. M., Bergot, A.-S., Hogarth, P. M., … Sweet, M. J. (2015). TLR3 drives IRF6-dependent IL-23p19 expression and p19/EBI3 heterodimer formation in keratinocytes. Immunology and cell biology, 93(9), 771–9.

Rawashdeh, M. A., & Abu Sirdaneh, E. O. (2009). Crown morphologic abnormalities in the permanent dentition of patients with cleft lip and palate. The Journal of craniofacial surgery, 20(2), 465–70.

Reija, M. F. G., Gordillo, D. P. L., Palacio, J. C. B., Abascal, L. B., & Perea, B. G.-M. (2013). Bilateral submandibular gland aplasia with hypertrophy of the sublingual glands of a patient with a cleft lip and palate: case report. The Journal of craniofacial surgery, 24(5), e532–3.

Restivo, G., Nguyen, B.-C., Dziunycz, P., Ristorcelli, E., Ryan, R. J. H., Özuysal, Ö. Y., … Dotto, G. P. (2011). IRF6 is a mediator of Notch pro-differentiation and tumour suppressive function in keratinocytes. The EMBO journal, 30(22), 4571–85.

Ribelles Llop, M., Guinot Jimeno, F., Mayné Acién, R., & Bellet Dalmau, L. J. (2010). Effects of xylitol chewing gum on salivary flow rate, pH, buffering capacity and presence of Streptococcus mutans in saliva. European journal of paediatric dentistry : official journal of European Academy of Paediatric Dentistry, 11(1), 9–14.

Richardson, R. J., Dixon, J., Jiang, R., & Dixon, M. J. (2009). Integration of IRF6 and Jagged2 signalling is essential for controlling palatal adhesion and fusion competence. Human molecular genetics, 18(14), 2632–42.

Richardson, R. J., Dixon, J., Malhotra, S., Hardman, M. J., Knowles, L., Boot-Handford, R. P., … Dixon, M. J. (2006). Irf6 is a key determinant of the keratinocyte proliferation-differentiation switch. Nature genetics, 38(11), 1329–34.

Risheim, H., Arneberg, P., & Birkhed, D. (1992). Oral sugar clearance and root caries prevalence in rheumatic patients with dry mouth symptoms. Caries research, 26(6), 439–44.

Rockville, MD: U.S. Department of Health and Human Services, N. I. of D. and C. R. (2000). Oral Health in America: A Report of the Surgeon General. National Institutes of Health.

Romano, R.-A., Smalley, K., Magraw, C., Serna, V. A., Kurita, T., Raghavan, S., & Sinha, S. (2012). ΔNp63 knockout mice reveal its indispensable role as a master regulator of epithelial development and differentiation. Development (Cambridge, England), 139(4), 772–82.

Rothová, M., Peterková, R., & Tucker, A. S. (2012). Fate map of the dental mesenchyme: dynamic development of the dental papilla and follicle. Developmental biology, 366(2), 244–54.

Royer, C., & Lu, X. (2011). Epithelial cell polarity: a major gatekeeper against cancer? Cell death and differentiation, 18(9), 1470–7.

Rudney, J. D. (1989). Relationships between human parotid saliva lysozyme lactoferrin, salivary peroxidase and secretory immunoglobulin A in a large sample population. Archives of oral biology, 34(7), 499–506.

Rudney, J. D., Krig, M. A., & Neuvar, E. K. (1993). Longitudinal study of relations between human salivary antimicrobial proteins and measures of dental plaque accumulation and composition. Archives of oral biology, 38(5), 377–86.

Rudney, J. D., Krig, M. A., Neuvar, E. K., Soberay, A. H., & Iverson, L. (1991). Antimicrobial proteins in human unstimulated whole saliva in relation to each other, and to measures of health status, dental plaque accumulation and composition. Archives of oral biology, 36(7), 497–506.

Ruiz, L. A., Maya, R. R., D'Alpino, P. H. P., Atta, M. T., & da Rocha Svizero, N. (2013). Prevalence of enamel defects in permanent teeth of patients with complete cleft lip and palate. The Cleft palate-craniofacial journal : official publication of the American Cleft Palate-Craniofacial Association, 50(4), 394–9.

Rutledge, K. D., Barger, C., Grant, J. H., & Robin, N. H. (2010). IRF6 mutations in mixed isolated familial clefting. American journal of medical genetics. Part A, 152A(12), 3107–9.

Salahshourifar, I., Wan Sulaiman, W. A., Halim, A. S., & Zilfalil, B. A. (2012). Mutation screening of IRF6 among families with non-syndromic oral clefts and identification of two novel variants: review of the literature. European journal of medical genetics, 55(6-7), 389–93.

Sánchez, G. A., & Fernandez De Preliasco, M. V. (2003). Salivary pH changes during soft drinks consumption in children. International journal of paediatric dentistry / the British Paedodontic Society [and] the International Association of Dentistry for Children, 13(4), 251–7.

Sandell, L. L., & Trainor, P. A. (2006). Neural crest cell plasticity. size matters. Advances in experimental medicine and biology, 589, 78–95.

Sasagawa, I., & Ishiyama, M. (2005). Fine structural and cytochemical mapping of enamel organ during the enameloid formation stages in gars, Lepisosteus oculatus, Actinopterygii. Archives of oral biology, 50(4), 373–91.

Sasaki, T., & Garant, P. R. (1986). Ultracytochemical demonstration of ATP-dependent calcium pump in ameloblasts of rat incisor enamel organ. Calcified Tissue International, 39(2), 86–96.

Shashni, R., Goyal, A., Gauba, K., Utreja, A. K., Ray, P., & Jena, A. K. (2015). Comparison of risk indicators of dental caries in children with and without cleft lip and palate deformities. Contemporary clinical dentistry, 6(1), 58–62.

Shin, K., Fogg, V. C., & Margolis, B. (2006). Tight junctions and cell polarity. Annual review of cell and developmental biology, 22, 207–35.

Shu, M., Morou-Bermudez, E., Suárez-Pérez, E., Rivera-Miranda, C., Browngardt, C. M., Chen, Y.-Y. M., … Burne, R. A. (2007). The relationship between dental caries status and dental plaque urease activity. Oral microbiology and immunology, 22(1), 61–6.

Simmer, J. P., & Fincham, A. G. (1995). Molecular mechanisms of dental enamel formation. Critical reviews in oral biology and medicine : an official publication of the American Association of Oral Biologists, 6(2), 84–108.

Simmer, J. P., Papagerakis, P., Smith, C. E., Fisher, D. C., Rountrey, A. N., Zheng, L., & Hu, J. C. C. (2010). Regulation of dental enamel shape and hardness. Journal of dental research, 89(10), 1024–38.

Slayton, R. L., Cooper, M. E., & Marazita, M. L. (2005). Tuftelin, Mutans Streptococci, and Dental Caries Susceptibility. Journal of Dental Research, 84(8), 711–714.

Smith, C. E. (1998). Cellular and chemical events during enamel maturation. Critical reviews in oral biology and medicine : an official publication of the American Association of Oral Biologists, 9(2), 128–61.

Stanier, P., & Moore, G. E. (2004). Genetics of cleft lip and palate: syndromic genes contribute to the incidence of non-syndromic clefts. Human molecular genetics, 13 Spec No, R73–81.

Steinfeld, S., Cogan, E., King, L. S., Agre, P., Kiss, R., & Delporte, C. (2001). Abnormal Distribution of Aquaporin-5 Water Channel Protein in Salivary Glands from Sjögren's Syndrome Patients. Laboratory Investigation, 81(2), 143–148.

Stookey, G. K. (2008). The effect of saliva on dental caries. Journal of the American Dental Association (1939), 139 Suppl, 11S–17S.

Sundell, A. L., Ullbro, C., Marcusson, A., & Twetman, S. (2015). Comparing caries risk profiles between 5- and 10- year-old children with cleft lip and/or palate and non-cleft controls. BMC oral health, 15(1), 85.

Takaishi, K., Sasaki, T., Kameyama, T., Tsukita, S., & Takai, Y. (1995). Translocation of activated Rho from the cytoplasm to membrane ruffling area, cell-cell adhesion sites and cleavage furrows. Oncogene, 11(1), 39–48.

Takaishi, K., Sasaki, T., Kotani, H., Nishioka, H., & Takai, Y. (1997). Regulation of cell-cell

adhesion by rac and rho small G proteins in MDCK cells. The Journal of cell biology, 139(4), 1047–59.

Tan, E. L. Y., Yow, M., Kuek, M. C., & Wong, H. C. (2012). Dental maturation of unilateral cleft lip and palate. Annals of maxillofacial surgery, 2(2), 158–62.

Tanida, T., Okamoto, T., Okamoto, A., Wang, H., Hamada, T., Ueta, E., & Osaki, T. (2003). Decreased excretion of antimicrobial proteins and peptides in saliva of patients with oral candidiasis. Journal of oral pathology & medicine : official publication of the International Association of Oral Pathologists and the American Academy of Oral Pathology, 32(10), 586–94.

Taniguchi, T., Ogasawara, K., Takaoka, A., & Tanaka, N. (2001). IRF family of transcription factors as regulators of host defense. Annual review of immunology, 19, 623–55.

Thesleff, I. (2006). The genetic basis of tooth development and dental defects. American journal of medical genetics. Part A, 140(23), 2530–2535.

Thesleff, I., & Hurmerinta, K. (1981). Tissue interactions in tooth development. Differentiation; research in biological diversity, 18(2), 75–88.

Thesleff, I., Vaahtokari, A., Vainio, S., & Jowett, A. (1996). Molecular mechanisms of cell and tissue interactions during early tooth development. The Anatomical record, 245(2), 151–61.

Thomas, B. L., Tucker, A. S., Qui, M., Ferguson, C. A., Hardcastle, Z., Rubenstein, J. L., & Sharpe, P. T. (1997). Role of Dlx-1 and Dlx-2 genes in patterning of the murine dentition. Development (Cambridge, England), 124(23), 4811–8.

Thomason, H. A., Zhou, H., Kouwenhoven, E. N., Dotto, G., Restivo, G., Nguyen, B., … Dixon, J. (2010). Cooperation between the transcription factors p63 and IRF6 is essential to prevent cleft palate in mice, 120(5), 1561–1569.

Tucker, a S., & Sharpe, P. T. (1999). Molecular genetics of tooth morphogenesis and patterning: the right shape in the right place. Journal of dental research, 78(4), 826–834.

Tucker, A. S. (2007). Salivary gland development. Seminars in cell & developmental biology, 18(2), 237–44.

Turner, C., Zagirova, A. F., Frolova, L. E., Courts, F. J., & Williams, W. N. (1998). Oral health status of Russian children with unilateral cleft lip and palate. The Cleft palate-craniofacial journal : official publication of the American Cleft Palate-Craniofacial Association, 35(6), 489–94.

Tzioufas, A. G., & Voulgarelis, M. (2007). Update on Sjögren's syndrome autoimmune epithelitis: from classification to increased neoplasias. Best practice & research. Clinical rheumatology, 21(6), 989–1010.

Vaezi, A., Bauer, C., Vasioukhin, V., & Fuchs, E. (2002). Actin cable dynamics and Rho/Rock orchestrate a polarized cytoskeletal architecture in the early steps of assembling a stratified

epithelium. Developmental cell, 3(3), 367–81.

van den Boogaard, M.-J., Créton, M., Bronkhorst, Y., van der Hout, A., Hennekam, E., Lindhout, D., … Ploos van Amstel, H. K. (2012). Mutations in WNT10A are present in more than half of isolated hypodontia cases. Journal of medical genetics, 49(5), 327–31.

van Houte, J., Lopman, J., & Kent, R. (1996). The final pH of bacteria comprising the predominant flora on sound and carious human root and enamel surfaces. Journal of dental research, 75(4), 1008–14.

van Loveren, C., Buijs, J. F., Bokhout, B., Prahl-Andersen, B., & Ten Cate, J. M. (1998). Incidence of mutans streptococci and lactobacilli in oral cleft children wearing acrylic plates from shortly after birth. Oral microbiology and immunology, 13(5), 286–91.

van Straten, C., & Butow, K.-W. (2013). Gene p63: In ectrodactyly-ectodermal dysplasia clefting, ankyloblepharon-ectodermal dysplasia, Rapp-Hodgkin syndrome. Annals of maxillofacial surgery, 3(1), 58–61.

Walker, J. L., Menko, A. S., Khalil, S., Rebustini, I., Hoffman, M. P., Kreidberg, J. A., & Kukuruzinska, M. A. (2008). Diverse roles of E-cadherin in the morphogenesis of the submandibular gland: insights into the formation of acinar and ductal structures. Developmental dynamics : an official publication of the American Association of Anatomists, 237(11), 3128–41.

Walker, S. C., Mattick, C. R., Hobson, R. S., & Steen, I. N. (2009). Abnormal tooth size and morphology in subjects with cleft lip and/or palate in the north of England. European journal of orthodontics, 31(1), 68–75.

Wang, J.-D., Chen, X., Frencken, J., Du, M.-Q., & Chen, Z. (2012a). Dental caries and first permanent molar pit and fissure morphology in 7- to 8-year-old children in Wuhan, China. International journal of oral science, 4(3), 157–60.

Wang, X., Liu, J., Zhang, H., Xiao, M., Li, J., Yang, C., … Kong, X. (2003). Novel mutations in the IRF6 gene for Van der Woude syndrome. Human genetics, 113(5), 382–6.

Wang, X. P., Zhong, B., Chen, Z. K., Stewart, M. E., Zhang, C., Zhang, K., … Miller, L. E. (2012b). History of frequent gum chewing is associated with higher unstimulated salivary flow rate and lower caries severity in healthy Chinese adults. Caries research, 46(6), 513–8.

Weiss, M., Weiss, J., Müller-Hartwich, R., Meier, B., & Jost-Brinkmann, P.-G. (2005). Chlorhexidine in cleft lip and palate patients with multibracket appliances. Results of a prospective study on the effectiveness of two different chlorhexidine preparations in cleft lip and palate patients with multibracket appliances. Journal of orofacial orthopedics = Fortschritte der Kieferorthopädie : Organ/official journal Deutsche Gesellschaft für Kieferorthopädie, 66(5), 349–62.

Wells, K. L., & Patel, N. (2010). Lumen formation in salivary gland development. Frontiers of oral biology, 14, 78–89.

Wells, M. (2014). Review suggests that cleft lip and palate patients have more caries. Evidence-based dentistry, 15(3), 79.

Woods, L. T., Camden, J. M., El-Sayed, F. G., Khalafalla, M. G., Petris, M. J., Erb, L., & Weisman, G. A. (2015). Increased Expression of TGF-β Signaling Components in a Mouse Model of Fibrosis Induced by Submandibular Gland Duct Ligation. PloS one, 10(5), e0123641.

Wu, T.-T., Chen, P. K. T., Lo, L.-J., Cheng, M.-C., & Ko, E. W.-C. (2011). The characteristics and distribution of dental anomalies in patients with cleft. Chang Gung medical journal, 34(3), 306–14.

Yang, J., Wang, S.-K., Choi, M., Reid, B. M., Hu, Y., Lee, Y.-L., … Hu, J. C.-C. (2014). Taurodontism, variations in tooth number, and misshapened crowns in Wnt10a null mice and human kindreds. Molecular Genetics & Genomic Medicine, n/a–n/a.

Yeh, C.-K., Harris, S. E., Mohan, S., Horn, D., Fajardo, R., Chun, Y.-H. P., … Abboud-Werner, S. (2012). Hyperglycemia and xerostomia are key determinants of tooth decay in type 1 diabetic mice. Laboratory investigation; a journal of technical methods and pathology, 92(6), 868–82.

Yildirim, M., Yorgancilar, E., Gun, R., & Topcu, I. (2012). Ectodermal dysplasia: otolaryngologic evaluation of 23 cases. Ear, nose, & throat journal, 91(2), E28–33.

Yildirim, S. (2013). Tooth Development, 5–17.

Zhang, Z., Tian, H., Lv, P., Wang, W., Jia, Z., Wang, S., … Gao, X. (2015). Transcriptional factor DLX3 promotes the gene expression of enamel matrix proteins during amelogenesis. PloS one, 10(3), e0121288.

Zhou, J., Wang, H., Yang, G., Wang, X., Sun, Y., Song, T., … Wang, S. (2010). Histological and ultrastructural characterization of developing miniature pig salivary glands. Anatomical record (Hoboken, N.J. : 2007), 293(7), 1227–39.